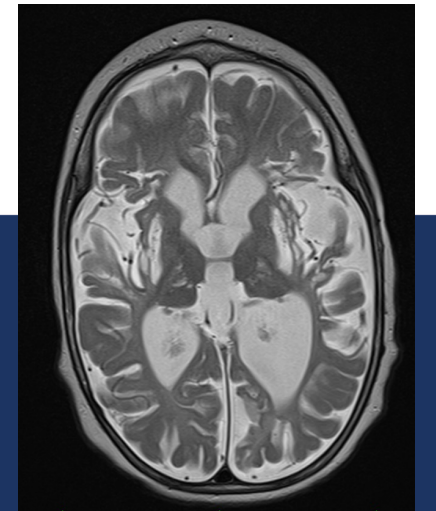# HYPOXIC – ISCHEMIC BRAIN INJURY

Shalen Misser
2022

Declarations

- Nothing to disclose

- The images are from our published articles. Two additional quoted references.

- Thank you to the patients we image and in the care of whom we aim to improve their lives

- Thank you to all my colleagues, co-investigators and supervisors

HYPOXIC – ISCHEMIC BRAIN INJURY

Research Plan

* Categorise the patterns

* Classify the central patterns

       Identify a new undescribed pattern

* Classify the watershed patterns

       Identify a biomarker for HIBI in watershed patterns

* Other aspects

AOSIS

A pictorial review of the pathophysiology and classification of the magnetic resonance imaging patterns of perinatal term hypoxic ischemic brain injury – What the radiologist needs to know…

CrossMark
click for updates

Authors:
Shalendra K. Misser[1,2] ©
Anthony J. Barkovich[3] ©
Jan W. Lotz[4] ©
Moherndran Archary[5] ©

Affiliations:
[1]Department of Radiology, Faculty of Health Sciences Medicine, College of Health Sciences, Nelson R. Mandela School of Medicine, University of KwaZulu-Natal, Durban, South Africa

[2]Department of Radiology,

This article provides a correlation of the pathophysiology and magnetic resonance imaging (MRI) patterns identified on imaging of children with hypoxic ischemic brain injury (HIBI). The purpose of this pictorial review is to empower the reading radiologist with a simplified classification of the patterns of cerebral injury matched to images of patients demonstrating each subtype. A background narrative literature review was undertaken of the regional, continental and international databases looking at specific patterns of cerebral injury related to perinatal HIBI. In addition, a database of MRI studies accumulated over a decade (including a total of 314 studies) was analysed and subclassified into the various patterns of cerebral injury. Selected cases were annotated to highlight the areas involved and for ease of identification of the affected substrate in daily practice.

Keywords: Hypoxic ischemic encephalopathy; Magnetic resonance imaging; Acute profound; Partial prolonged; Hypoxic ischemic brain injury; Ulegyria; Multicystic; Encephalopathy.
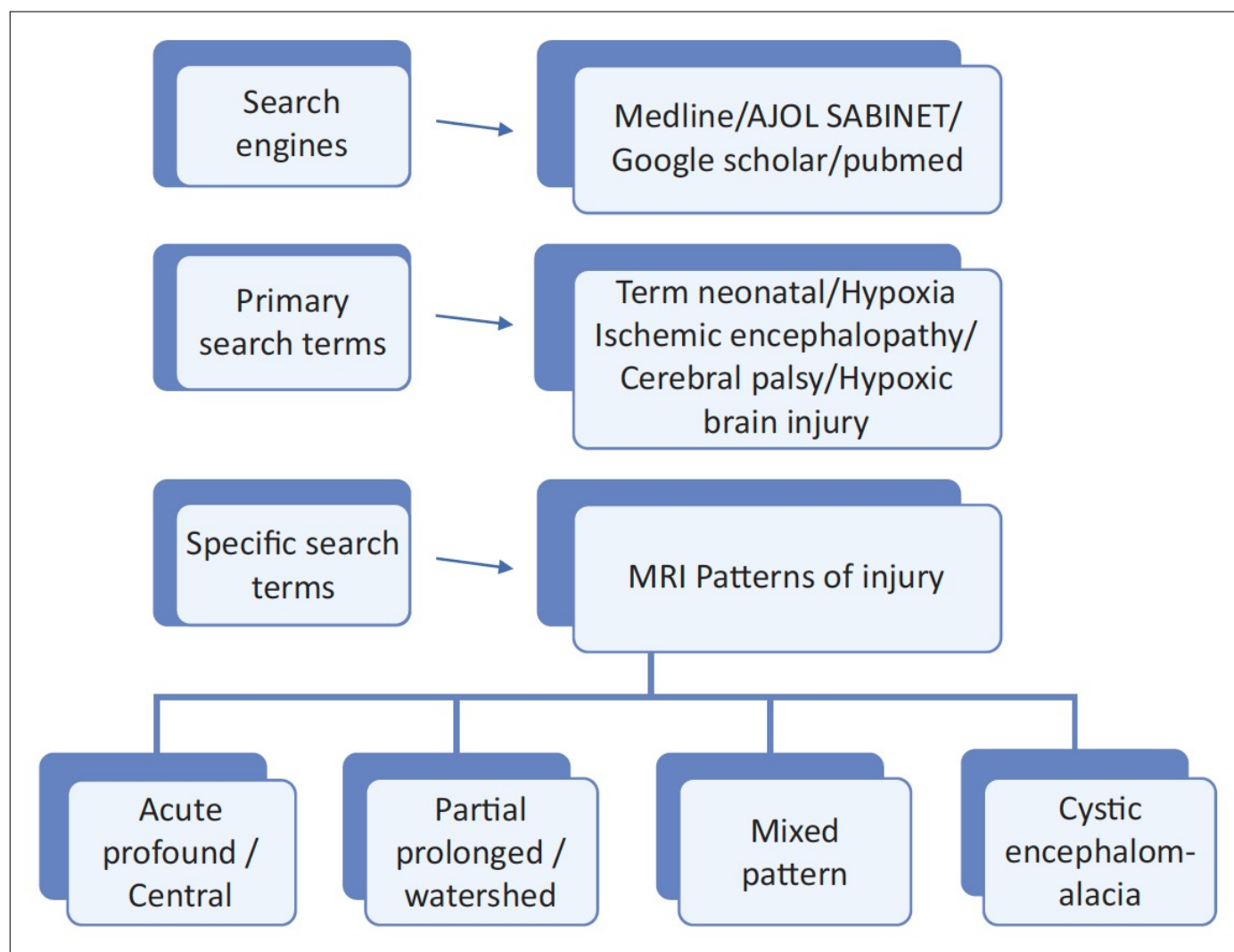
Misser SK, Barkovich AJ, Lotz JW, Archary M. A pictorial review of the pathophysiology and classification of the magnetic resonance imaging patterns of perinatal term hypoxic ischemic brain injury – What the radiologist needs to know… S Afr J Rad. 2020;24(1), a1915. https://doi.org/10.4102/sajr.v24i1.1915

FIGURE 2: Contextual framework of the narrative review process for term neonatal hypoxic ischemic encephalopathy and the resultant neuroimaging patterns.

Misser SK, Barkovich AJ, Lotz JW, Archary M. A pictorial review of the pathophysiology and classification of the magnetic resonance imaging patterns of perinatal term hypoxic ischemic brain injury – What the radiologist needs to know... S Afr J Rad. 2020;24(1), a1915. https://doi.org/10.4102/sajr.v24i1.1915

TABLE 1: The basic patterns of magnetic resonance imaging abnormalities in hypoxic ischemic encephalopathy.

Subtype of HIBI	Anatomical structure involved	Timing and severity of insult
Acute profound ischemia	Deep nuclei/perirolandic/hippocampus	Sudden/profound hypoxic episode
Partial prolonged ischemia	Cerebral intervascular watershed areas	Prolonged, moderate/or intermittent
Mixed injury	Deep nuclei/cortex and watershed areas	Severe, relatively brief. May be prolonged.
Type 1 cystic encephalomalacia	Cerebral cortex, white matter sparing the basal nuclei	Severe prolonged anoxia
Type 2 cystic encephalomalacia	Cerebral cortex, white matter as well as basal nuclei	Severe, with acute profound anoxia

Cerebral = Cortex and subcortical/central white matter involvement, especially parasagittal/watershed territory.
Deep nuclei = Thalamus, Putamen, ±Caudate nucleus.
White matter = Periventricular and central cerebral white matter.

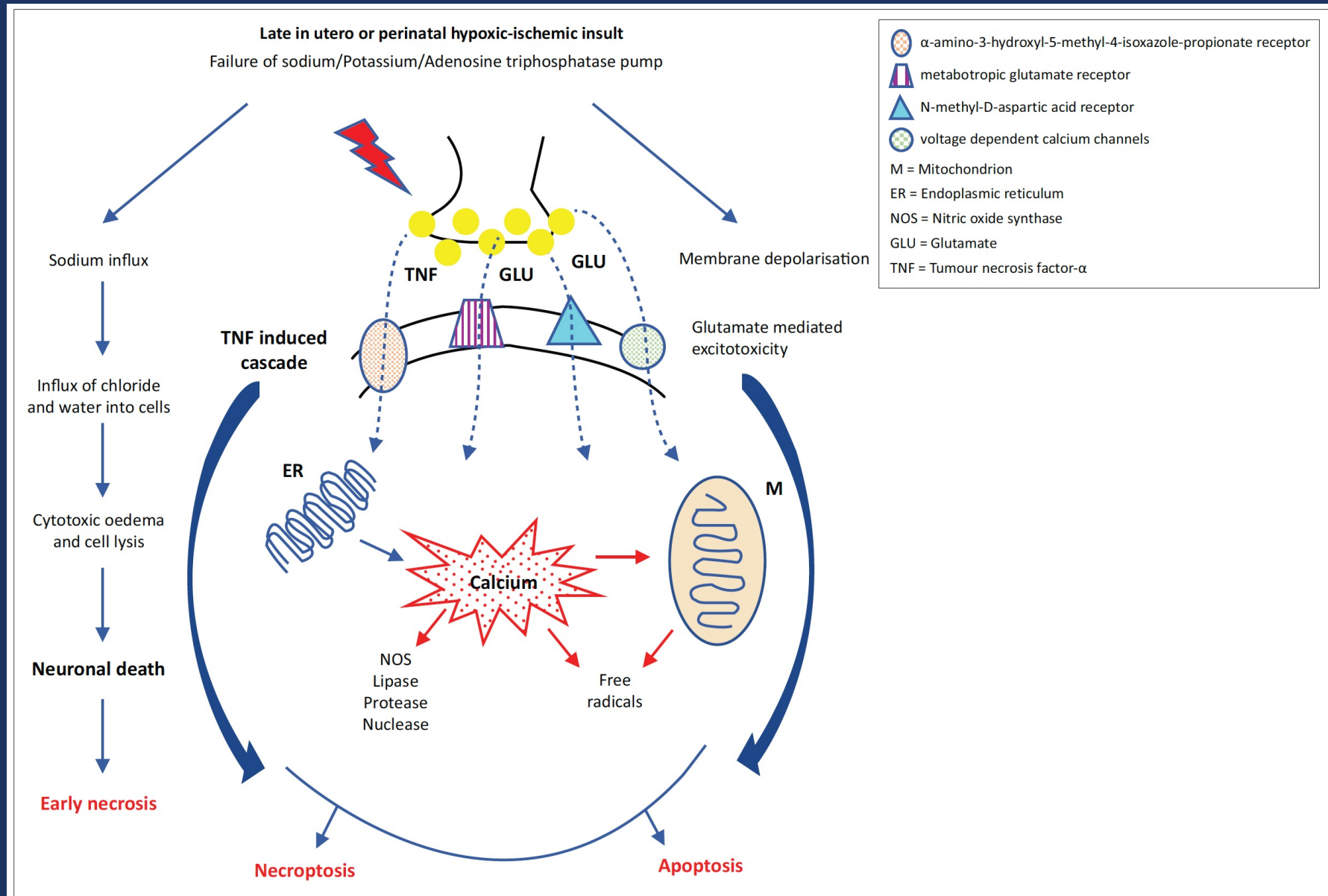HIBI, hypoxic ischemic brain injury.

FIGURE 1: Pathogenesis of hypoxic ischemic encephalopathy[12] mediated by sodium potassium adenosine triphosphatase pump failure leading to cytotoxic oedema and early cell necrosis, apoptosis via glutamate-induced excitotoxicity and necroptosis by tumour necrosis factor-α-induced cascade.
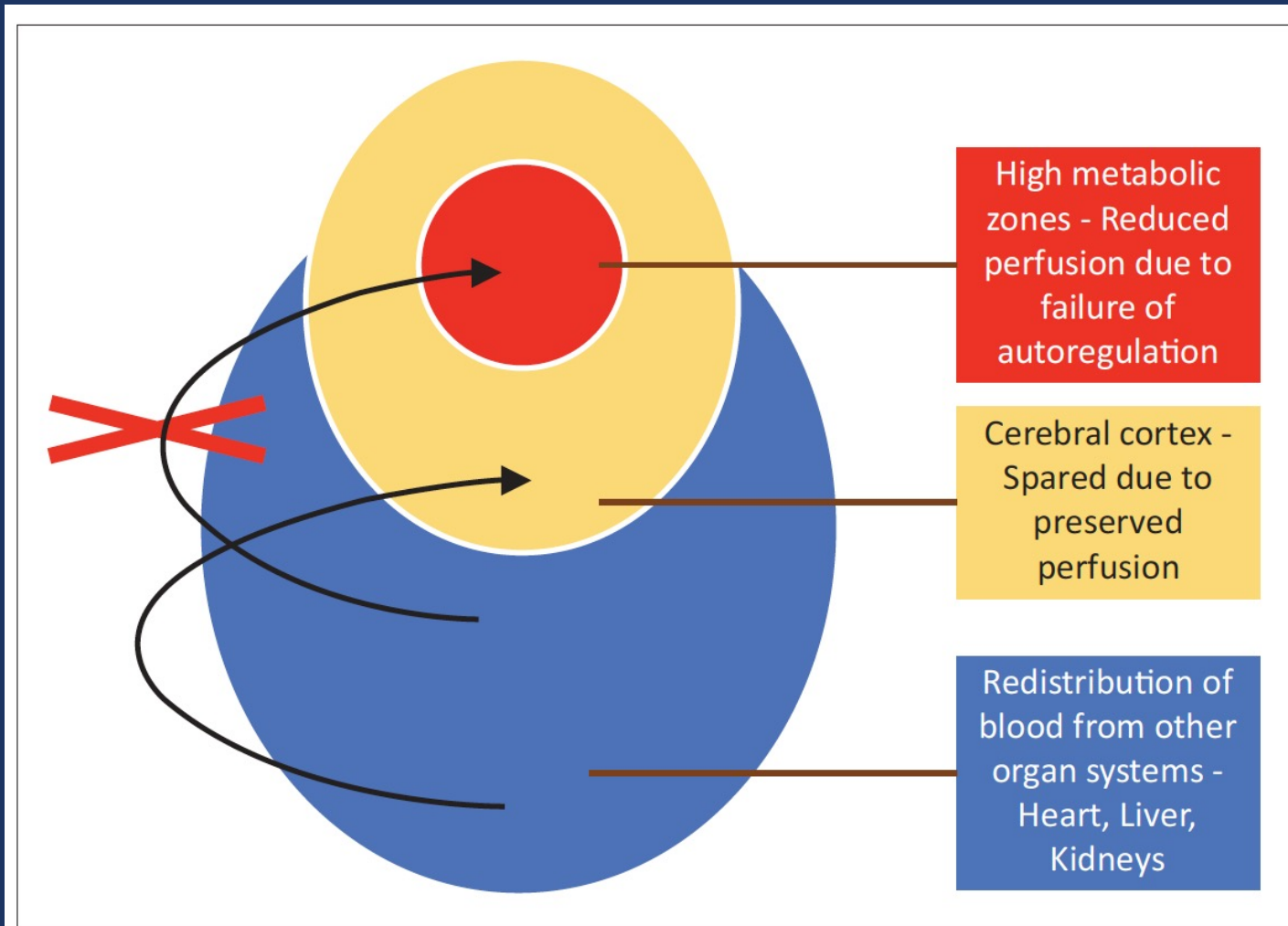
FIGURE 3: Diagrammatic representation showing redistribution of visceral blood supply to the brain, but failure of cerebral autoregulatory mechanisms to redirect perfusion to the high metabolic zones of the brain.

TABLE 3: High metabolic zones of the brain with highest concentration of N-methyl-D-aspartate receptors.

Perirolandic sensorimotor strip

Thalami (ventral posterior lateral nuclei)

Lentiform nuclei (posterior putamen)

Hippocampi and parahippoocampal gyri

Optic radiation

Heschl's gyrus at primary auditory cortex

Anterior superior cerebellar vermis
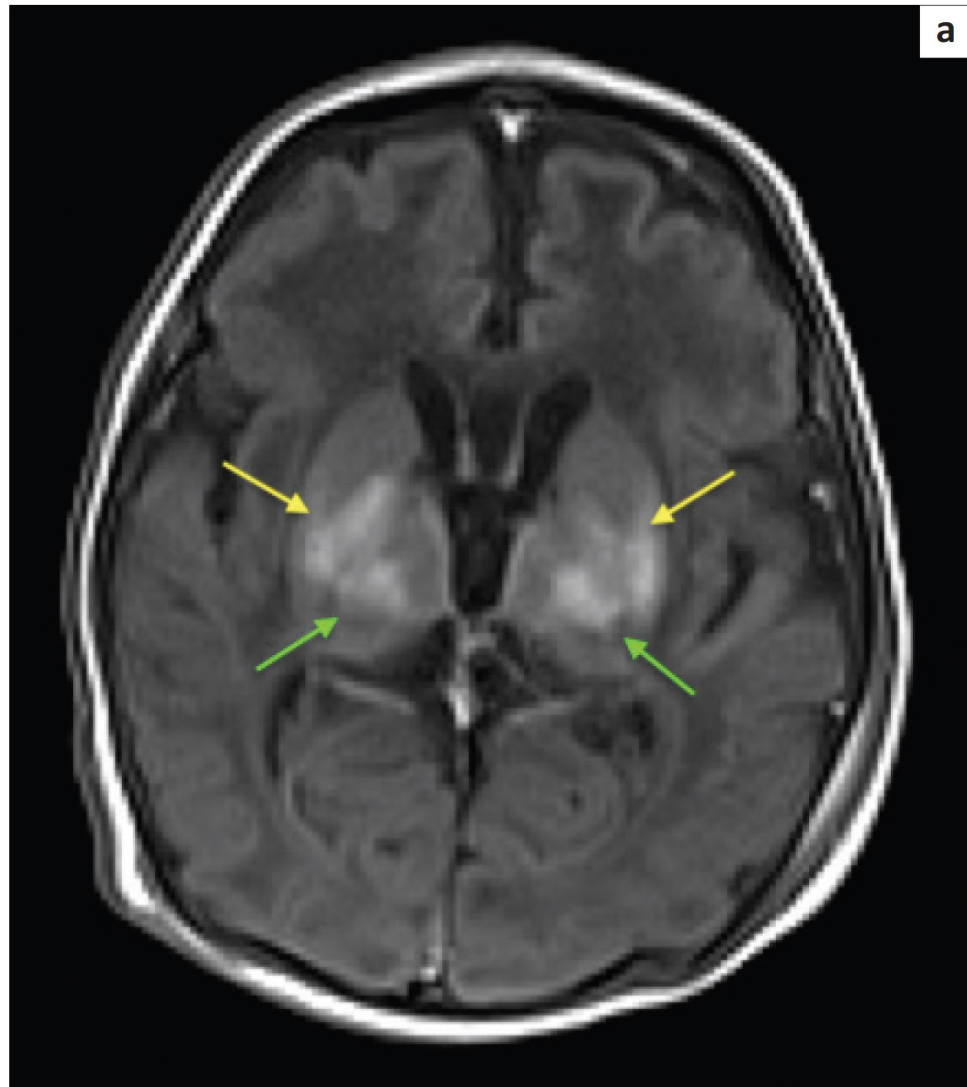
Tegmentum of midbrain and pons
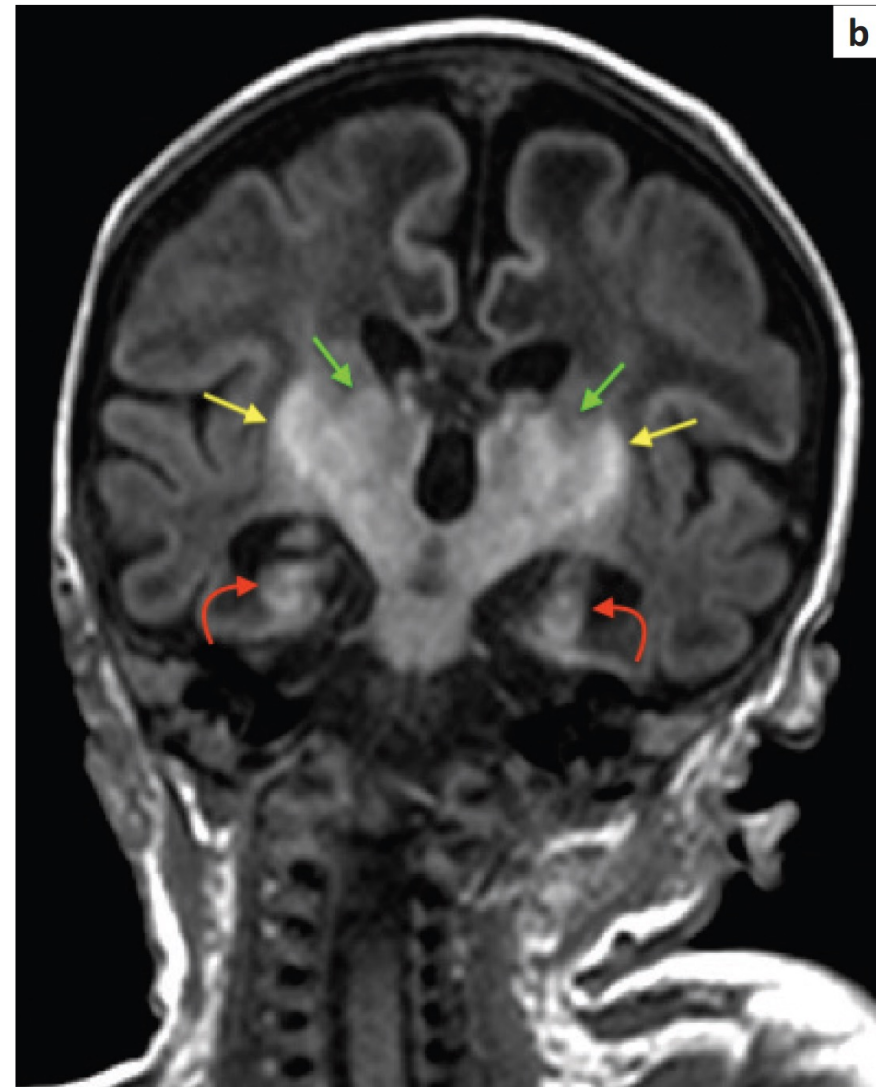
FIGURE 4: Two-week-old neonate born with grade 3 hypoxic ischemic brain injury and neonatal seizures. (a) An axial T1-weighted sequence showing signal shortening at the dorsal putamina (yellow arrows) and ventral thalami (green arrows). (b) Note, in addition to the basal ganglia and thalamic changes, the hyperintense signal and volume loss at both hippocampi (red arrows).
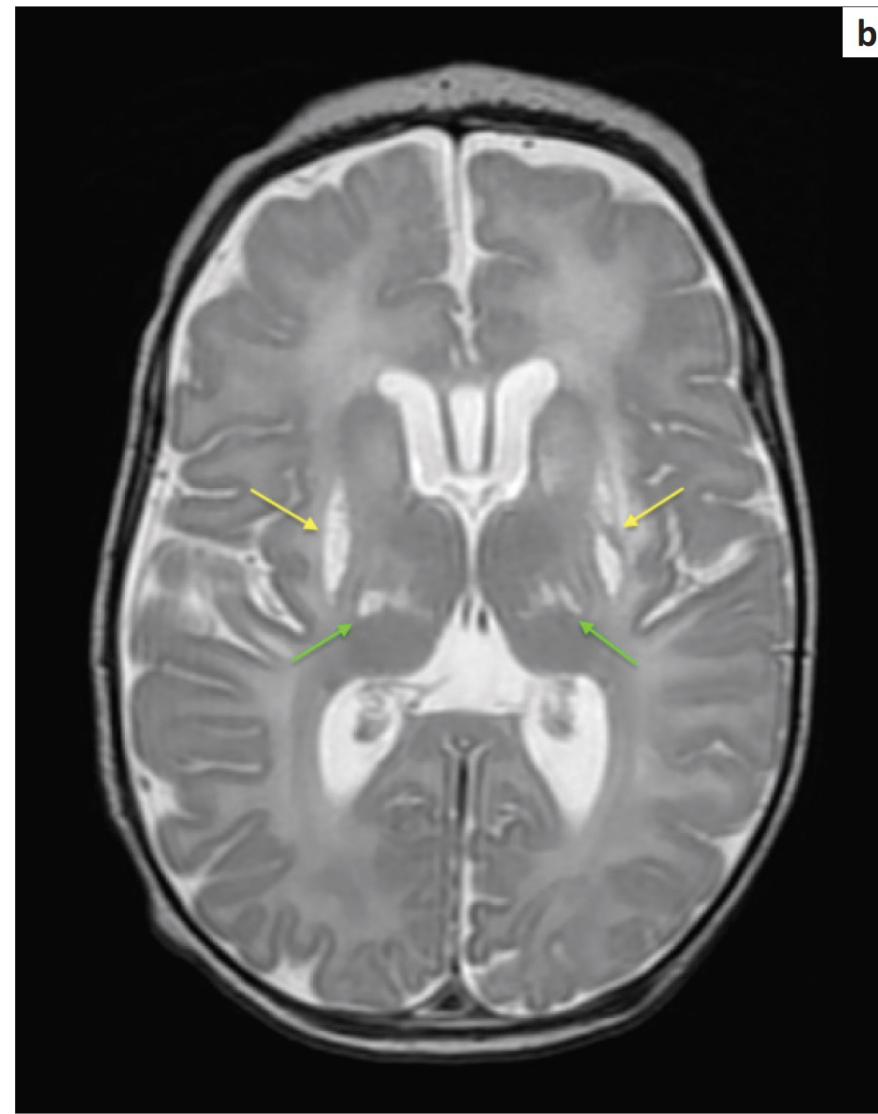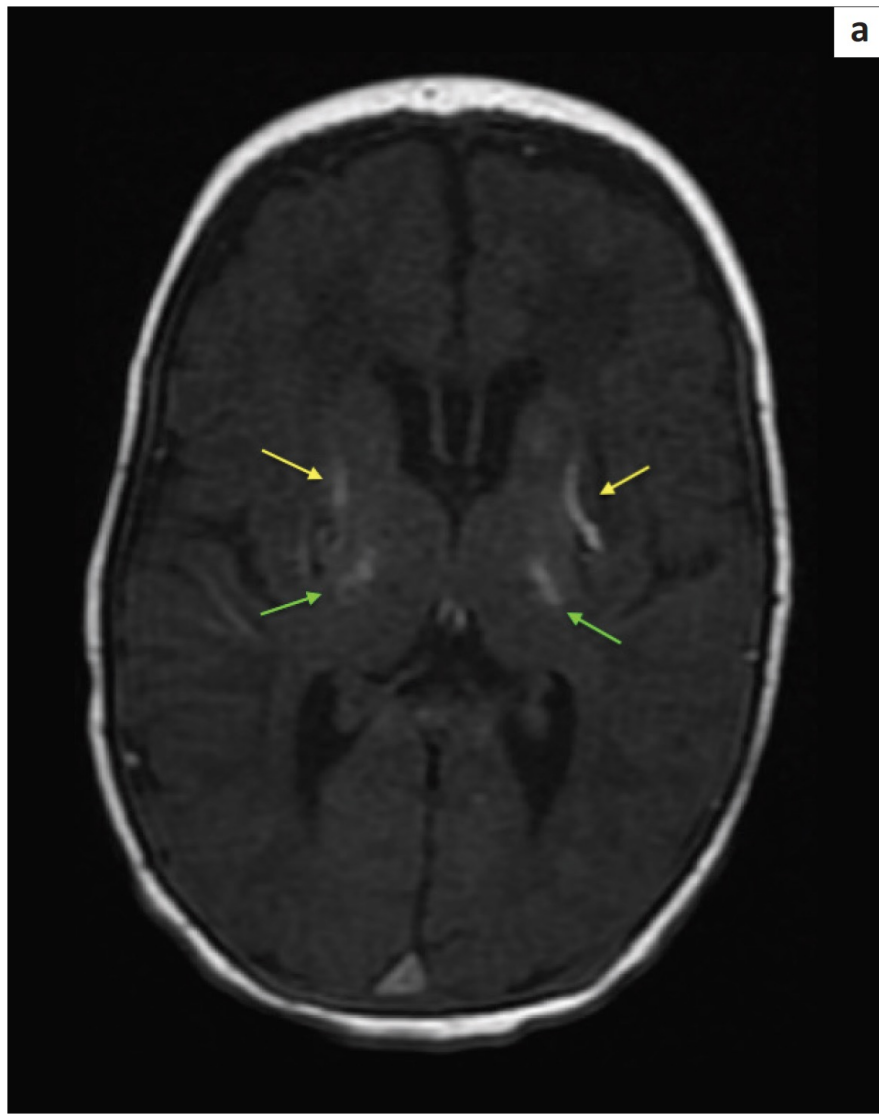
FIGURE 6: Twenty-seven-day-old male child delivered after abruptio placentae. Axial magnetic resonance imaging images at the level of the basal ganglia demonstrating bilateral fairly symmetrical dorsal putaminal (yellow arrows) and ventral thalamic (green arrows) hyperintensity because of T1 shortening (a) and corresponding T2-weighted hyperintensity and established atrophy of these structures (b). Note that the changes have evolved within the first month of life.
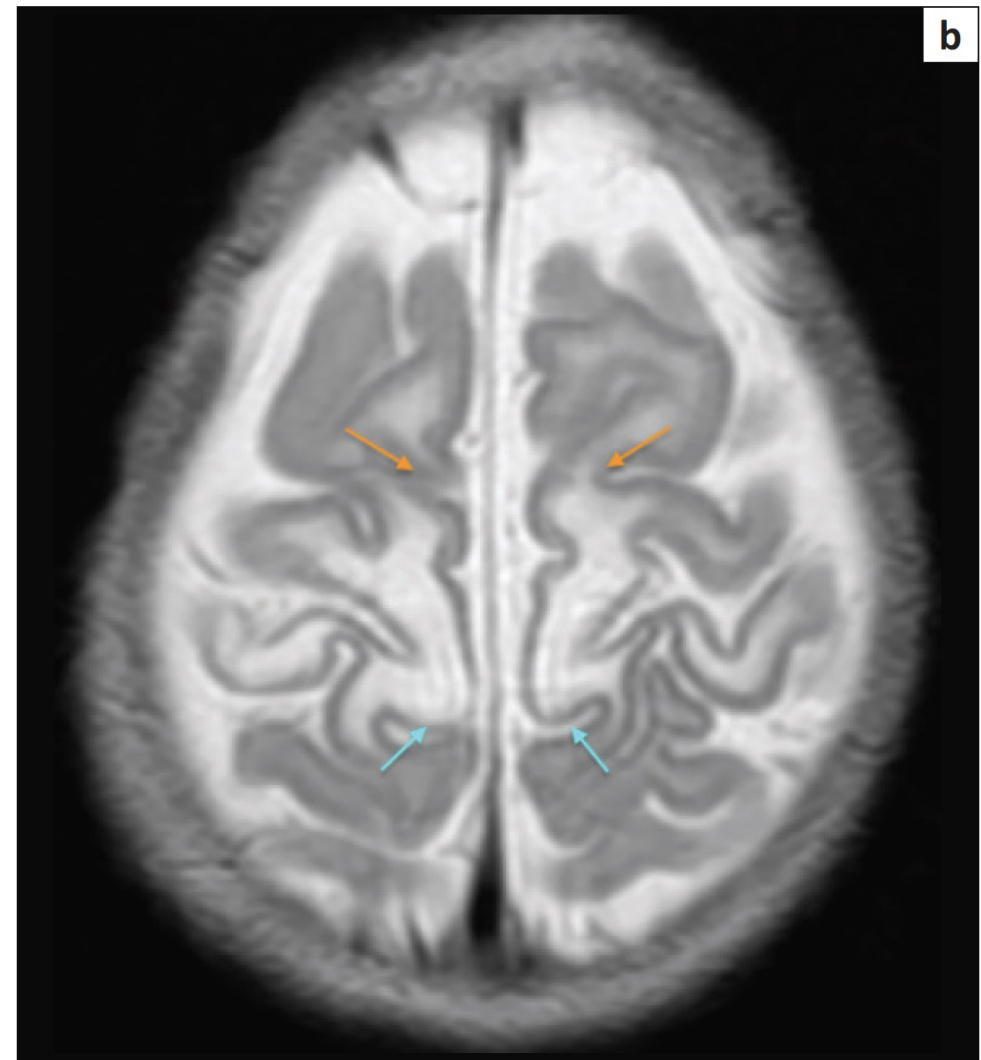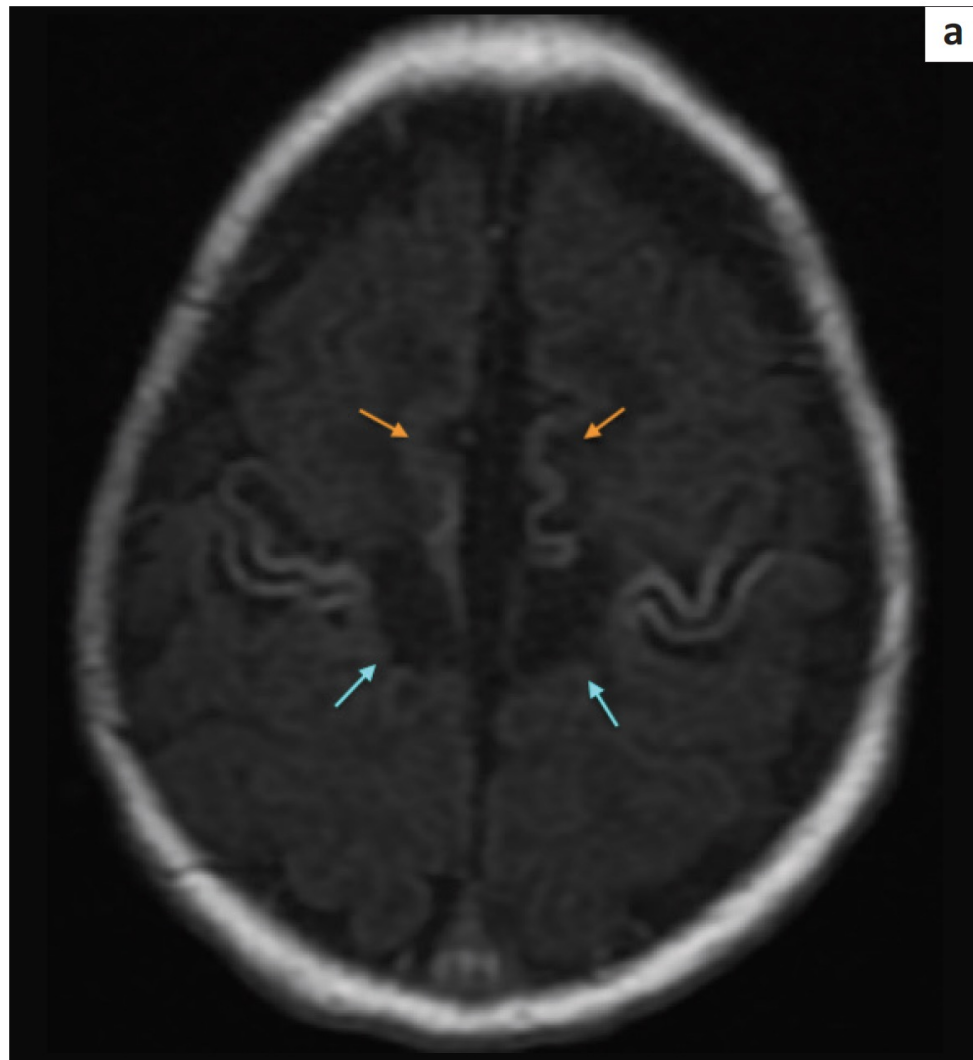
Misser SK, Barkovich AJ, Lotz JW, Archary M. A pictorial review of the pathophysiology and classification of the magnetic resonance imaging patterns of perinatal term hypoxic ischemic brain injury – What the radiologist needs to know... S Afr J Rad. 2020;24(1), a1915. https://doi.org/10.4102/sajr.v24i1.1915

FIGURE 7: The same child as in Figure 6. Axial magnetic resonance imaging at the superior cerebral convexity demonstrating perirolandic cortical ribbon hyperintensity with T1 shortening (a) on both sides of the central sulcus and T2-weighted hyperintensity of the surrounding sensorimotor cortex (b). Note associated localised parasagittal cortex (orange arrows) and paracentral lobule (cyanide arrows) involvement.
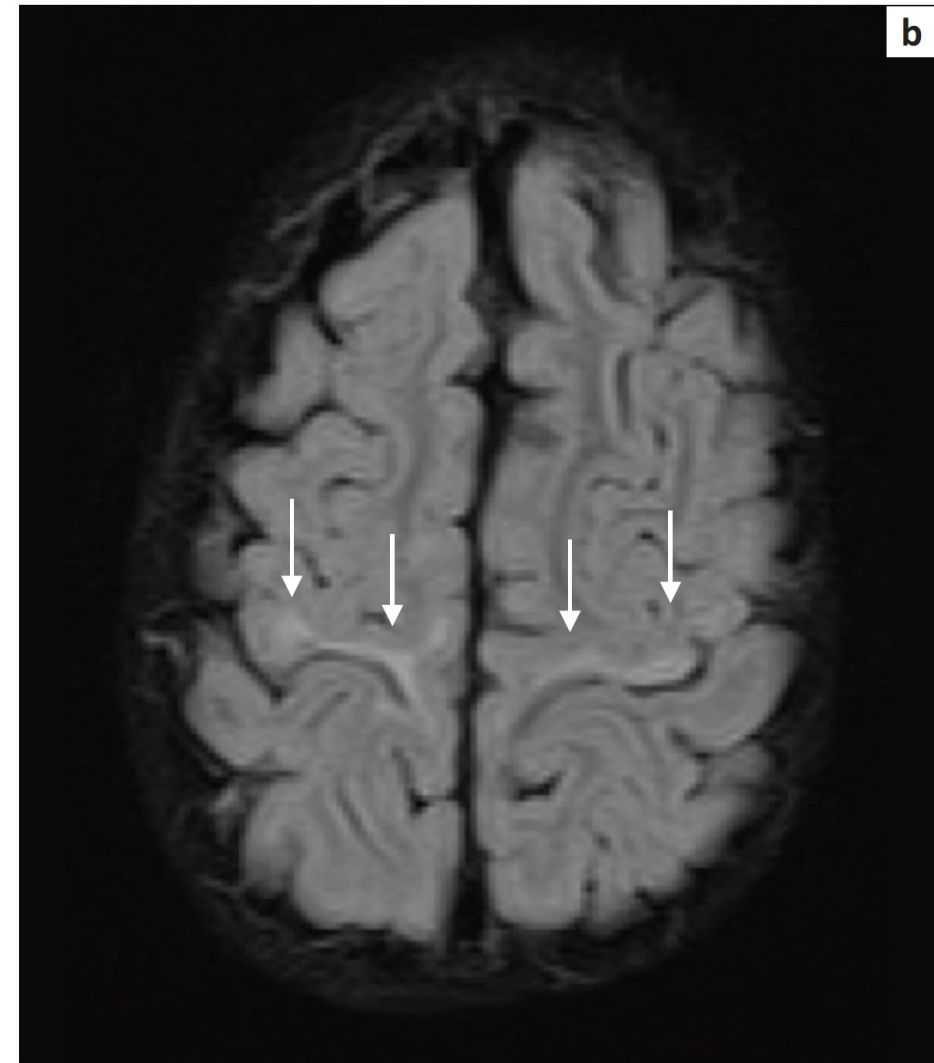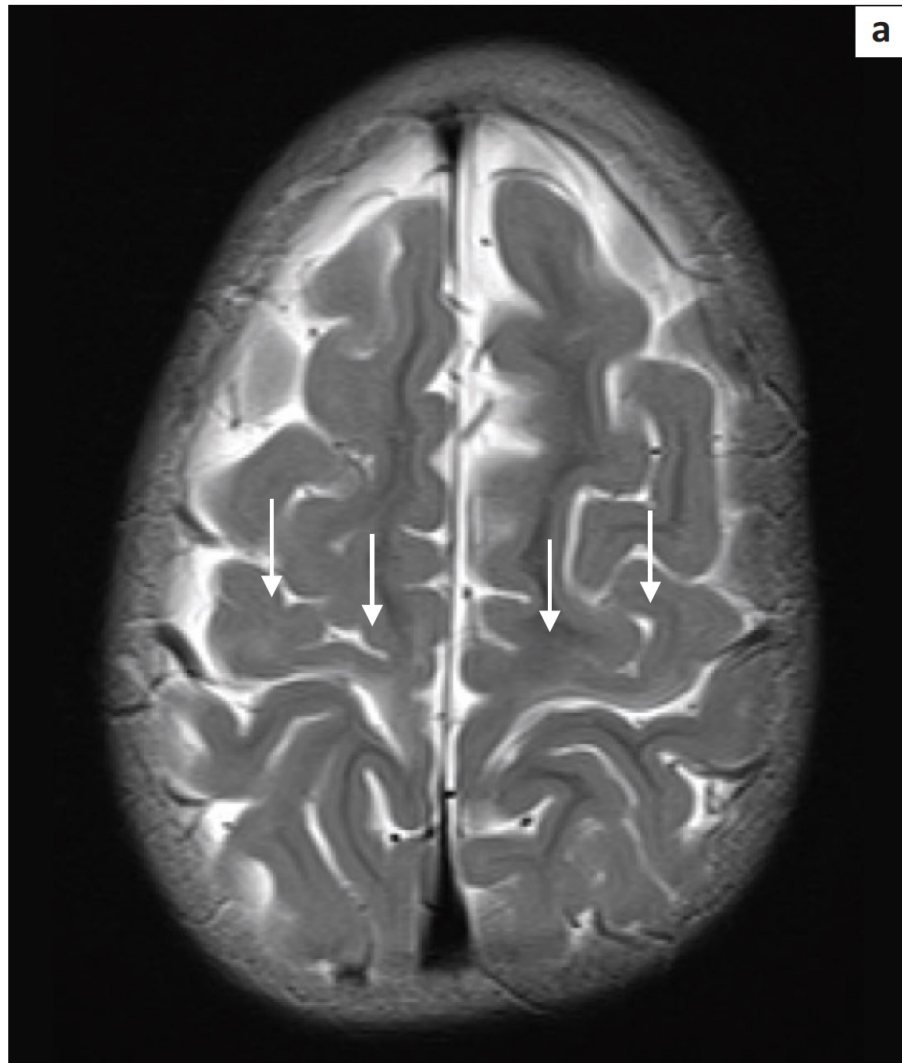
FIGURE 8: Three-year-old male child with history of neonatal encephalopathy, low Apgar scores and seizures. (a) An axial T2-weighted sequence image, which does not demonstrate the perirolandic changes adequately, and these changes would be difficult to diagnose without the axial FLAIR sequence image (b) which shows that the changes are almost exclusively involving the precentral gyrus.
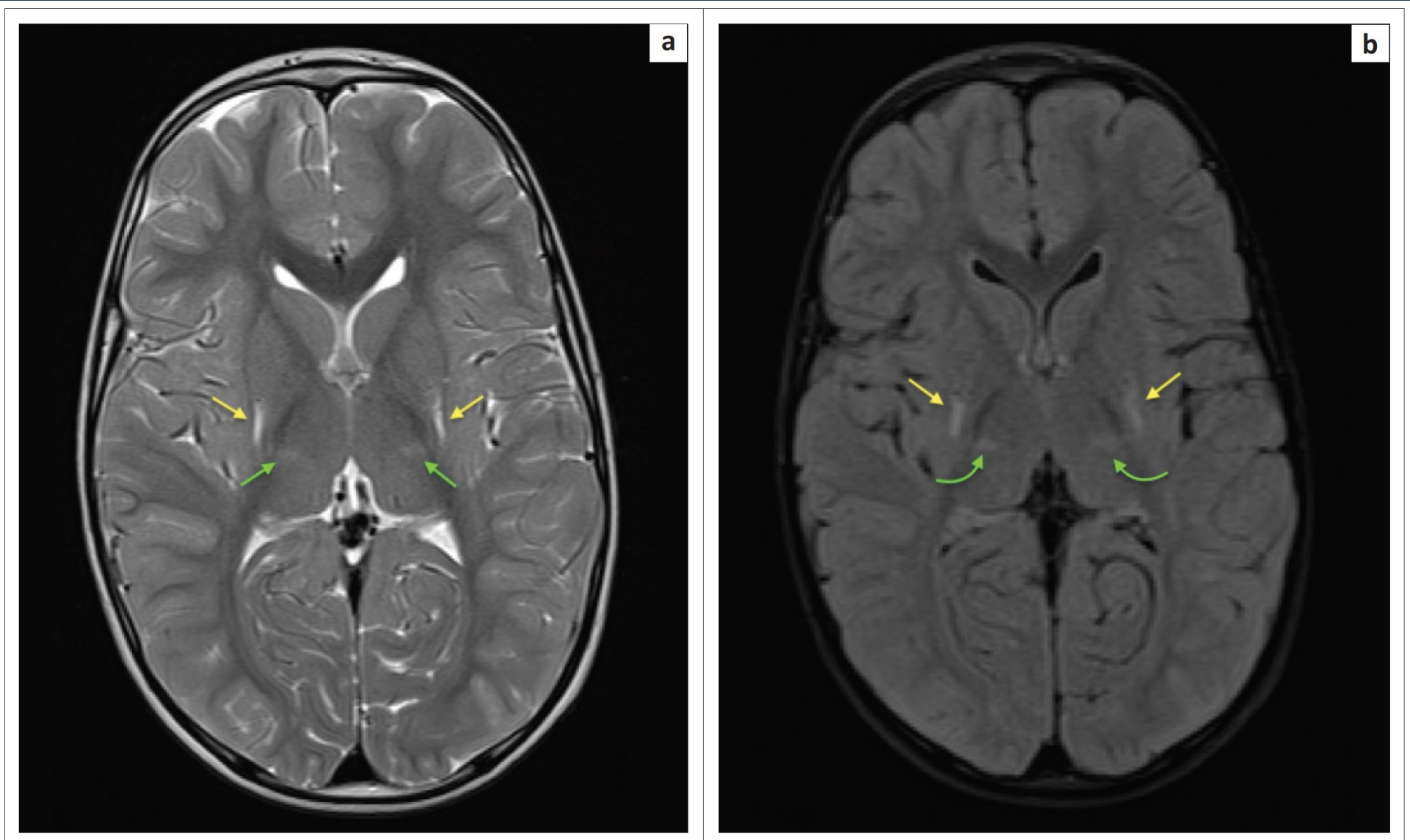
Misser SK, Barkovich AJ, Lotz JW, Archary M. A pictorial review of the pathophysiology and classification of the magnetic resonance imaging patterns of perinatal term hypoxic ischemic brain injury – What the radiologist needs to know… S Afr J Rad. 2020;24(1), a1915. https://doi.org/10.4102/sajr.v24i1.1915

FIGURE 9: Four-year-old male child with cerebral palsy. Neonatal history of hypoxic ischemic brain injury-related encephalopathy, seizures, requiring ventilation and prolonged 4 week stay in ICU. (a) An axial T2-weighted sequence and (b) an axial FLAIR sequence image showing subtle flame shaped dorsal putaminal (yellow arrows) hyperintensity and smudge-like ventral thalamic (green arrows) hyperintensity bilaterally.
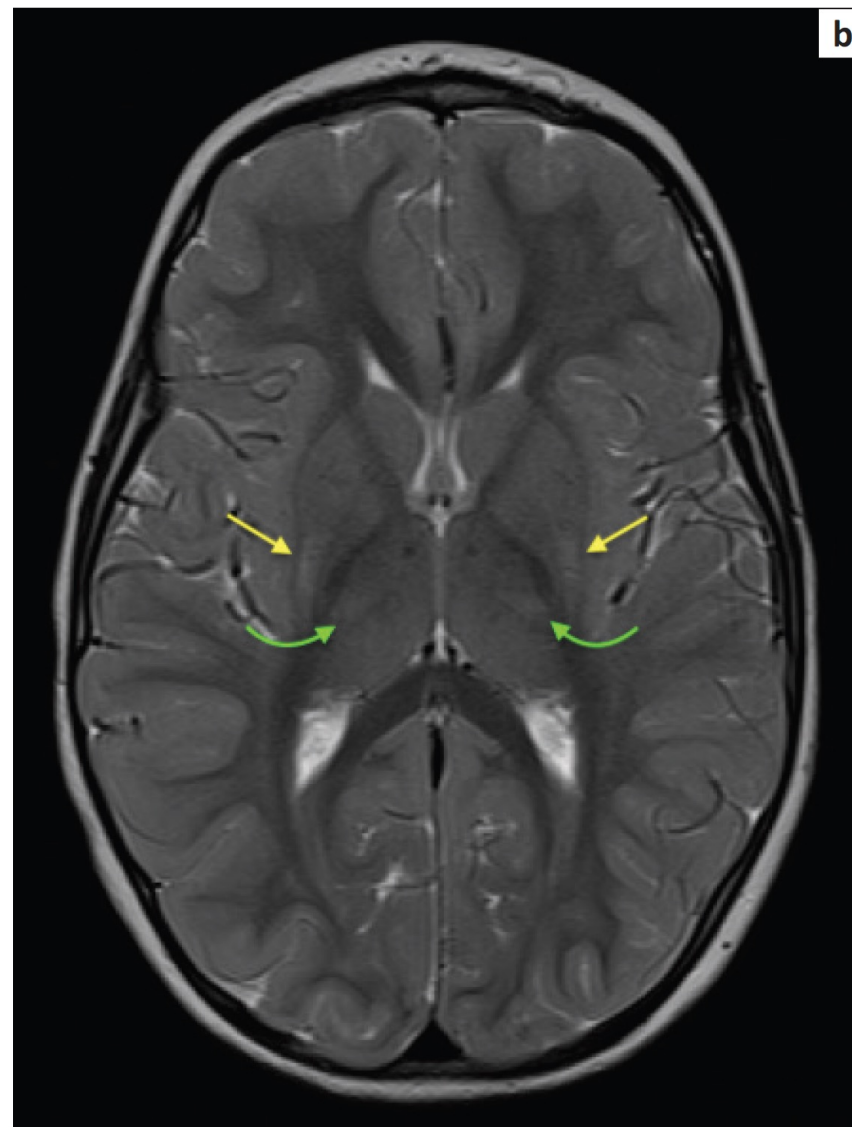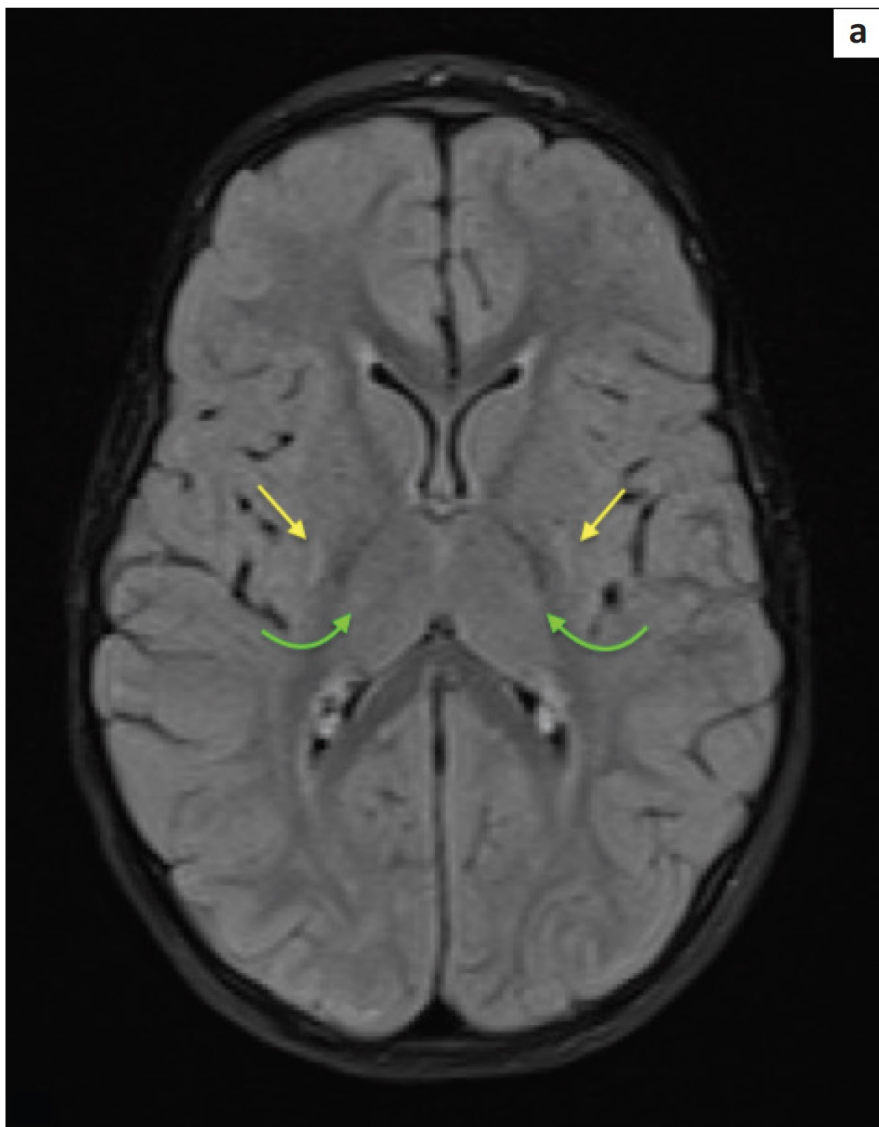
Misser SK, Barkovich AJ, Lotz JW, Archary M. A pictorial review of the pathophysiology and classification of the magnetic resonance imaging patterns of perinatal term hypoxic ischemic brain injury – What the radiologist needs to know… S Afr J Rad. 2020;24(1), a1915. https://doi.org/10.4102/sajr.v24i1.1915

FIGURE 10: A 2-year-old female child with dystonic cerebral palsy. (a) An axial FLAIR sequence image and (b) an axial T2-weighted image demonstrating even more subtle signal abnormalities at the dorsal putamina (yellow arrows) and ventral thalami (green arrows). These changes can be very difficult to detect and may be omitted by the unsuspecting reporter.
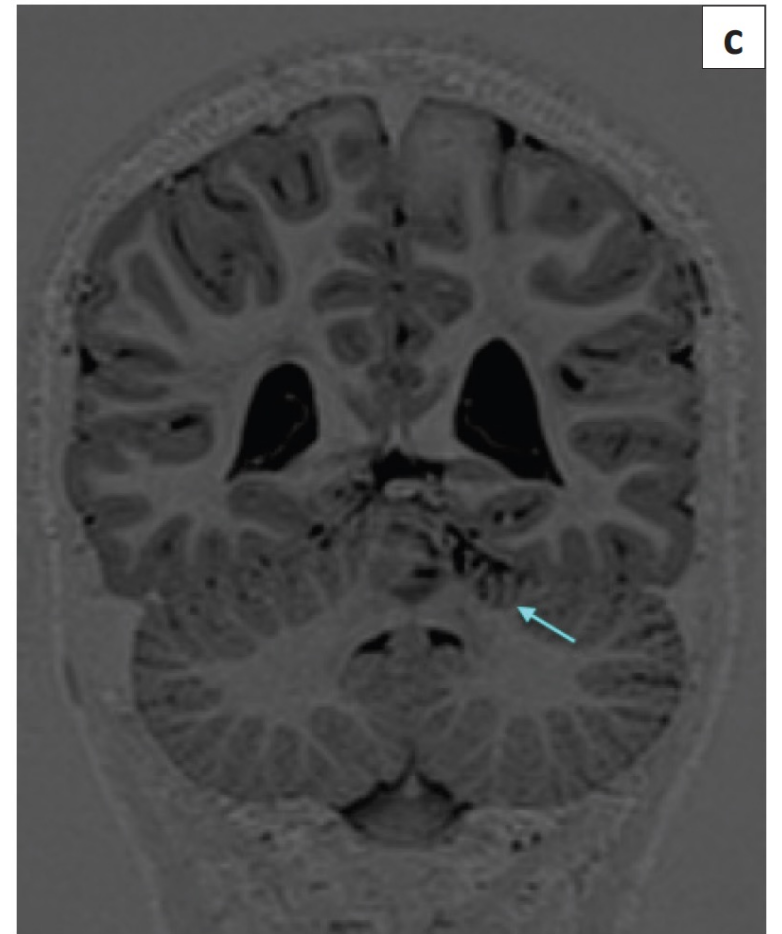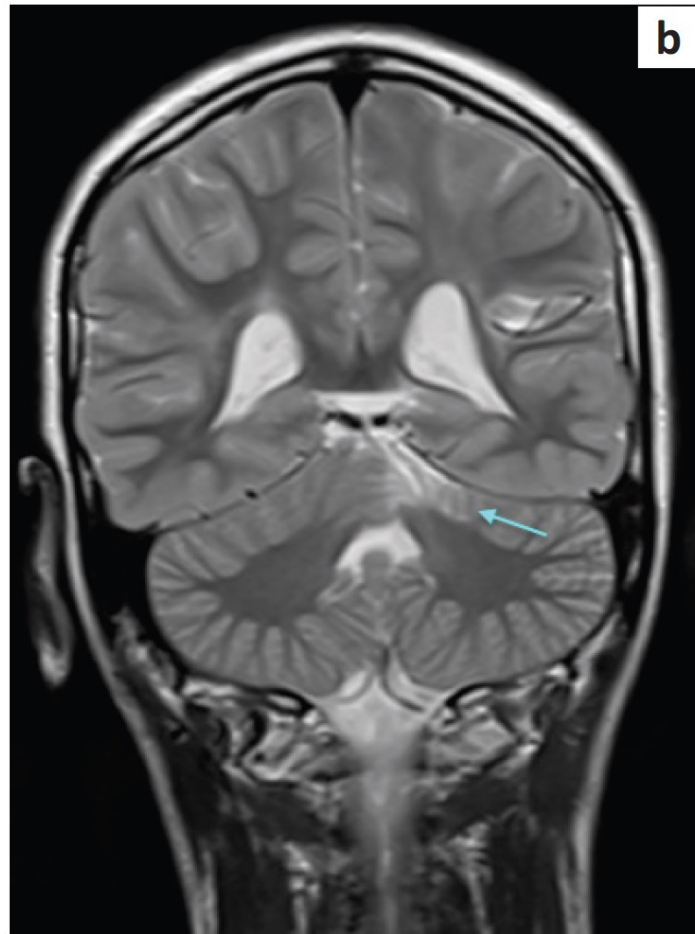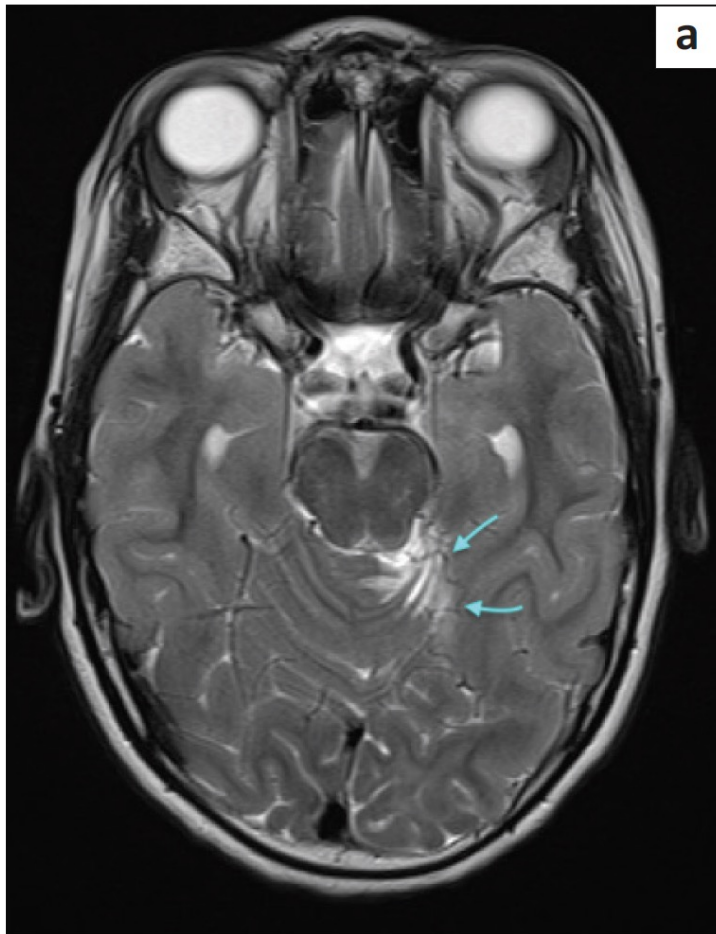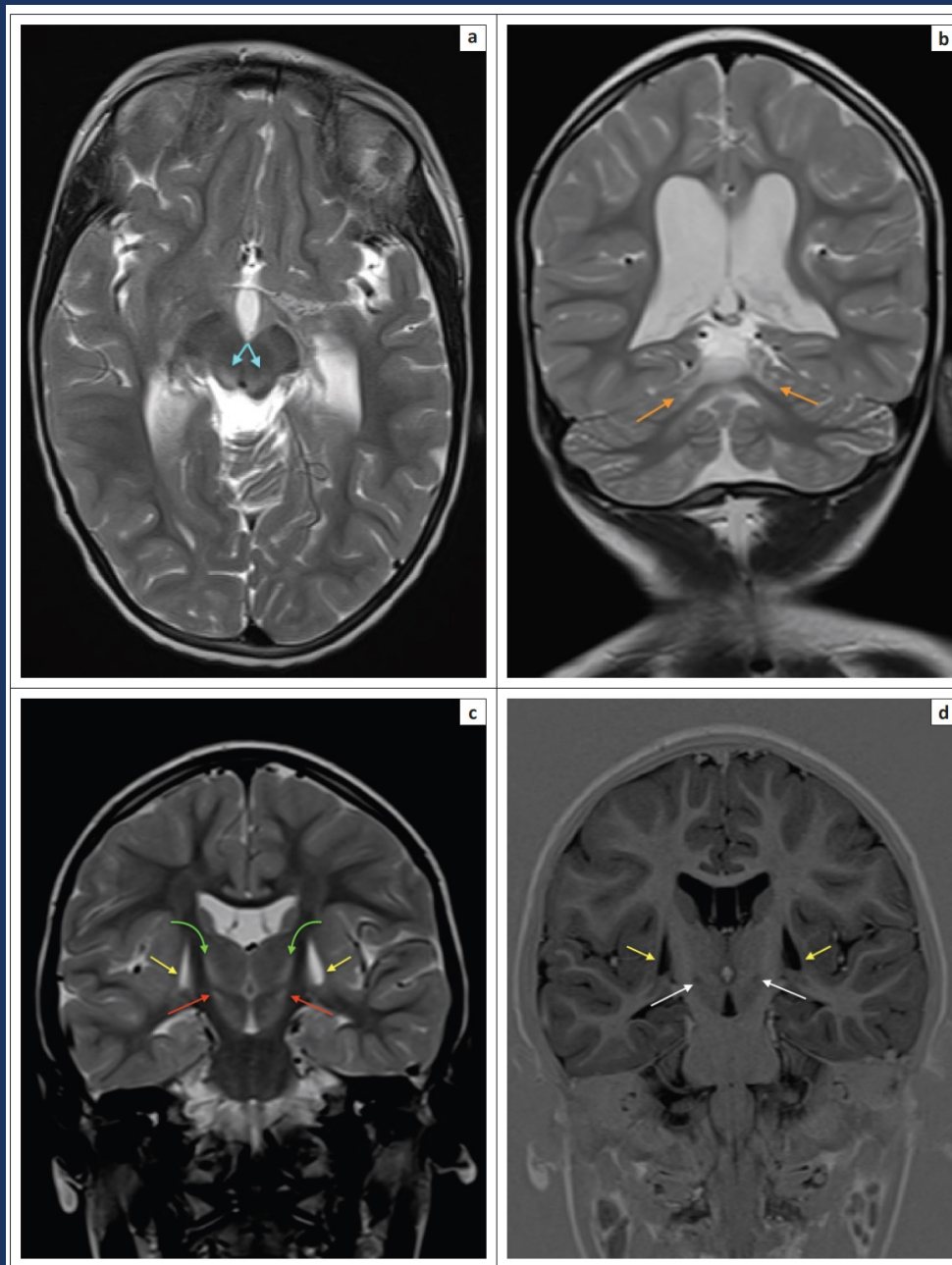
Misser SK, Barkovich AJ, Lotz JW, Archary M. A pictorial review of the pathophysiology and classification of the magnetic resonance imaging patterns of perinatal term hypoxic ischemic brain injury – What the radiologist needs to know... S Afr J Rad. 2020;24(1), a1915. https://doi.org/10.4102/sajr.v24i1.1915

FIGURE 11: A 9-year-old male child who suffered grade 3 hypoxic ischemic brain injury with Apgar scores of zero at 1 min and 7 at 5 min. (a) An axial T2-weighted, (b) a coronal T2-weighted and (c) a coronal inversion recovery (IR) sequence image demonstrating the left superior cerebellar cortex injury (cyan blue arrows) with localised atrophy involving the left half of the quadrangular lobule. This is an important review area, as in this case, the injury was omitted by the first reporter.

FIGURE 12: (a) and (b) are T2-weighted images in a 3-year-old female child with acute profound HIBI. (a) Dorsal midbrain tegmentum (cyan blue arrows) signal changes and (b) superior cerebellar (orange arrows) injury. (c) and (d) are coronal T2-weighted and IR sequences in a 7-year-old female child who presents with dyskinetic cerebral palsy after grade 2 hypoxic ischemic encephalopathy. (c) Hyperintensity at the subthalamic nucleus (red arrows) of the upper midbrain and (d) corresponding low signal intensity (white arrows) extending close to the periaqueductal gray (yellow arrows indicate putamen and green arrows indicate thalamus).

Misser SK, Barkovich AJ, Lotz JW, Archary M. A pictorial review of the pathophysiology and classification of the magnetic resonance imaging patterns of perinatal term hypoxic ischemic brain injury – What the radiologist needs to know... S Afr J Rad. 2020;24(1), a1915. https://doi.org/10.4102/sajr.v24i1.1915
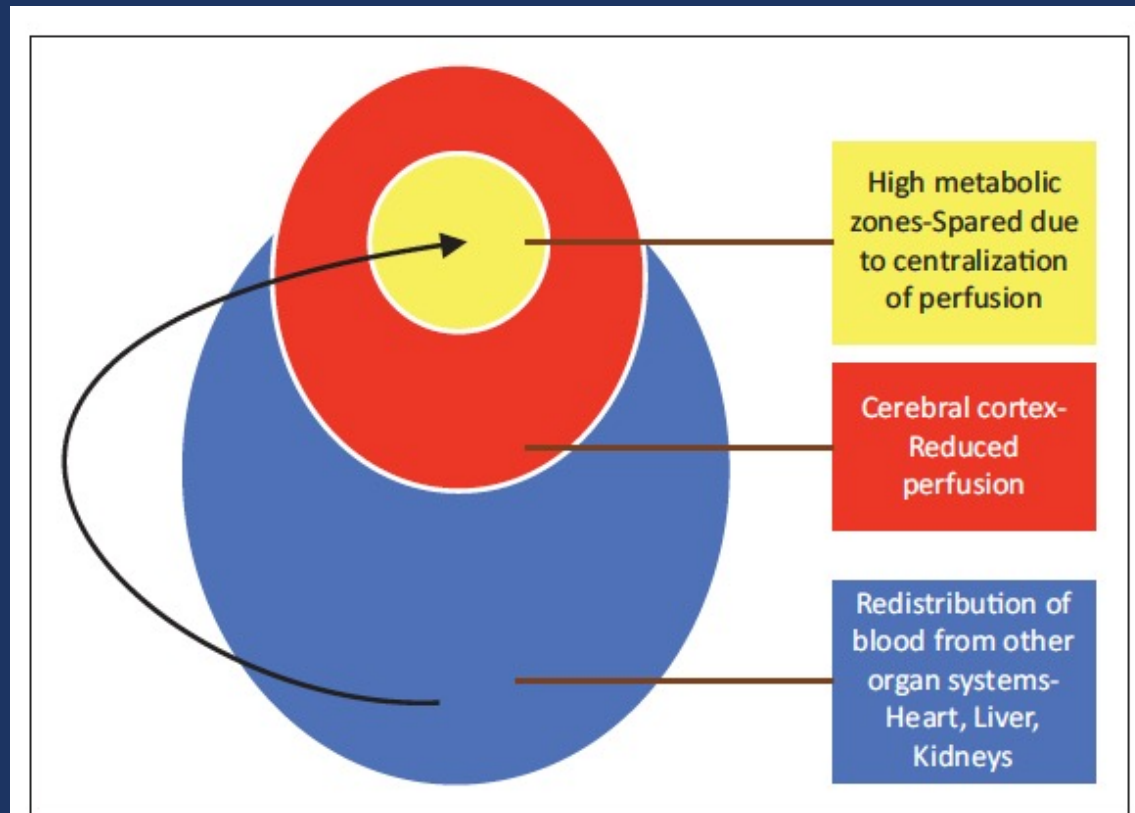
FIGURE 13: Diagrammatic representation of the redistribution of blood away from the visceral organ systems and cerebral cortex in favour of the most important central brain structures.
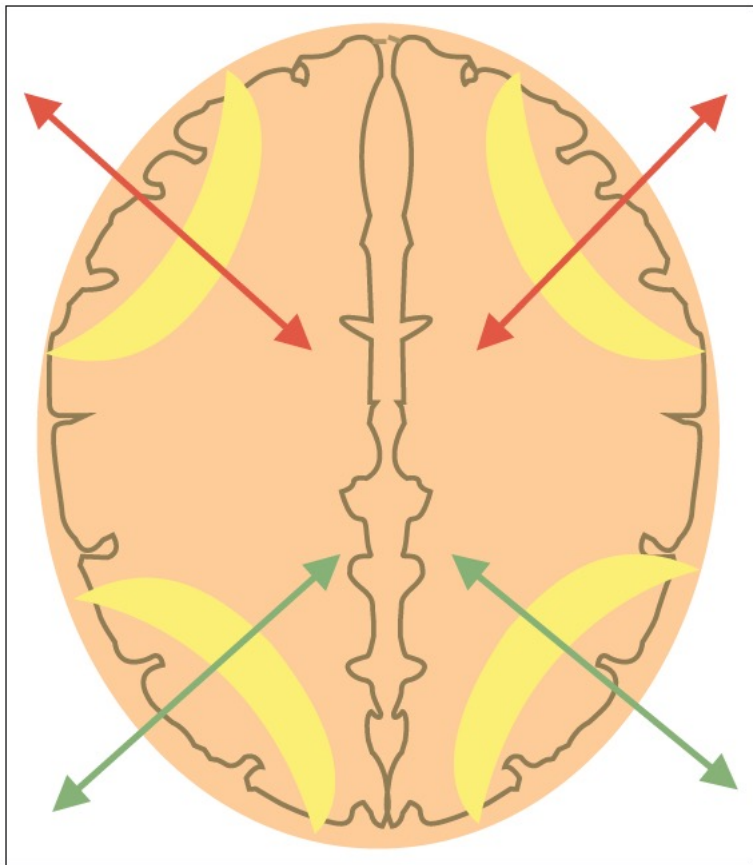
Misser SK, Barkovich AJ, Lotz JW, Archary M. A pictorial review of the pathophysiology and classification of the magnetic resonance imaging patterns of perinatal term hypoxic ischemic brain injury – What the radiologist needs to know… S Afr J Rad. 2020;24(1), a1915. https://doi.org/10.4102/sajr.v24i1.1915

FIGURE 14: Schematic representation of the interarterial external watershed regions (depicted in yellow overlay) at the centrum ovale. The red arrows indicate the border zone between anterior cerebral artery and middle cerebral artery territories. The green arrows indicate the border zone between middle cerebral artery and posterior cerebral artery territories.
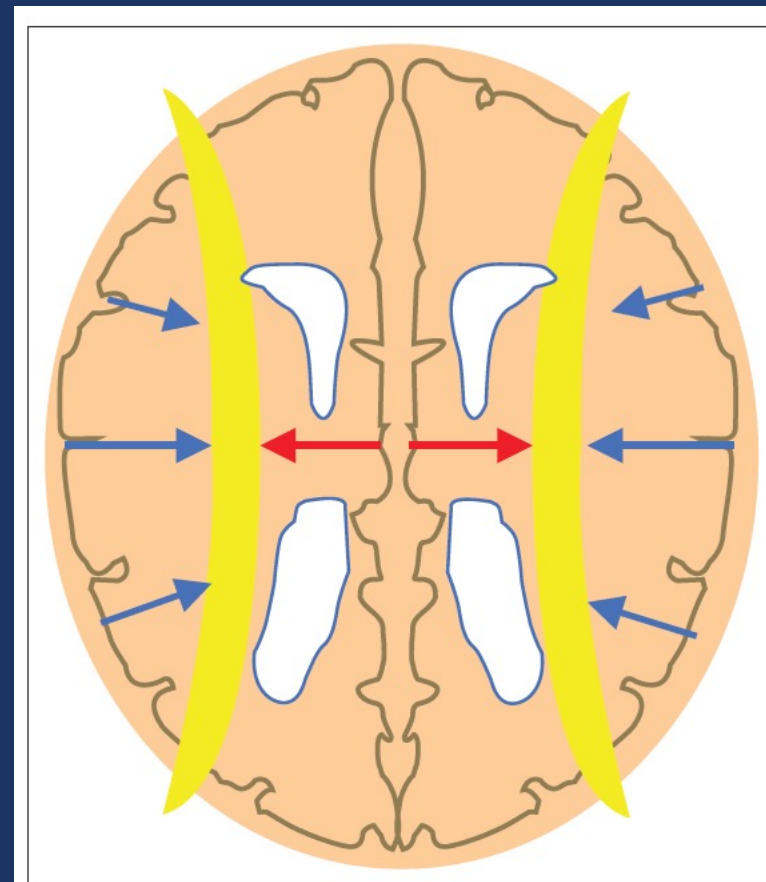
FIGURE 15: Schematic representation of the internal watershed regions (depicted in yellow overlay). The red arrows indicate the susceptible junction zones of the ventriculofugal vessels coursing away from the ventricles and ventriculopetal vessels coursing inward from the cortex (blue arrows).
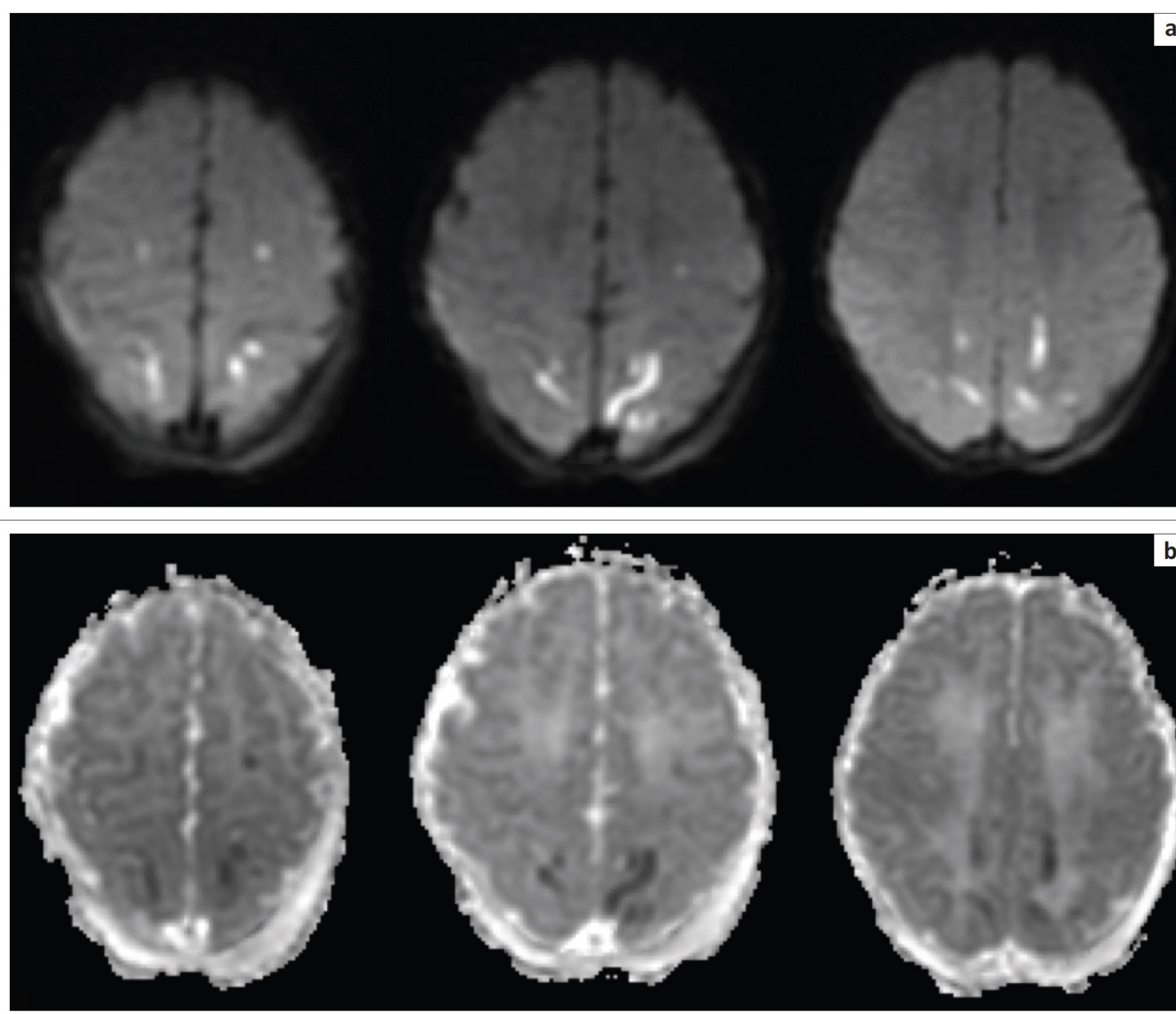
Misser SK, Barkovich AJ, Lotz JW, Archary M. A pictorial review of the pathophysiology and classification of the magnetic resonance imaging patterns of perinatal term hypoxic ischemic brain injury – What the radiologist needs to know... S Afr J Rad. 2020;24(1), a1915. https://doi.org/10.4102/sajr.v24i1.1915

FIGURE 16: A 2-day-old baby boy presenting with grade 2 hypoxic ischemic brain injury. (a) The diffusion B-1000 trace sequences and (b) the corresponding ADC maps at each level. There are focal areas of restricted diffusion involving the parasagittal watershed zones of both cerebral hemispheres.
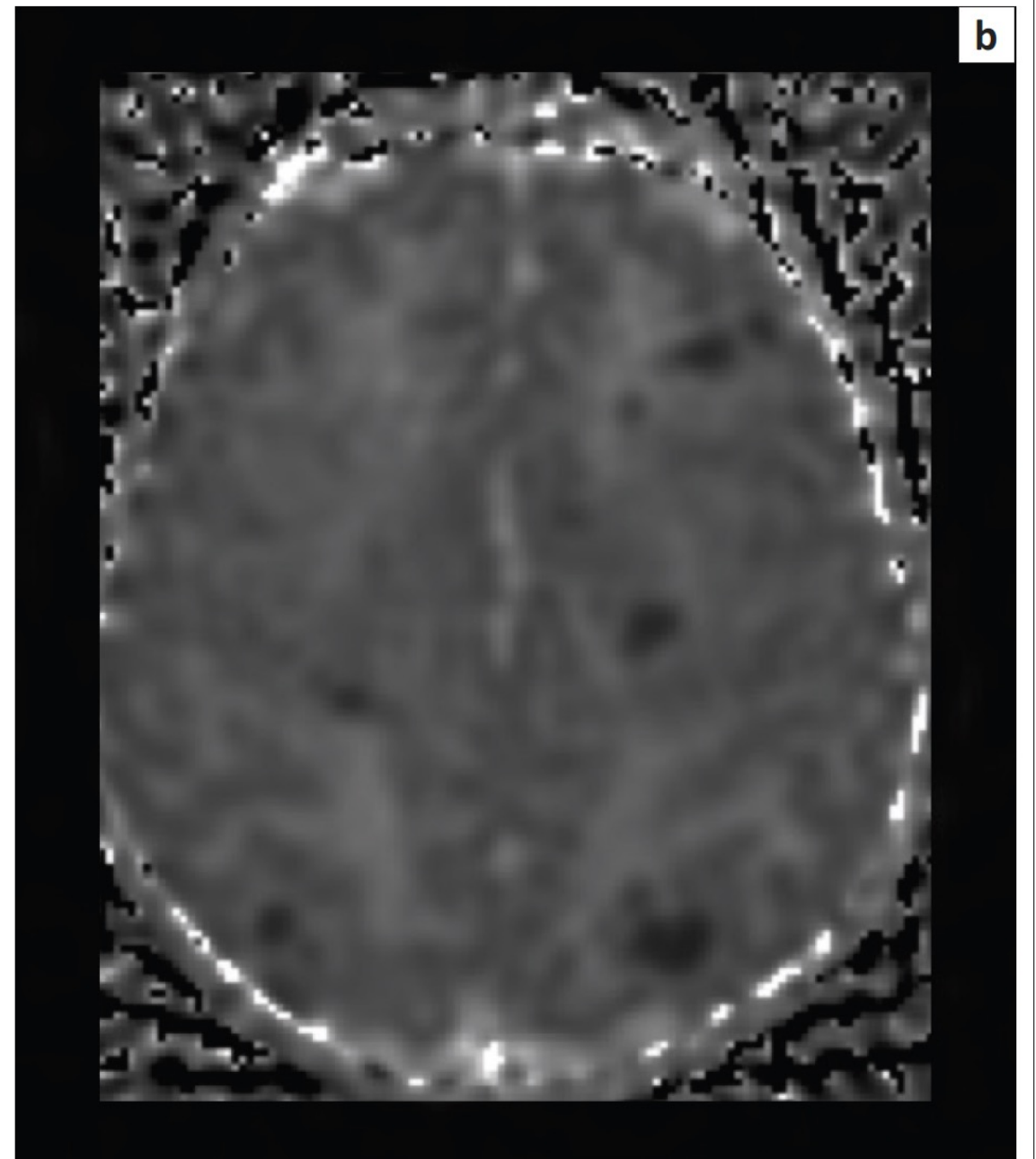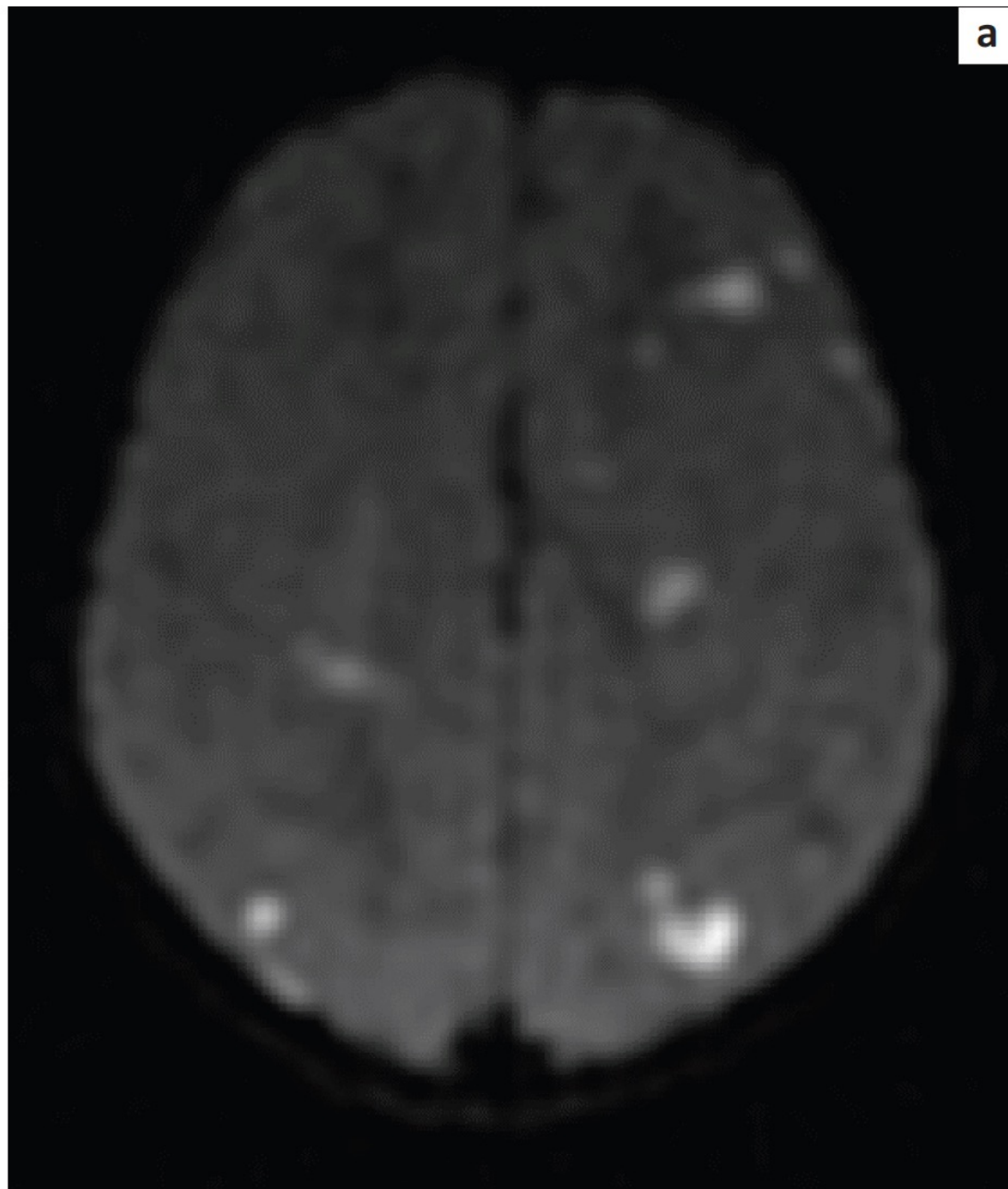
Misser SK, Barkovich AJ, Lotz JW, Archary M. A pictorial review of the pathophysiology and classification of the magnetic resonance imaging patterns of perinatal term hypoxic ischemic brain injury – What the radiologist needs to know... S Afr J Rad. 2020;24(1), a1915. https://doi.org/10.4102/sajr.v24i1.1915

FIGURE 17: A 3-day-old baby boy with neonatal seizures after grade 2 neonatal hypoxic ischemic brain injury. (a) The diffusion B-1000 trace sequence and (b) the corresponding ADC map. Note that the watershed territory involvement in this child is asymmetric, and this is often seen in partial prolonged ischemia subtype.
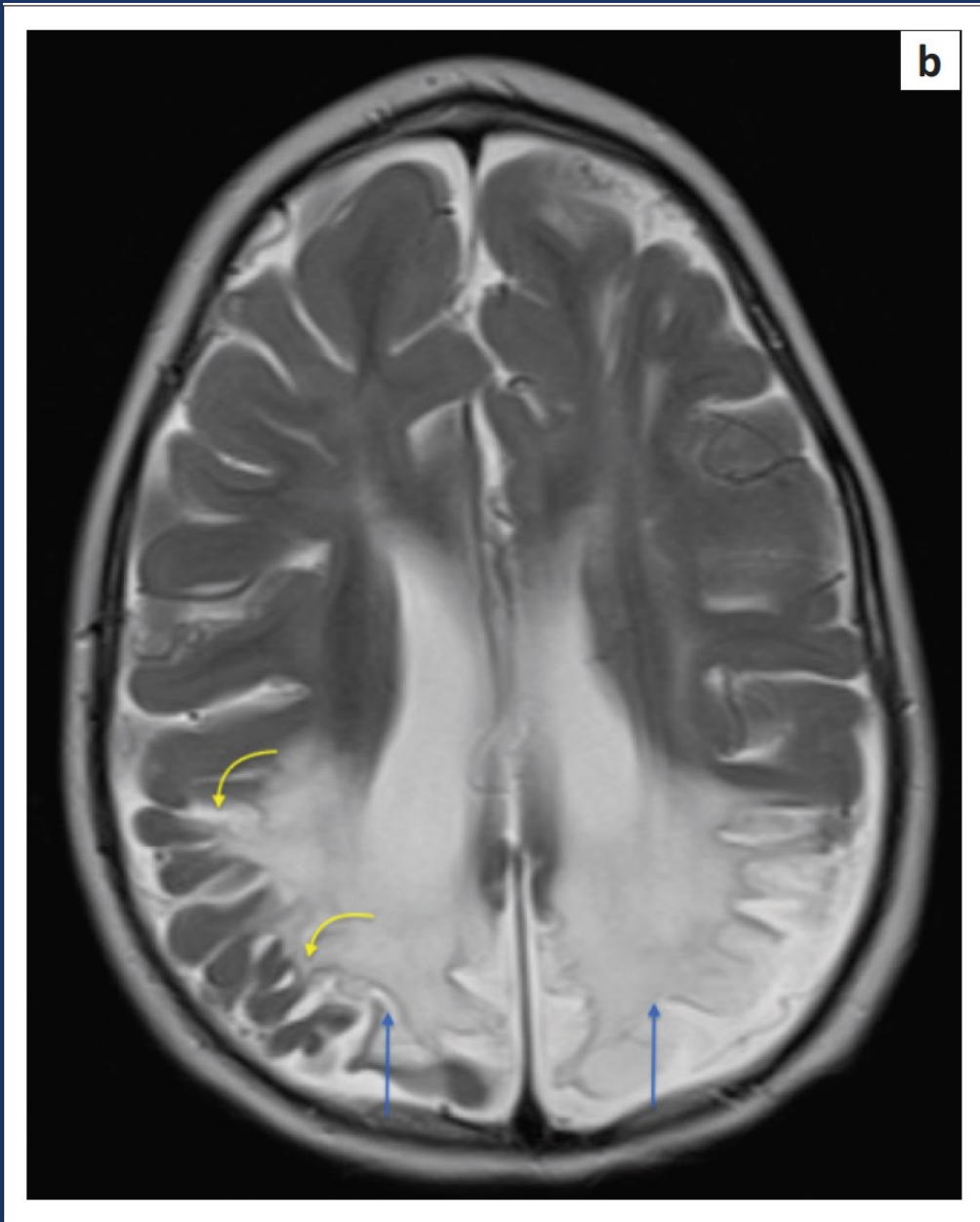
Pearls of imaging…

Bilateral medial frontal, parietal and occipital watershed injuries may be asymmetric.

Look out for mushroom-shaped gyri of the ulegyria phenomenon.

Note secondary features of corpus callosum thinning and ex vacuo dilatation of ventricles.
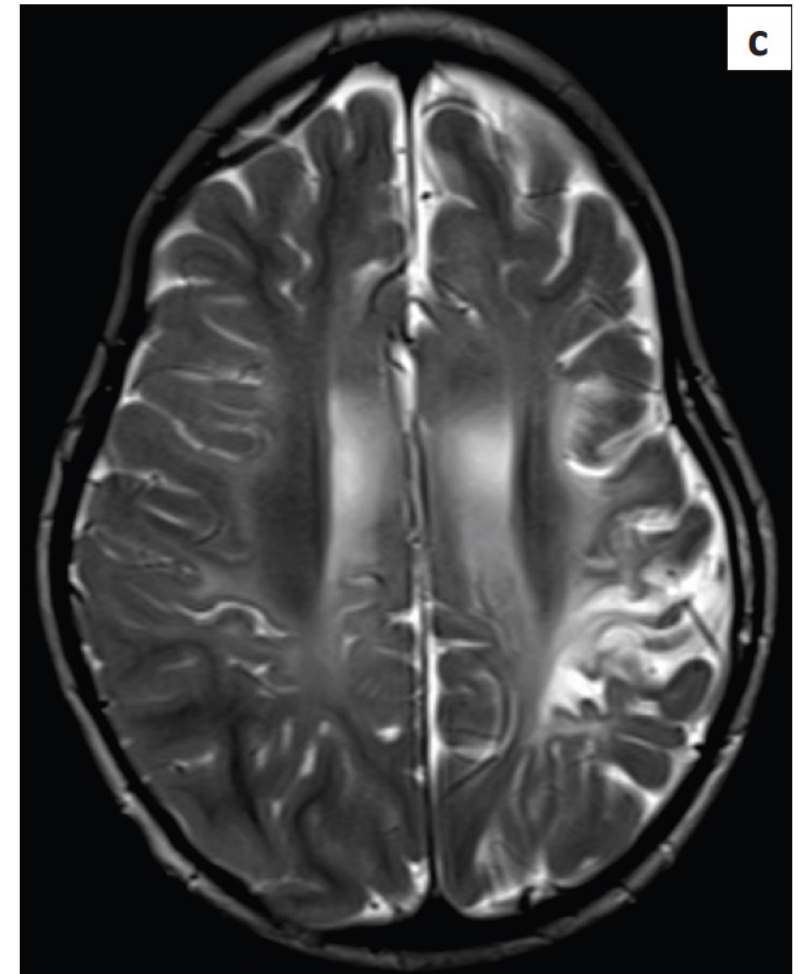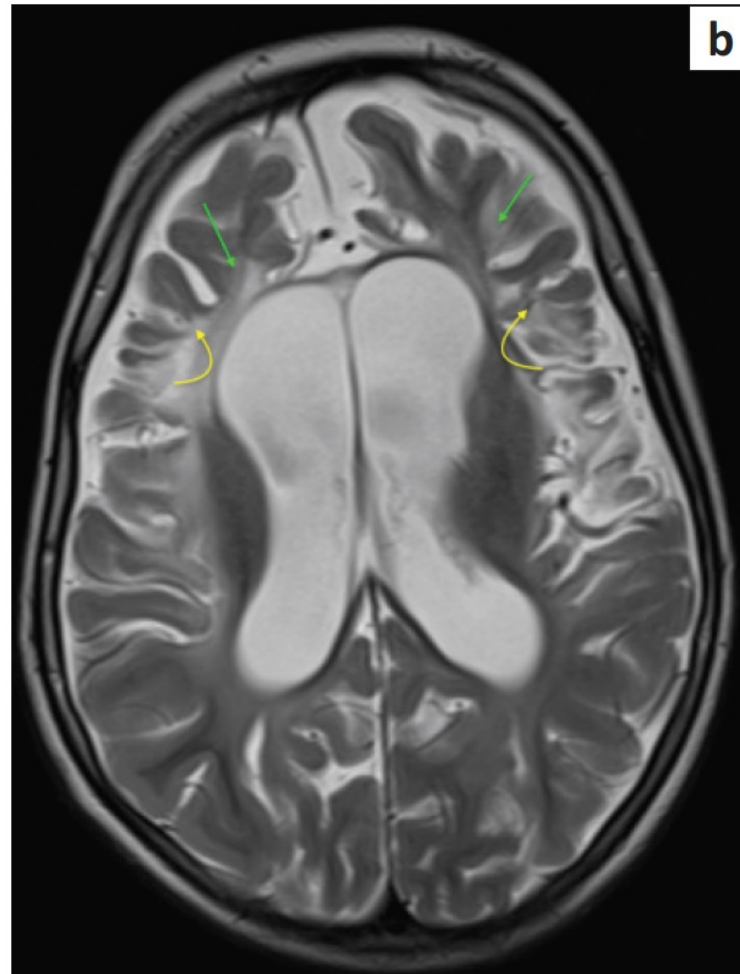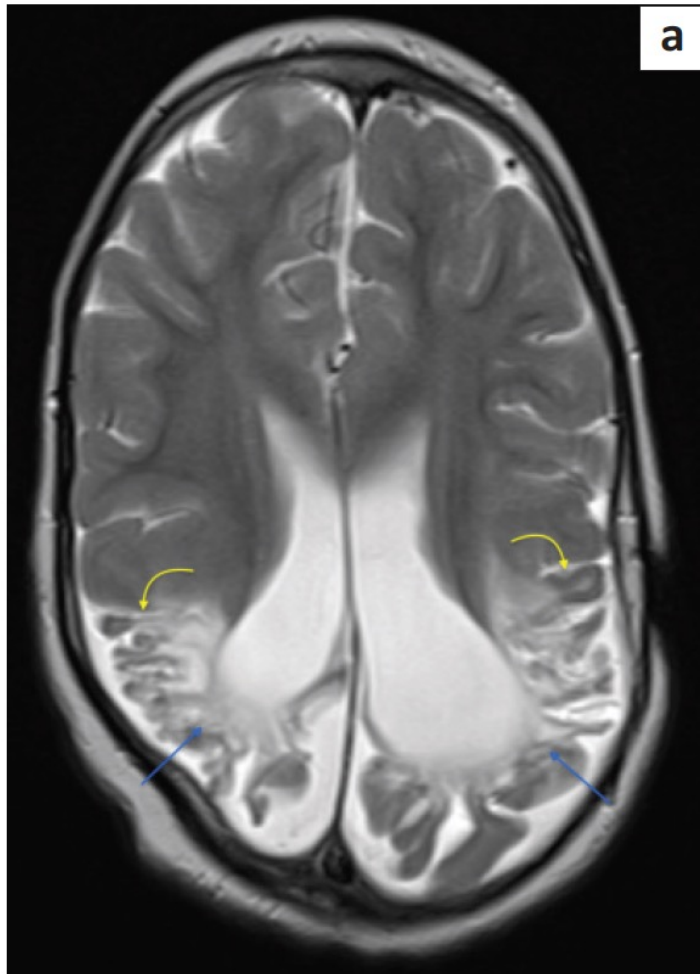
FIGURE 19: Axial T2-weighted magnetic resonance images demonstrating severe post-hypoxic injury because of partial prolonged ischemia in three different patients. Note the spongiosis of the parietal lobes (blue arrows) (a) and frontal lobes (green arrows) (b) associated with ulegyria (yellow arrows) and secondary ventriculomegaly. (c) The level of centrum ovale demonstrating asymmetric hypoxic ischemic brain injury changes, greater in the left frontal and parietal lobes. This latter pattern of asymmetric involvement is not an uncommon finding.

Misser SK, Barkovich AJ, Lotz JW, Archary M. A pictorial review of the pathophysiology and classification of the magnetic resonance imaging patterns of perinatal term hypoxic ischemic brain injury – What the radiologist needs to know… S Afr J Rad. 2020;24(1), a1915. https://doi.org/10.4102/sajr.v24i1.1915
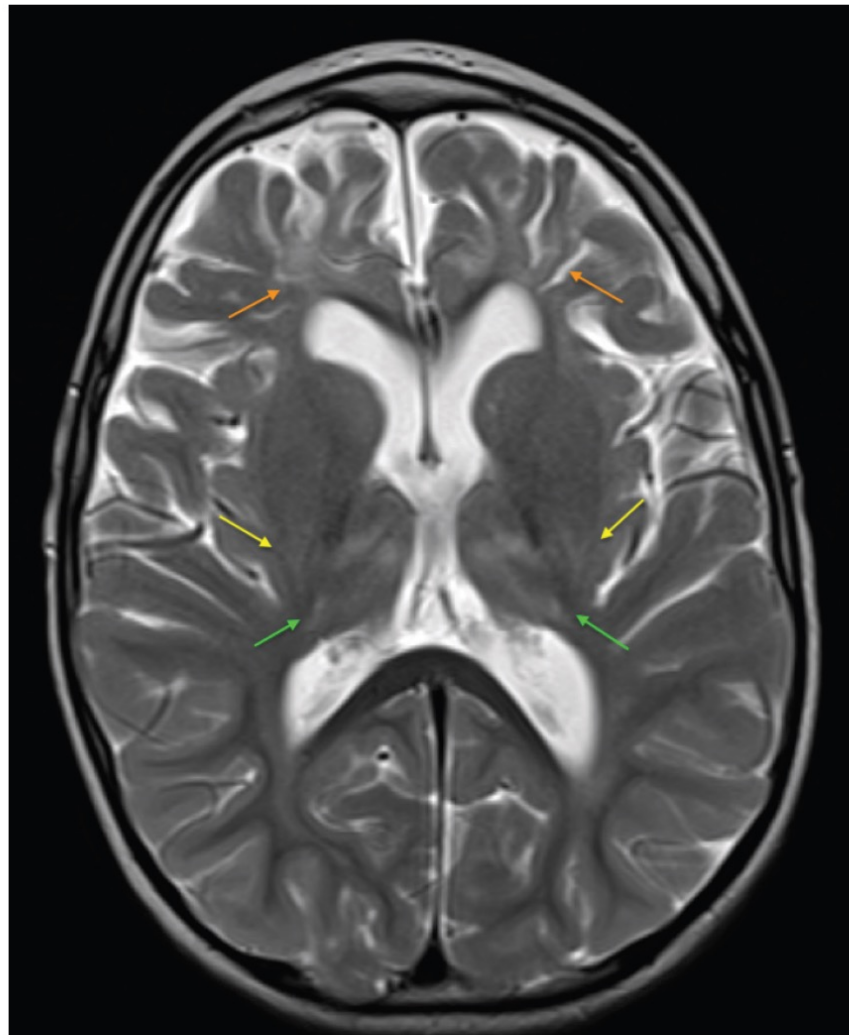
Mixed pattern

FIGURE 24: Axial T2-weighted image at the level of the basal nuclei performed on a 7-year-old male child. There is bifrontal encephalomalacia involving the middle and inferior frontal gyri (orange arrows) with ulegyria. Subtle hyperintensity is present at the posterior tips of the putamina (yellow arrows). Note in addition, loss of volume and more extensive hyperintensity of both thalami (green arrows). The combination is indicative of a mixed pattern of cerebral injury.
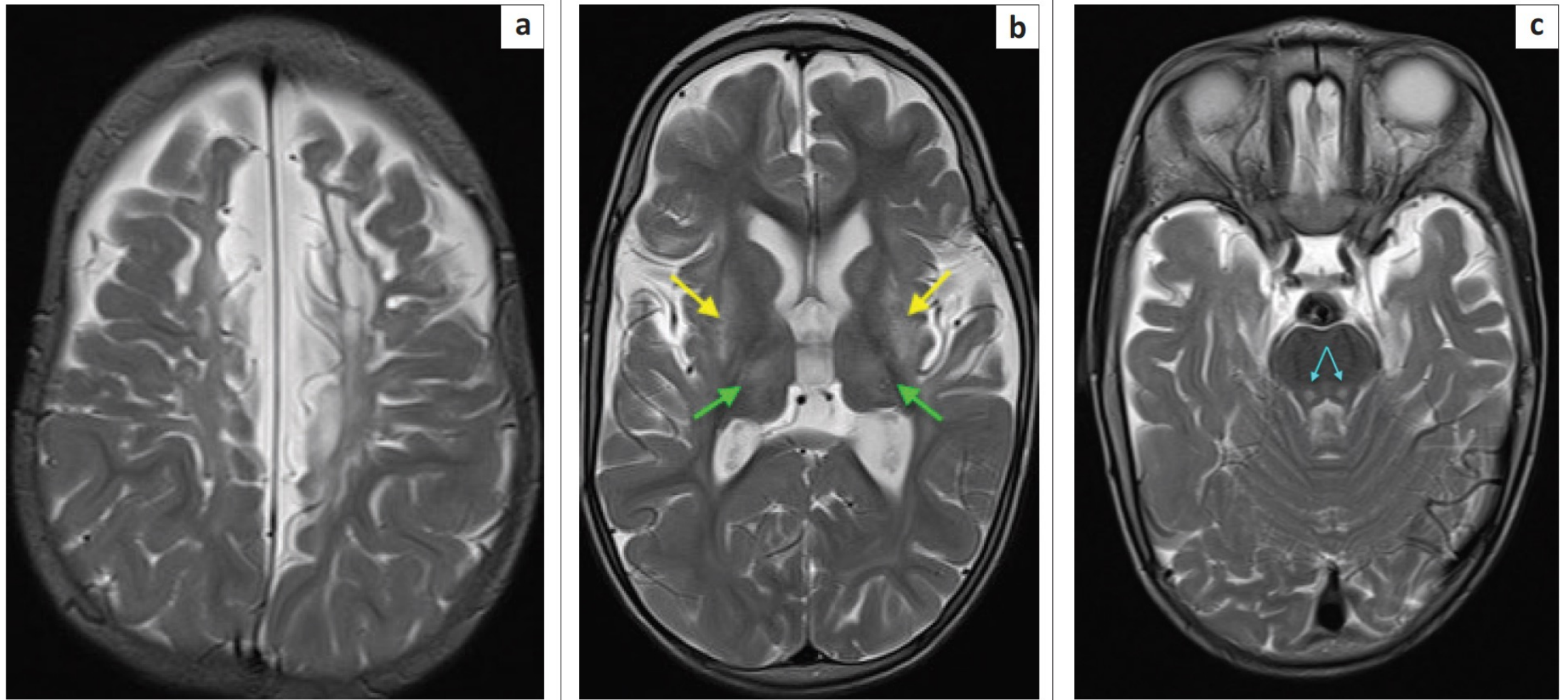
FIGURE 22: A 2-year-old male child with severe mixed type hypoxic ischemic brain injury. T2-weighted axial images (a) at the level of the centrum ovale demonstrating parasagittal frontal lobe injury with atrophy beyond the central sulcus and paracentral lobule, involving the superior frontal gyri with ulegyria, (b) at the level of the basal ganglia shows the hyperintense signal change at the dorsal putamina (yellow arrows) and ventral thalami (green arrows) and (c) at the level of the superior cerebellar peduncles reveals prominent central tegmental tract (cyan blue arrows) hyperintensity at the dorsum of the pons.
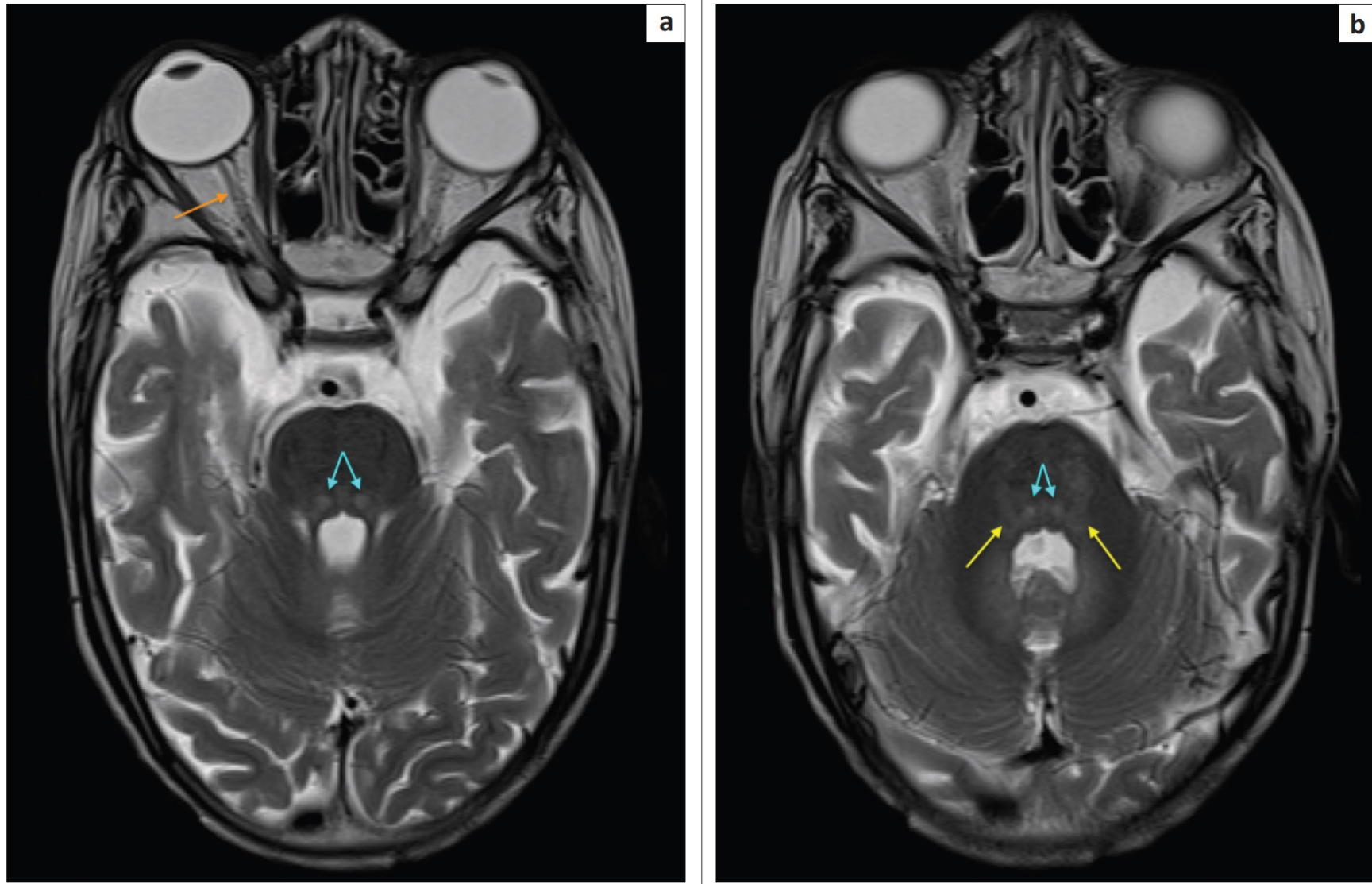
FIGURE 23: A 7-year-old male child with mixed subtype hypoxic ischemic brain injury. Axial T2-weighted sequence images through the midbrain and pons show dorsal tegmental (yellow arrows) and central tegmental tract (cyan blue arrows) hyperintensity. Note severe cerebral atrophy and optic atrophy (orange arrows).
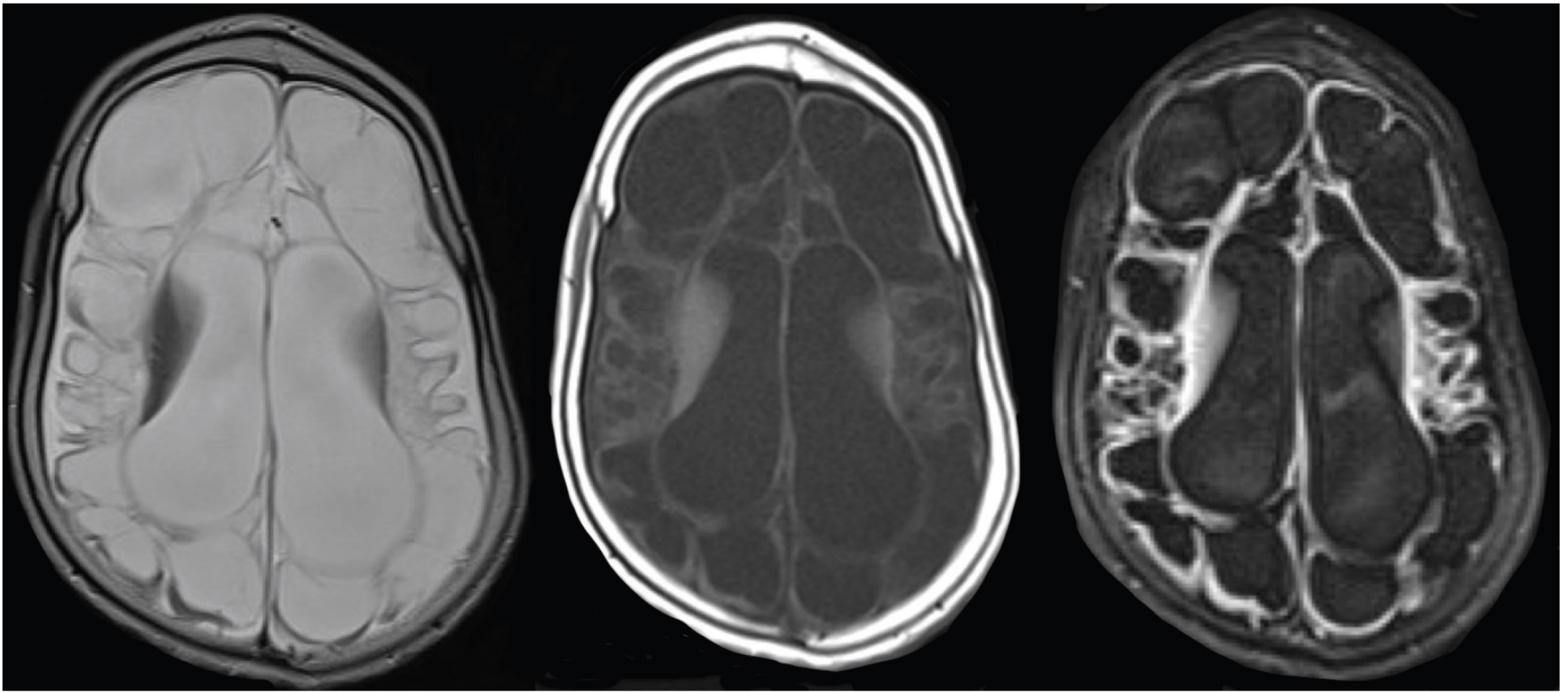
FIGURE 25: A 3-year-old male child with spastic cerebral palsy and blindness. Recorded neonatal encephalopathy with low Apgar scores and neonatal seizures. Axial T2-weighted, T1-weighted and FLAIR sequence images show extensive cerebral destruction with grey and white matter injury, cystic encephalomalacia and ex vacuo dilatation of the lateral ventricles.
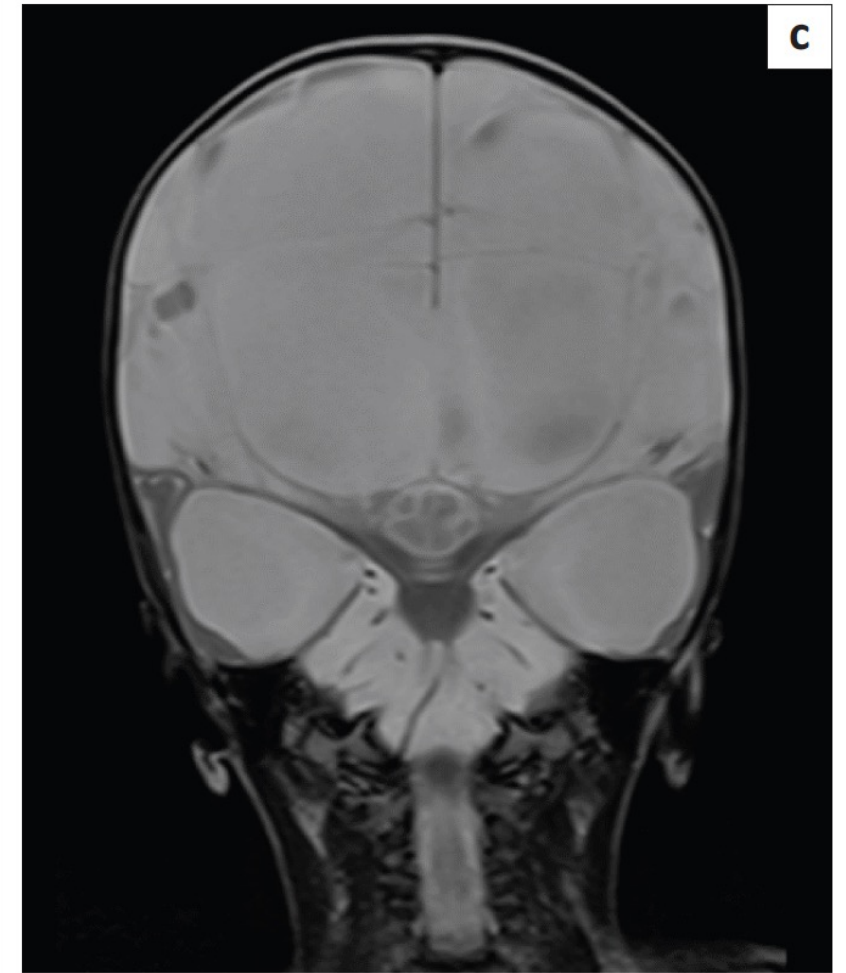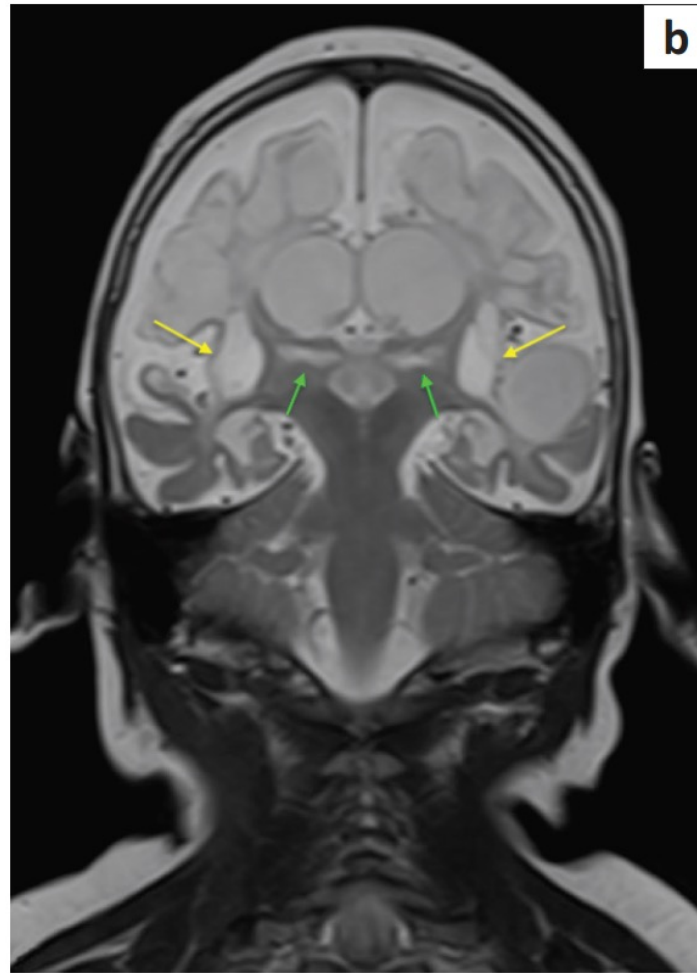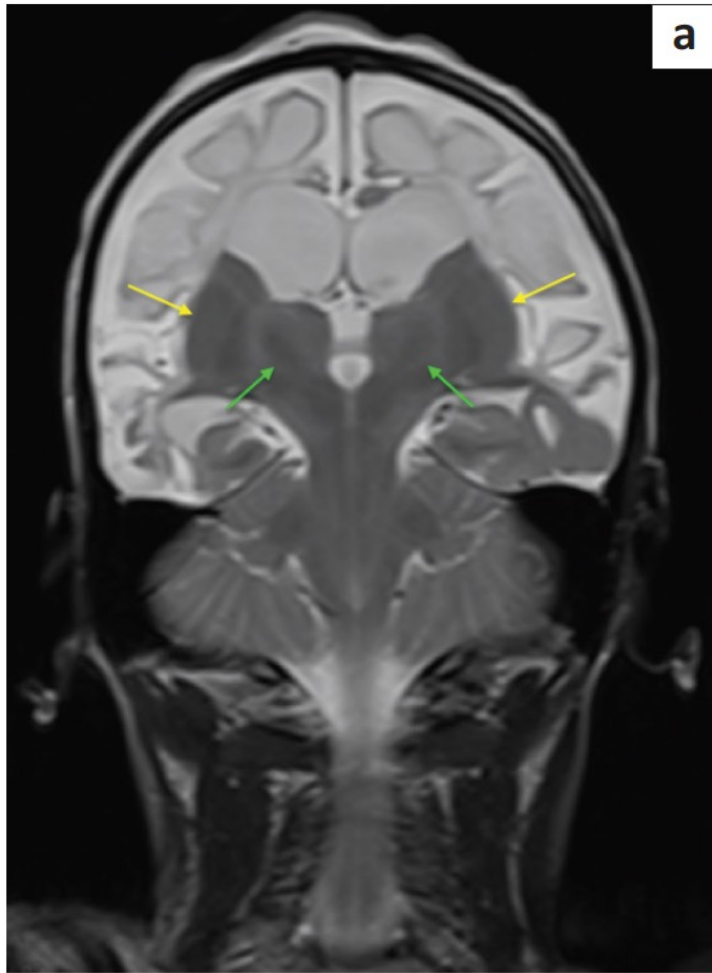
FIGURE 26: The spectrum of basal ganglia involvement in association with cystic encephalomalacia shown on coronal T2-weighted images in three children. (a) A 4-year-old female child with complete sparing of the basal ganglia, thalami and cerebellum. (b) A 2-year-old male child with necrosis of the putamen (yellow arrows) and ventral thalamus (green arrows) bilaterally. (c) A 4-year-old-male child who suffered severe total anoxia related to abruptio placentae, with birth weight of 3.35 kg and Apgar scores of 1/10 and 3/10. Note near-complete cerebral cystic encephalomalacia, atrophy of lentiform nuclei and severe thalamic destruction.
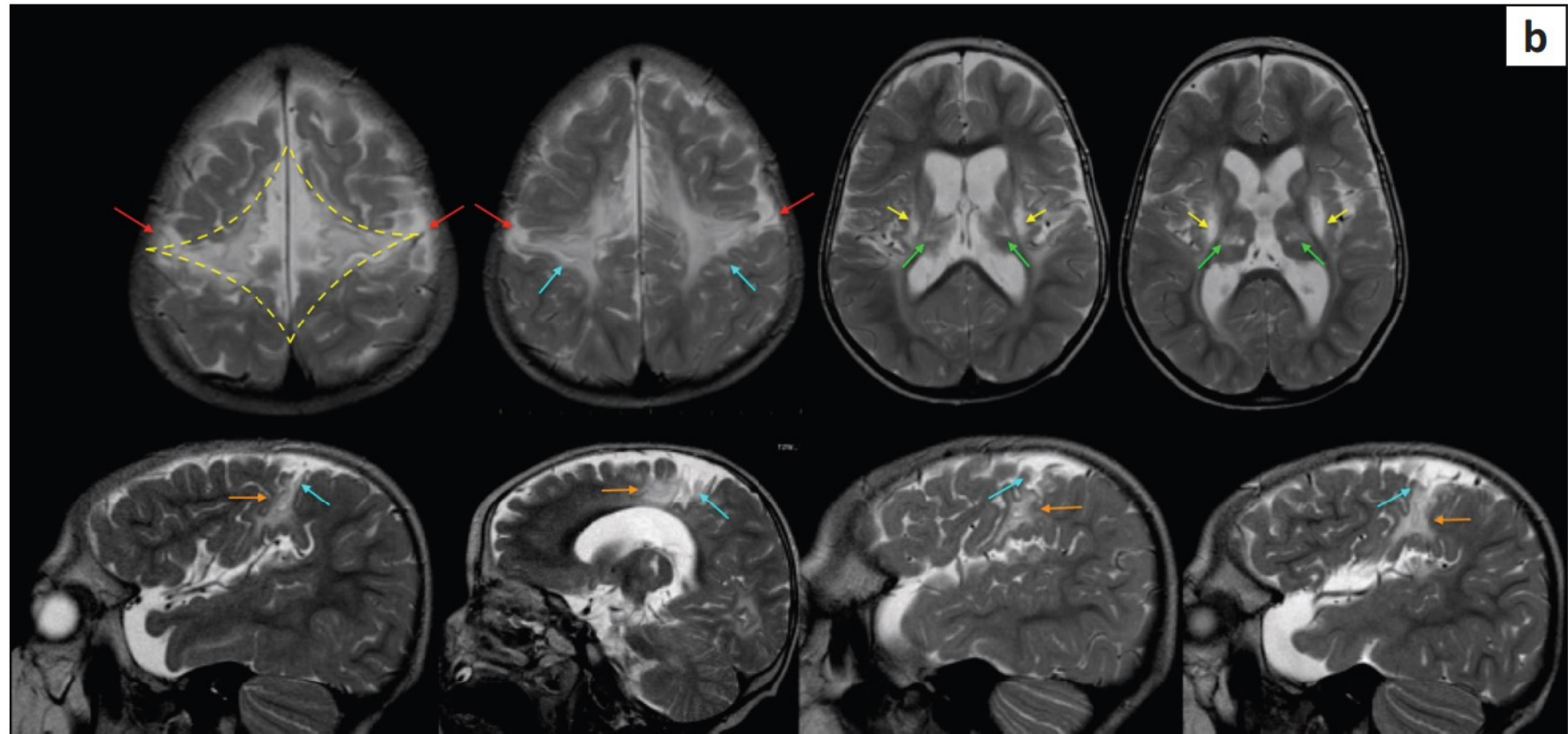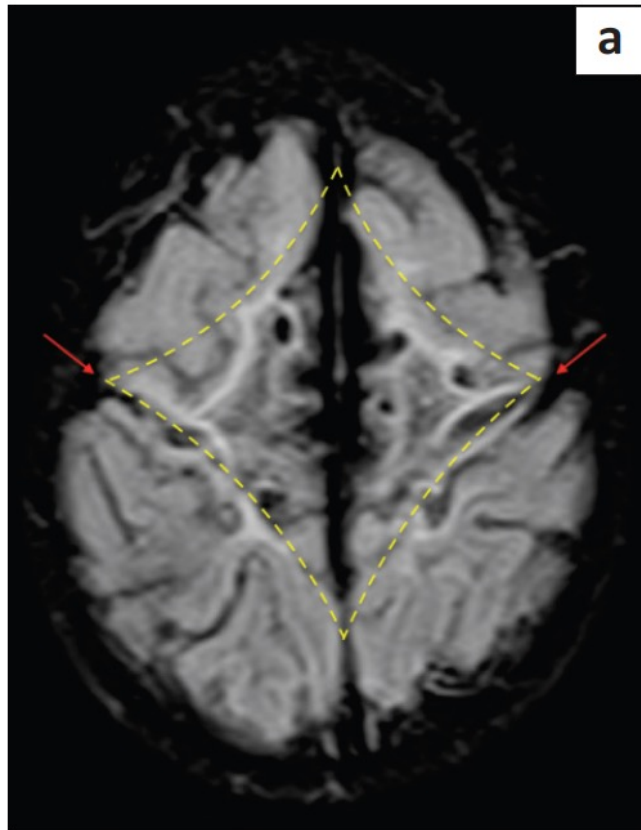
Misser SK, Barkovich AJ, Lotz JW, Archary M. A pictorial review of the pathophysiology and classification of the magnetic resonance imaging patterns of perinatal term hypoxic ischemic brain injury – What the radiologist needs to know... S Afr J Rad. 2020;24(1), a1915. https://doi.org/10.4102/sajr.v24i1.1915

FIGURE 20: Two examples of parasagittal cerebral injury in children who suffered sentinel events of placental abruption leading to acute profound ischemia (API). (a) This figure shows a diamond-shaped expansion of the frontoparietal parasagittal surface convexity, widening the interhemispheric fissure and tapering bilaterally at the far edge of each central sulcus (red arrows). (b) This figure reveals similar broadening of the extra-axial space because of parasagittal cortex and paracentral lobule injury. Note the contiguous corticospinal tract Wallerian degeneration (orange arrows), the subsiding centrum ovale scaffold (cyan blue arrows) as well as API-related basal ganglia (yellow arrows) and thalamic (green arrows) injury.

Misser SK, Barkovich AJ, Lotz JW, Archary M. A pictorial review of the pathophysiology and classification of the magnetic resonance imaging patterns of perinatal term hypoxic ischemic brain injury – What the radiologist needs to know… S Afr J Rad. 2020;24(1), a1915. https://doi.org/10.4102/sajr.v24i1.1915

HYPOXIC – ISCHEMIC BRAIN INJURY

Research Plan

* Categorise the patterns

* Classify the central patterns

        Identified a new undescribed pattern

* Classify the watershed patterns

        Identified a biomarker for HIBI in watershed patterns

* Other aspects

Insights into Imaging

ORIGINAL ARTICLE

Open Access

A proposed magnetic resonance imaging grading system for the spectrum of central neonatal parasagittal hypoxic–ischaemic brain injury

Shalendra Kumar Misser[1,2]*, Jan Willem Lotz[3], Stefan-Dan Zaharie[4], Nobuhle Mchunu[5,6], Moherndran Archary[7] and Anthony James Barkovich[8]

Abstract

Aim: To describe the spectrum of parasagittal injury on MRI studies performed on children following severe perinatal term hypoxia–ischaemia, using a novel MRI grading system, and propose a new central pattern correlated with neuropathologic features.

Methods: MR scans of 297 patients with perinatal term hypoxia–ischaemia were evaluated for typical patterns of brain injury. A total of 83 patients that demonstrated the central/basal ganglia–thalamus and perirolandic pattern of injury were categorised according to the degree of severity. The perirolandic injury was graded by the degree of interhemispheric widening, paracentral lobule involvement and perirolandic cortex destruction leading to a tiered categorisation. Of these 83 patients, 19 had the most severe subtype of injury. A detailed analysis of the clinical data of a subset of 11 of these 19 patients was conducted.

Results: We demonstrated the mild subtype in 21/83(25%), the moderate subtype in 22/83(27%) and the severe subtype in 21/83(25%). A fourth pattern was identified in 19/83(23%) patients with a diamond-shaped expansion of the interhemispheric fissure, concomitant thalamic, putaminal, hippocampal and other smaller substrate involvement indicative of the most destructive subtype.

Conclusions: We propose a new MR grading system of injury at the parasagittal perirolandic region related to severe, sustained central perinatal term hypoxia–ischaemia. We also introduce a previously undescribed pattern of injury, the most severe form of this spectrum, seen especially after prolongation of the second stage of labour. This constellation of high metabolic substrate, targeted tissue destruction is consistently demonstrated by MRI, termed the *massive paramedian injury* pattern.

Keywords: Hypoxia–ischaemia in term neonates, Brain, Magnetic resonance imaging, Massive paramedian injury

BACKGROUND

The pattern of hypoxic–ischaemic brain injury (HIBI) in cases of profound ischaemia has been well described.

There is generally a variable degree of involvement of the basal ganglia (especially the dorsal putamen) and the ventral thalamus which combines to create the basal ganglia–thalamus (BGT) pattern.

Associated perirolandic injury, which may be of varying degrees of severity, is found in combination with the central nuclei destruction, which we refer to in this review as the Rolandic Basal Ganglia–Thalamus (RBGT) pattern.

A
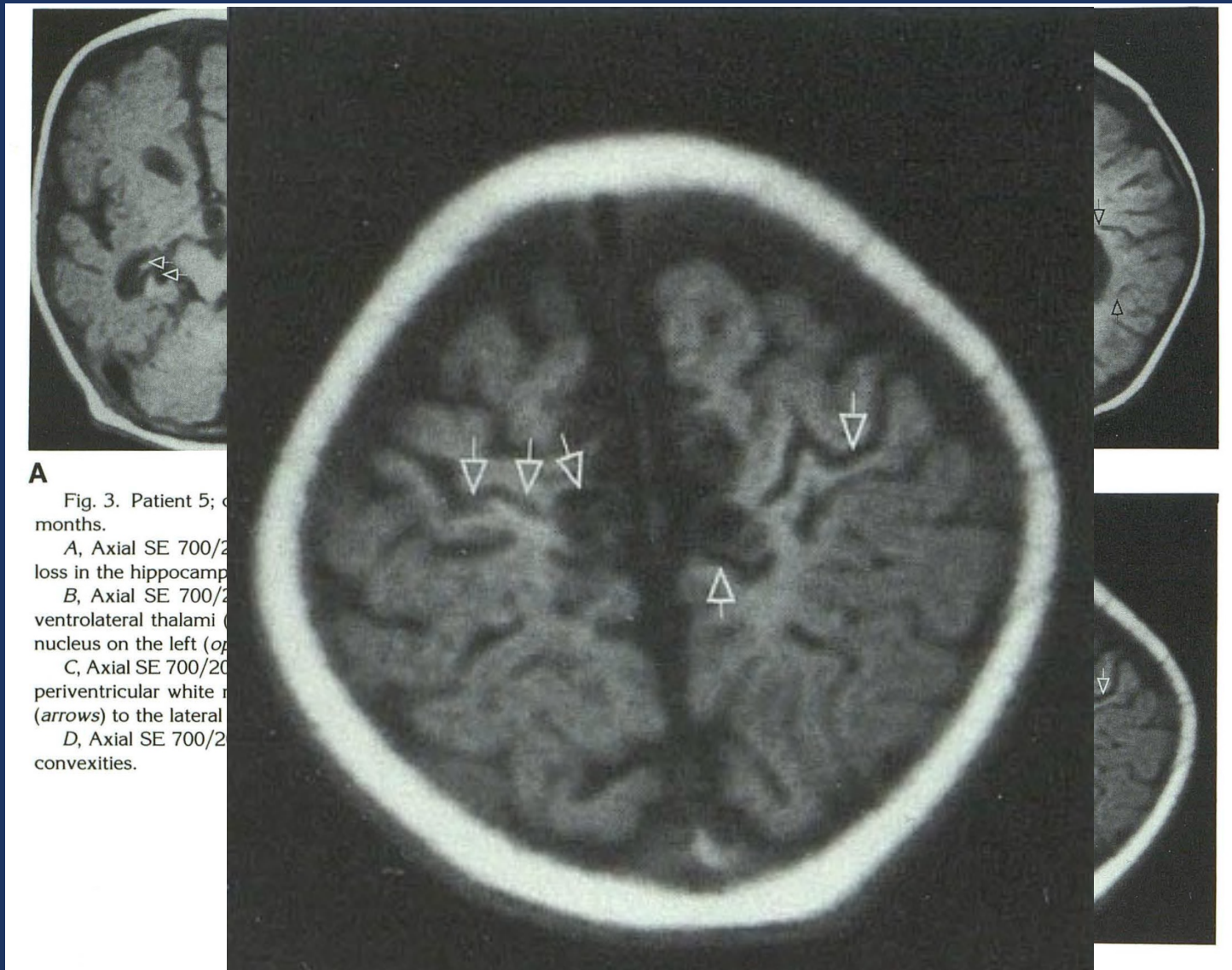
Fig. 3. Patient 5;
months.
A, Axial SE 700/2
loss in the hippocamp
B, Axial SE 700/2
ventrolateral thalami (
nucleus on the left (o
C, Axial SE 700/20
periventricular white
(arrows) to the lateral
D, Axial SE 700/2
convexities.

The term parasagittal cerebral hypoxic–ischaemic brain injury has been attributed predominantly to watershed territory involvement in partial prolonged type of HIBI.

The parasagittal cortex on either side of the inter-hemispheric fissure is traditionally recognised as a watershed zone, located between the major arterial territories supplying the cerebral cortex.

There are however instances where a perirolandic injury may extend to the far reaches of the primary motor cortex or Brodmann area 4 (BA4) and into the premotor cortex or Brodmann area 6 (BA6), including the supplementary motor area (SMA) and association cortex.

It is not uncommon for radiologists to report these injuries as "mixed patterns" of injury. However, careful examination reveals continuity of the lesions with no intervening normal cerebral substrate, indicating that all the affected structures are contiguously destroyed.
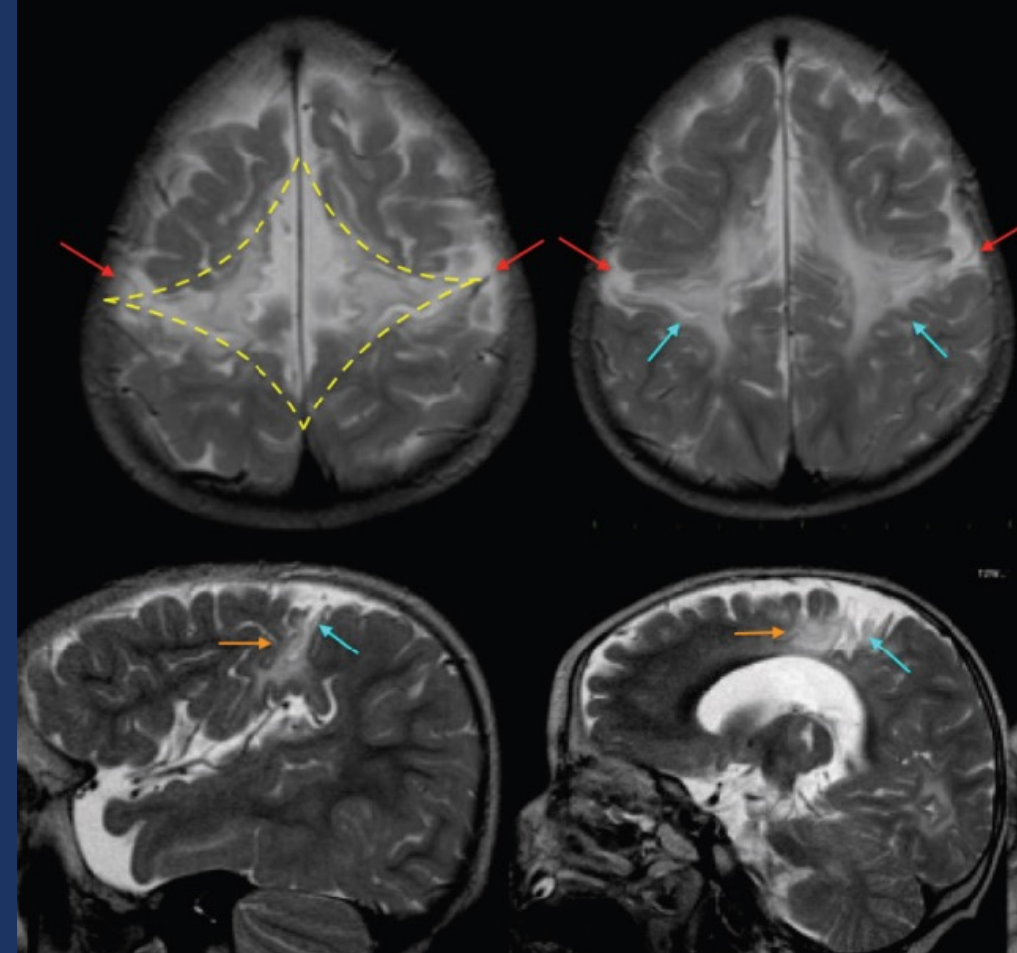
Aim: To describe the spectrum of parasagittal injury on MRI studies performed on children following severe perinatal term hypoxia–ischaemia, using a novel MRI grading system, and propose a new central pattern correlated with neuropathologic features.

The purpose of this study

* To describe the spectrum of parasagittal brain injuries identified at the perirolandic region in term neonates attributable to severe central type hypoxia–ischaemia.

* To show the extent of injury in each grade and the associated structural damage incurred, remote from the parasagittal area, including the basal ganglia, thalamus and other important substrates.

* to show that in addition to parasagittal injuries due to partial prolonged ischaemia, there is a gradation of injuries also identified at the parasagittal cortex, attributable to profound and sustained hypoxia–ischaemia of the central injury subtype.

Methods

Imaging was performed at different times after the perinatal injury, dependent on clinician referral, and showed a range of patterns of injury in the chronic phase of HIBI. The MRI scans were all performed on 1.5 T Siemens Scanners.

Sagittal volumetric, 1 mm slices GE 1900/2.95 (TR/TE (msec)) and coronal volumetric Inversion Recovery (IR) 1.1-mm slices SE 4000/363 (TR/ TE (msec)), coronal IR through temporal lobes, axial T2, axial FLAIR, axial diffusion-weighted/ADC, axial susceptibility- weighted and coronal T2-weighted sequences were obtained in all patients.

The MRI studies of these full-term infants were retrospectively independently reviewed by the principal investigator (S.K.M.) and coinvestigator (J.L.) with neuroradiological expertise of 15 years and 30 years, respectively.

From this database of 297 patients, we classified injuries into the four major patterns of HIBI [8] as per classification in Table 1.

Methods: MR scans of 297 patients with perinatal term hypoxia–ischaemia were evaluated for typical patterns of brain injury. A total of 83 patients that demonstrated the central/basal ganglia–thalamus and perirolandic pattern of injury were categorised according to the degree of severity. The perirolandic injury was graded by the degree of interhemispheric widening, paracentral lobule involvement and perirolandic cortex destruction leading to a tiered categorisation. Of these 83 patients, 19 had the most severe subtype of injury. A detailed analysis of the clinical data of a subset of 11 of these 19 patients was conducted.
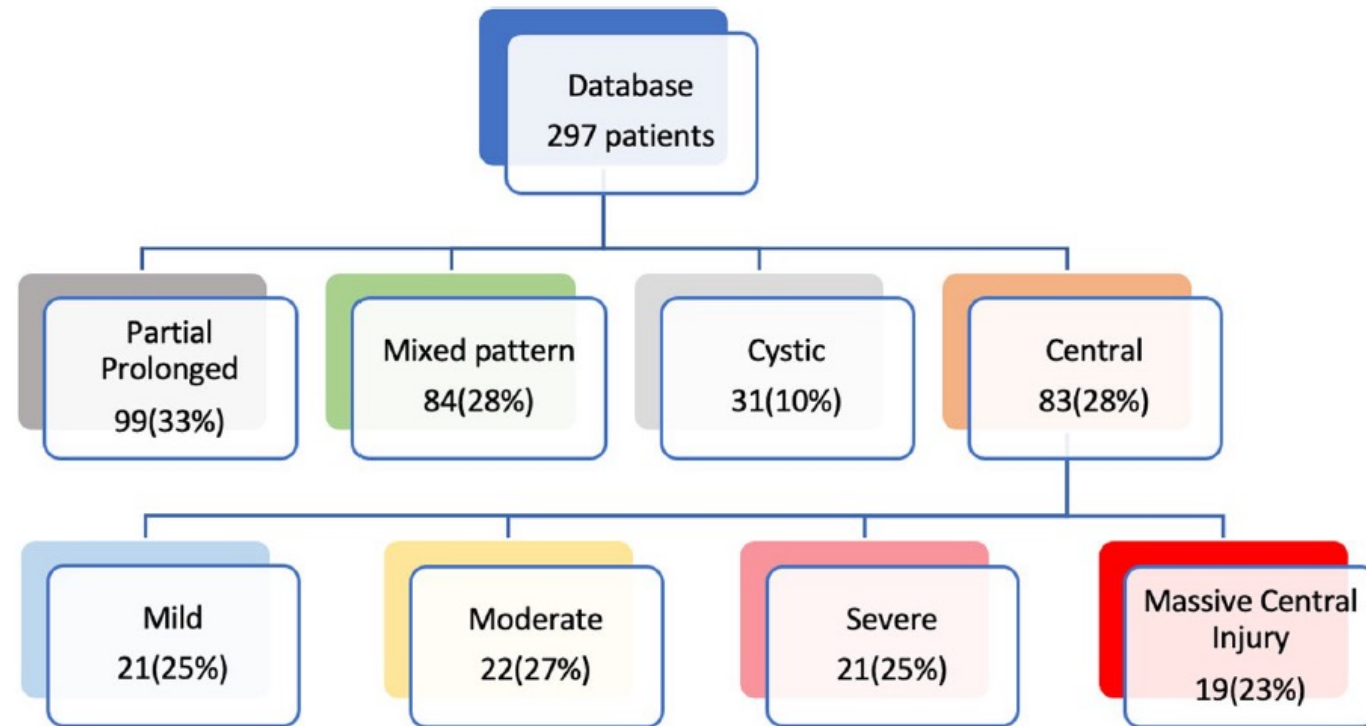
Fig. 1 Schematic diagram of the sequence of derivation of the individual subtypes from the sampled database

Table 1 The four main MRI patterns in patients with hypoxic–ischaemic brain injury [8]

Subtype of HIBI	Anatomical structure involved	Type of insult
Central RBGT pattern	Deep Nuclei/Perirolandic cortex/Hippocampus	Profound hypoxic episode
Partial Prolonged or Watershed Pattern	Cerebral Intervascular Watershed Areas	Prolonged, moderate or intermittent
Mixed RBGT + Watershed Pattern	Deep Nuclei/Cortex/Watershed Areas	Severe, variable in duration
Cystic Encephalomalacia	Cerebral Cortex White Matter/Basal Nuclei	Total Anoxia

RBGT Rolandic basal ganglia–thalamus pattern, *Deep nuclei* thalamus, putamen

The studies were evaluated for morphology and signal abnormalities of multiple specific structures in the brain using a devised grading system.

A simple 0–3 scoring system was applied to each region independently including
0 = no injury,
1 = mild injury (less than a third of the structure was injured),
2 = moderate injury (more than one third, but less than two thirds of the structure was injured)
3 = severe injury (more than two thirds, with up to near complete destruction of the substrate).

Particular attention was given to the substrates previously enumerated as being high metabolic areas of the brain including the perirolandic sensorimotor cortex,
Paracentral lobule, deep grey matter nuclei (especially putamina and thalami),
the brainstem, the hippocampi, the superficial and deep white matter, the visual cortex,
the primary auditory cortex, insular, mammillary bodies, fornix and the corpus callosum [8].
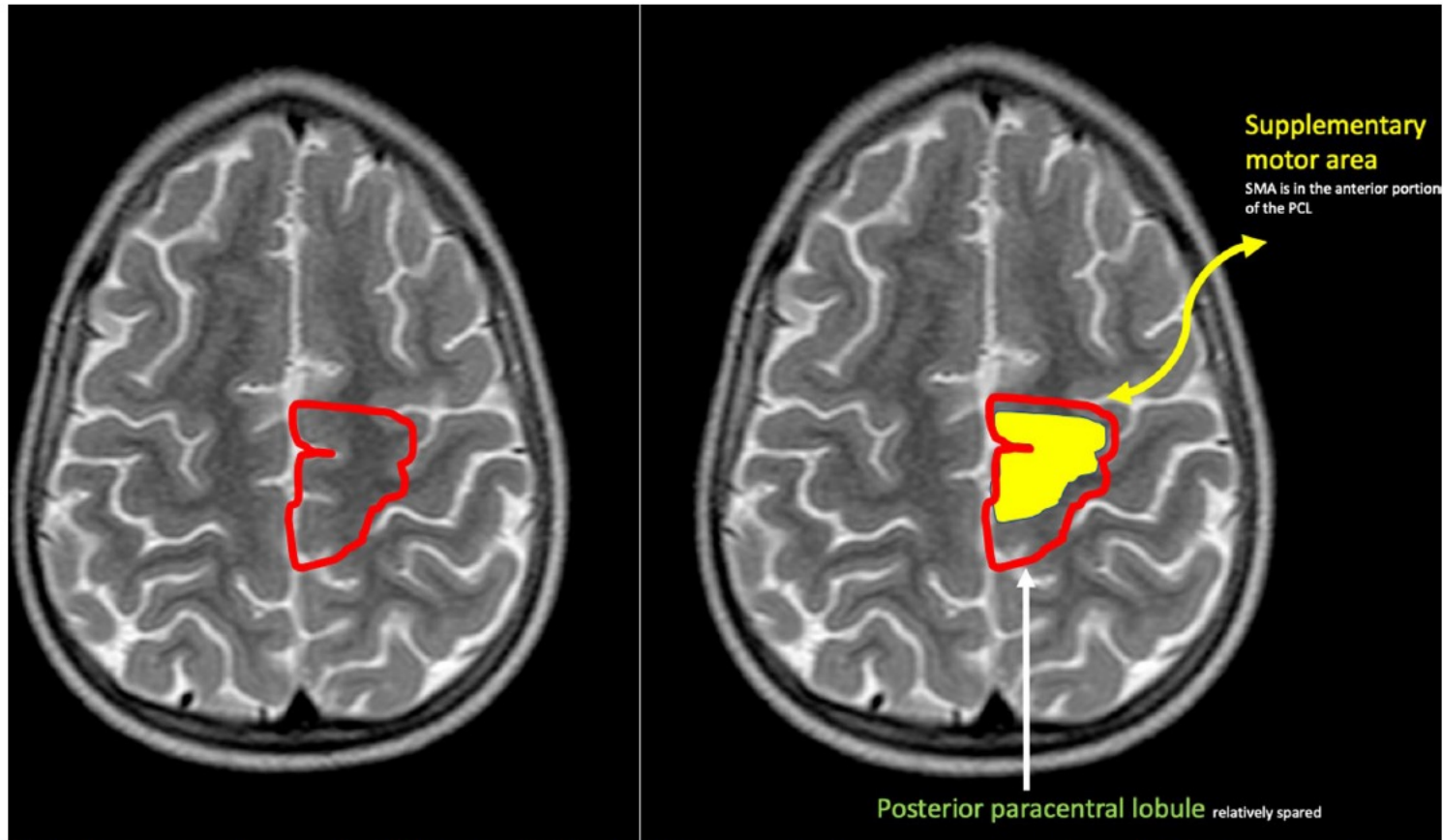
Fig. 8 The location of the paracentral lobule (PCL) with the anterior PCL connecting the supplementary motor area (SMA) to the precentral primary motor cortex and the posterior PCL connecting to the postcentral gyrus

Each study was assessed with a view to **accurate grading of the injuries** at each specific substrate.

Sixteen separate substrate assessments, listed in Table 2, were initially undertaken for each patient.

Regarding the **basal ganglia**, evaluation of injuries focussed upon the posterior aspect of the putamina and at the thalami, predominantly the ventral lateral aspect.

Hippocampal injuries were documented based upon assessment in the coronal plane with relevant inversion recovery sequences planned according to the triplanar axes of the hippocampus.

We subsequently focussed the evaluation to 5 specific parasagittal features listed in bold below (each evaluated from 0 to 3 as above) leading to a potential maximum parasagittal score out of 15.

In reviewing the perirolandic injuries, careful note was made of the involvement of the paracentral lobule (**PCL**) including the supplementary motor areas, the **superior frontal gyrus**, **precentral gyrus**, the **postcentral gyrus** and the degree of interhemispheric fissure (**IHF**) widening.
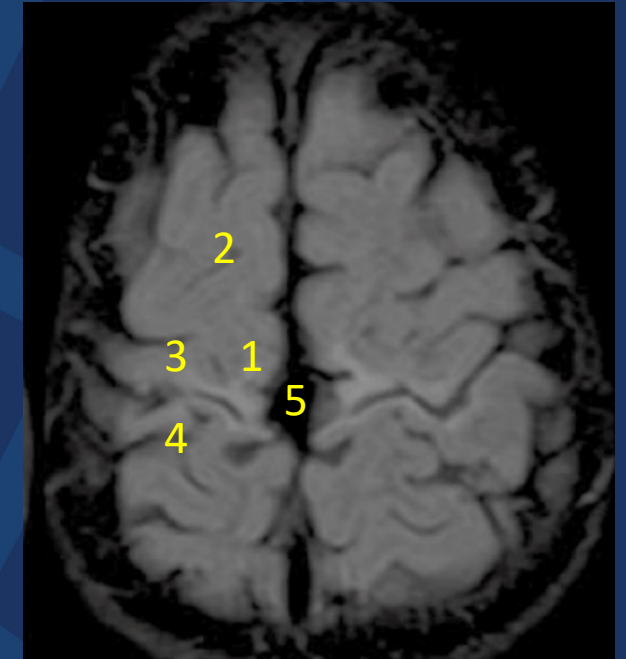
Table 3 Distribution of the parasagittal score between sub-groups

| Parasagittal score, N (%)	Mild (N=21)	Moderate (N=22)	Severe (N=21)	MPI (N=19)	Overall (N=83)
0	2 (9.5)				2 (2.4)
1		2 (9.1)			2 (2.4)
2	2 (9.5)				2 (2.4)
3	5 (23.8)				5 (6.0)
4	9 (42.9)	7 (31.8)			16 (19.3)
5	2 (9.5)	5 (22.7)			7 (8.4)
6	1 (4.8)	2 (9.1)			3 (3.6)
7		4 (18.2)	1 (4.8)		5 (6.0)
8		1 (4.5)	2 (9.5)	1 (5.3)	4 (4.8)
9			1 (4.8)		1 (1.2)
10			4 (19.0)		4 (4.8)
11		1 (4.5)	3 (14.3)	1 (5.3)	5 (6.0)
12			4 (19.0)	7 (36.8)	11 (13.3)
13			1 (4.8)	5 (26.3)	6 (7.2)
14			3 (14.3)	4 (21.1)	7 (8.4)
15			2 (9.5)	1 (5.3)	3 (3.6)

P value < 0.0001
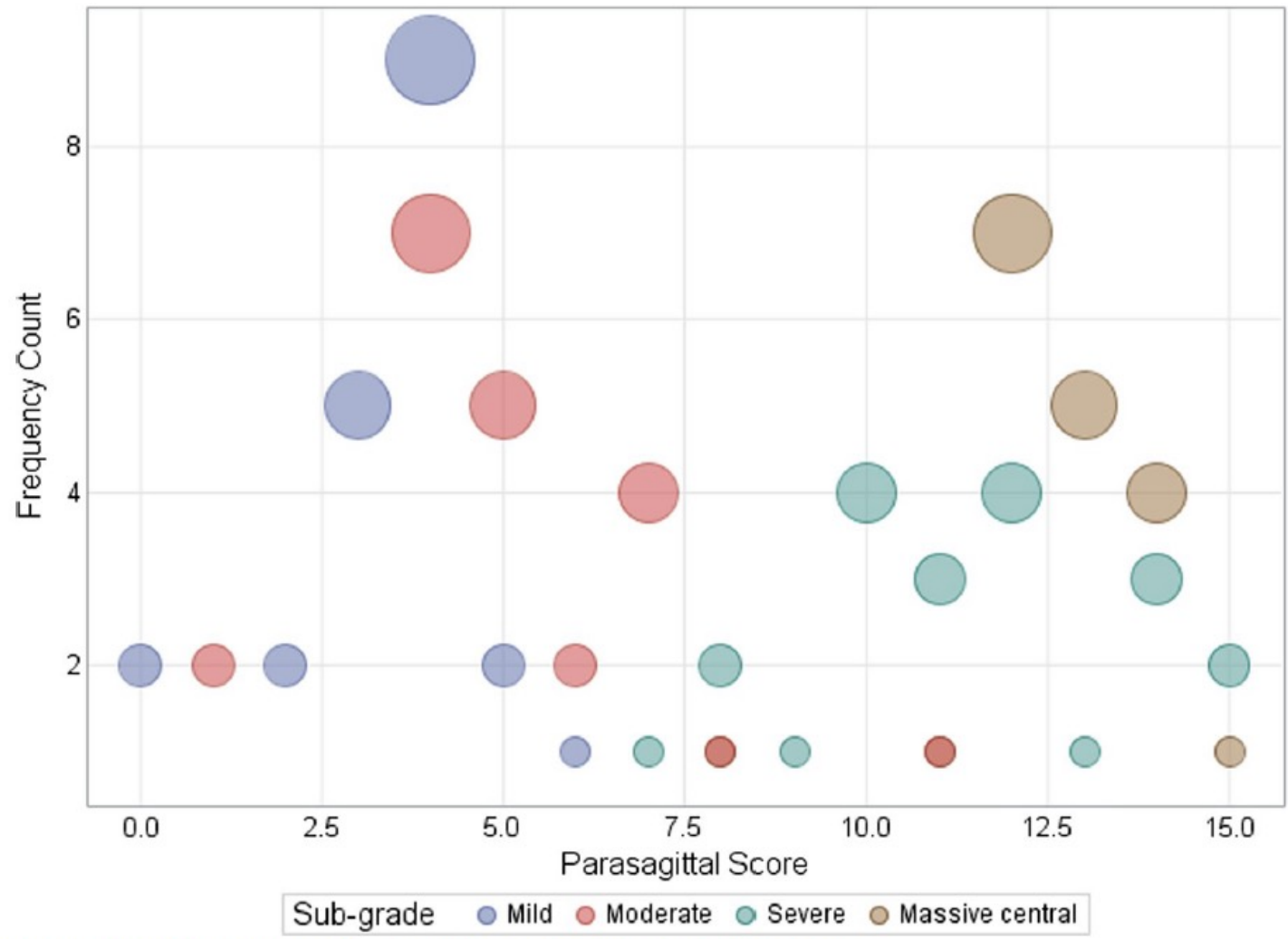
Fig. 6 Grid-bubble chart of the frequency of parasagittal scores for subtypes of central injury

Table 2 Key features of each subtype of parasagittal central hypoxic–ischaemic injury

	Mild	Moderate	Severe	Massive paramedian
Parasagittal structures affected	Sensorimotor cortex	Sensorimotor cortex, SMA	Sensorimotor cortex, SMA and more of the PCL	Sensorimotor cortex, SMA, PCL, extending to the SFG and SPL
Boundaries of the injury	Limited to perirolandic cortex only	Perirolandic cortex and anterior part of the PCL	Perirolandic cortex and PCL	Laterally to edge of central sulcus, anteriorly and posteriorly to the edges of the IHF
White matter destruction	Nil	Some reduction in WM volume	Slightly more WM volume reduction	Severe decrease in overall WM volume
Interhemispheric fissure widening	Apposed paramedian gyri	Slight widening of the fissure at the PCL	Inverted V-shaped opening of the fissure	Diamond-shaped widening of the fissure
Central cortico-spinal tract destruction	Usually none or minimal along the long tract	Mild hyperintensity along the long tracts	More significant destruction of the central WM tracts	Near complete destruction
Insular Cortex	Spared	Minimally involved	Moderately involved	Near complete destruction
Mammillary Bodies	Usually spared	Mildly injured	Moderately injured	Severely atrophied
Heschl Gyrus	Usually spared	Mildly injured	Moderately injured	Severely injured
Hippocampi	May be slightly decreased in volume	Moderately decreased in volume	Severely decreased in volume	Complete destruction
Calcarine cortex	Usually, normal	Mild signal change	Moderate signal change	Significant signal change and atrophy
Corpus callosum	Mild central CC atrophy	Moderate central CC atrophy	Marked central CC atrophy	Near complete central CC atrophy
BGT involvement	Mild signal change	Moderate signal change up to less than 50% volume involved	Marked signal change greater than 50% volume involved	Spongiotic cavitation at putamen and thalami

PCL paracentral lobule, *CC* corpus callosum, *SMA* supplementary motor area, *SFG* superior frontal gyrus, *SPL* superior parietal lobule, *IHF* Interhemispheric fissure, *WM* white matter
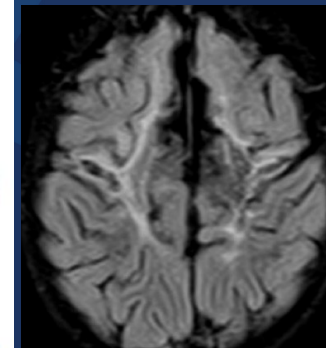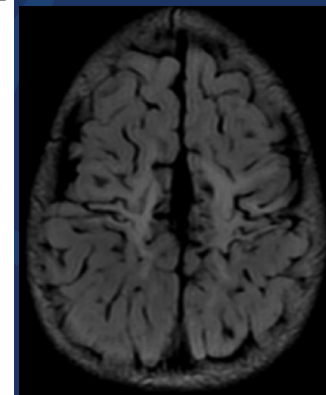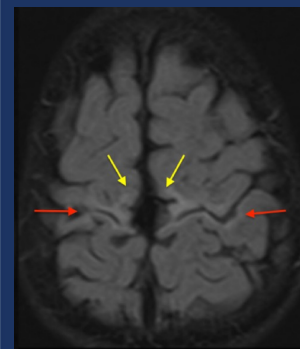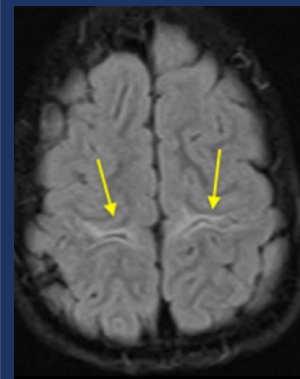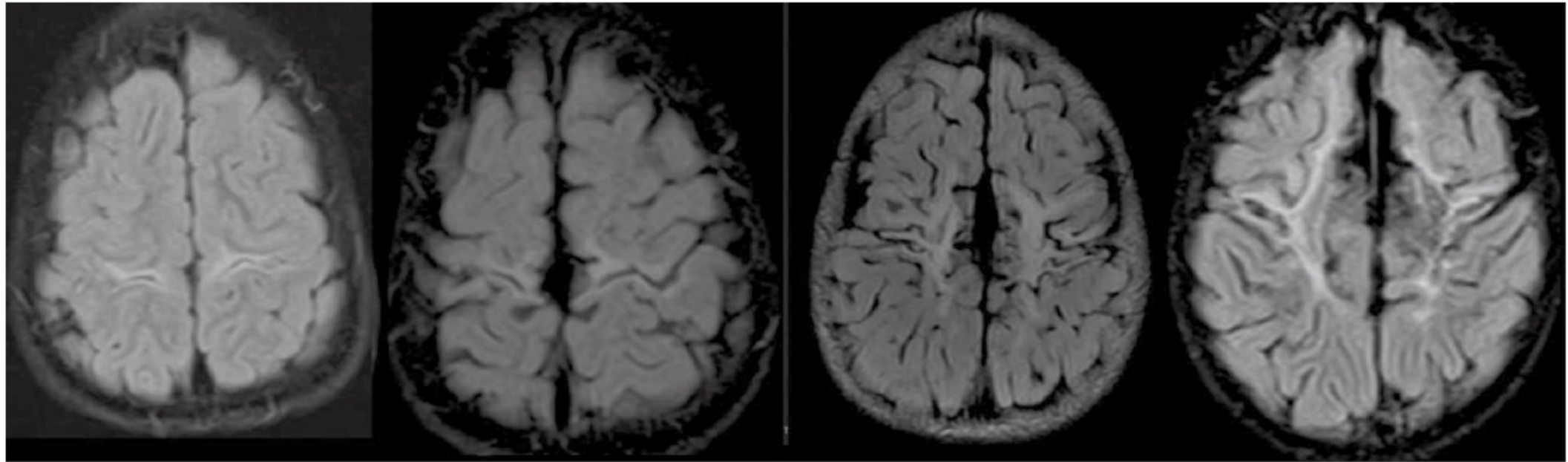
| Mild N=21(25%) | Moderate N=22(27%) | Severe N=21(25%) | Massive Paramedian Injury N=19(23%) |

Fig. 9 The proposed classification of parasagittal perirolandic central type injury

In the mild perirolandic (Grade 1) subtype, (N = 21/83, 25%) the central sulcus is outlined by hyperintensity on the axial FLAIR sequence, optimal to show (as in Fig. 2) this often-subtle injury.
In some children, the injury may be limited in size and located in the pre-rolandic or post-rolandic lip of the sensorimotor cortex, with sparing of the rest of the cerebral mantle.

When motor cortex injury predominantly involves the "hand knob" region of the homunculus, bilateral upper limb function is affected and there is no appreciable widening of the interhemispheric fissure.

The parasagittal score in this subgroup did not exceed 6/15 and the average score was 3/15.
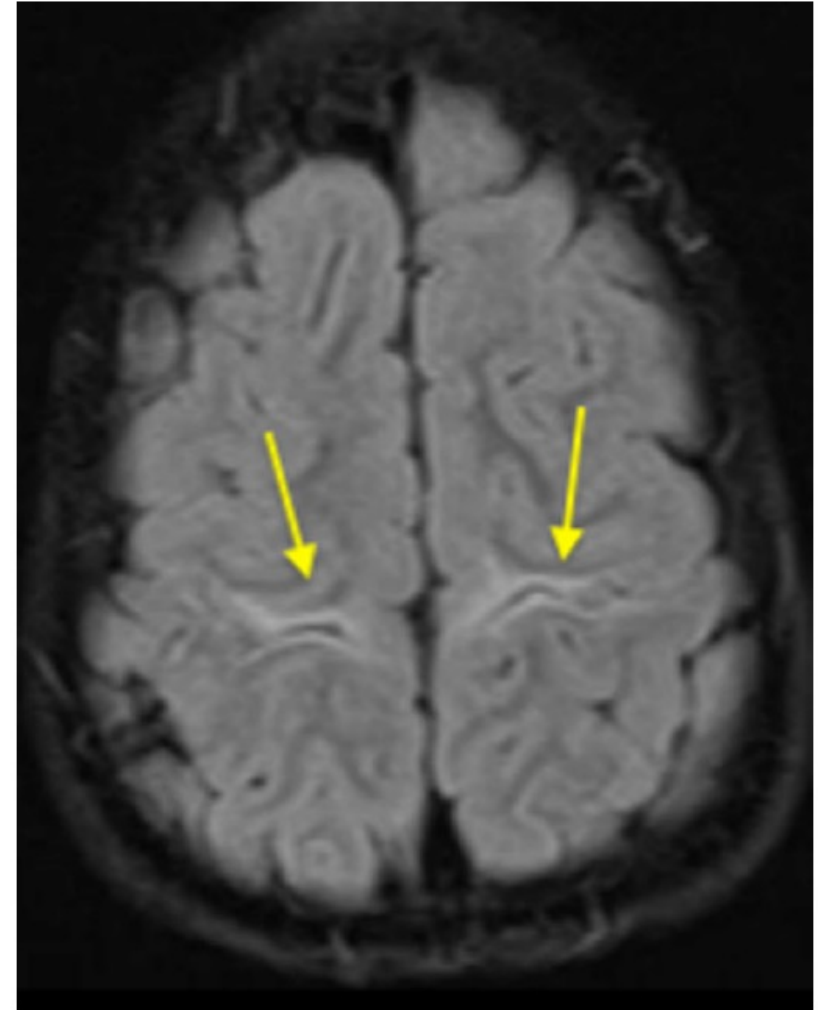
Fig. 2 The mild subtype of perirolandic (yellow arrows) primary motor cortex and postcentral gyrus involvement

Mild perirolandic (Grade 1) subtype

The moderate perirolandic (Grade 2) subtype
(N = 22/83, 27%) is manifested as partial injury of the
ventral aspect of the paracentral lobule in addition to
the perirolandic injury.

A particular involvement of the SMA is manifested in this
subgroup (shown in Fig. 3) resulting in a slight widening of the
interhemispheric fissure, in the region of the paracentral lobule
anteriorly with sparing of the margins of the paracentral lobule,
the lateral margins of the central sulci and absence of
extension towards the superior frontal gyrus (SFG) and
superior parietal lobules (SPL).

The average parasagittal score for this subgroup was 5/15.
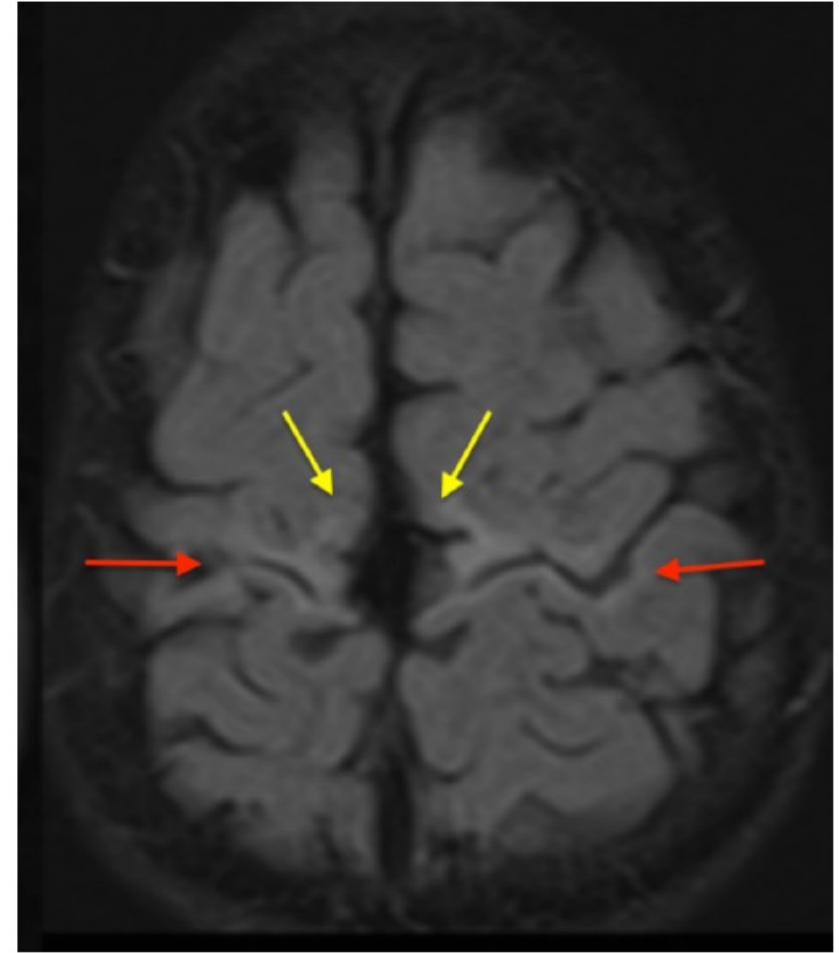
Fig. 3 The moderate subtype of perirolandic injury (red arrows)
including partial SMA involvement at the ventral aspect of the PCL
(yellow arrows)

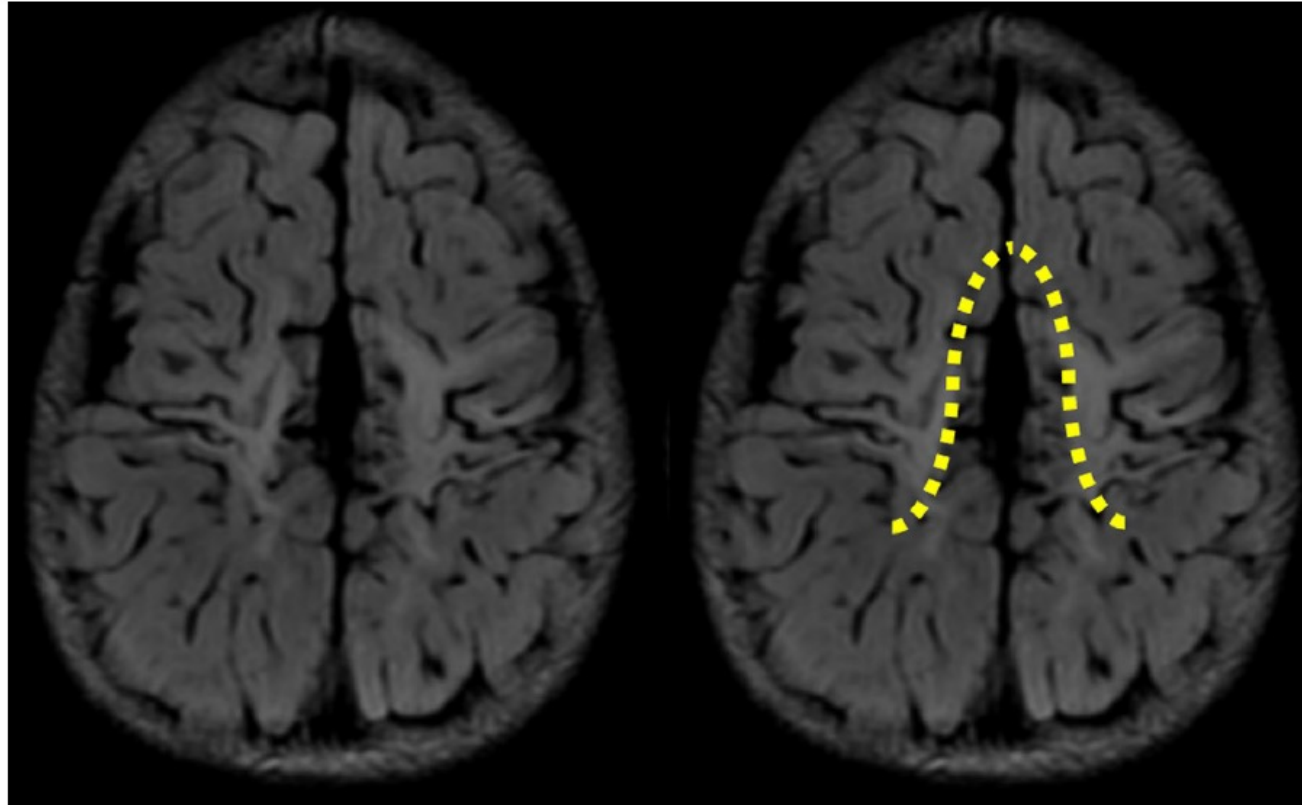Moderate perirolandic (Grade 2) subtype

Fig. 4 The severe subtype of perirolandic injury with greater PCL involvement and marked localised atrophy, widening the interhemispheric fissure, with an inverted-V configuration (yellow dotted line)

The severe perirolandic (Grade 3) subtype (N = 21/83, 25%) is associated with greater destruction of the anterior paracentral lobule including more of the SMA and surrounding premotor association cortex, more marked atrophy of the pre-central and post-central gyri, and greater widening of the interhemispheric fissure which has an inverted-V configuration, open dorsally and with a closed apex anteriorly at the superior frontal gyrus level (Fig. 4). The average parasagittal score in this subtype was 10/15.
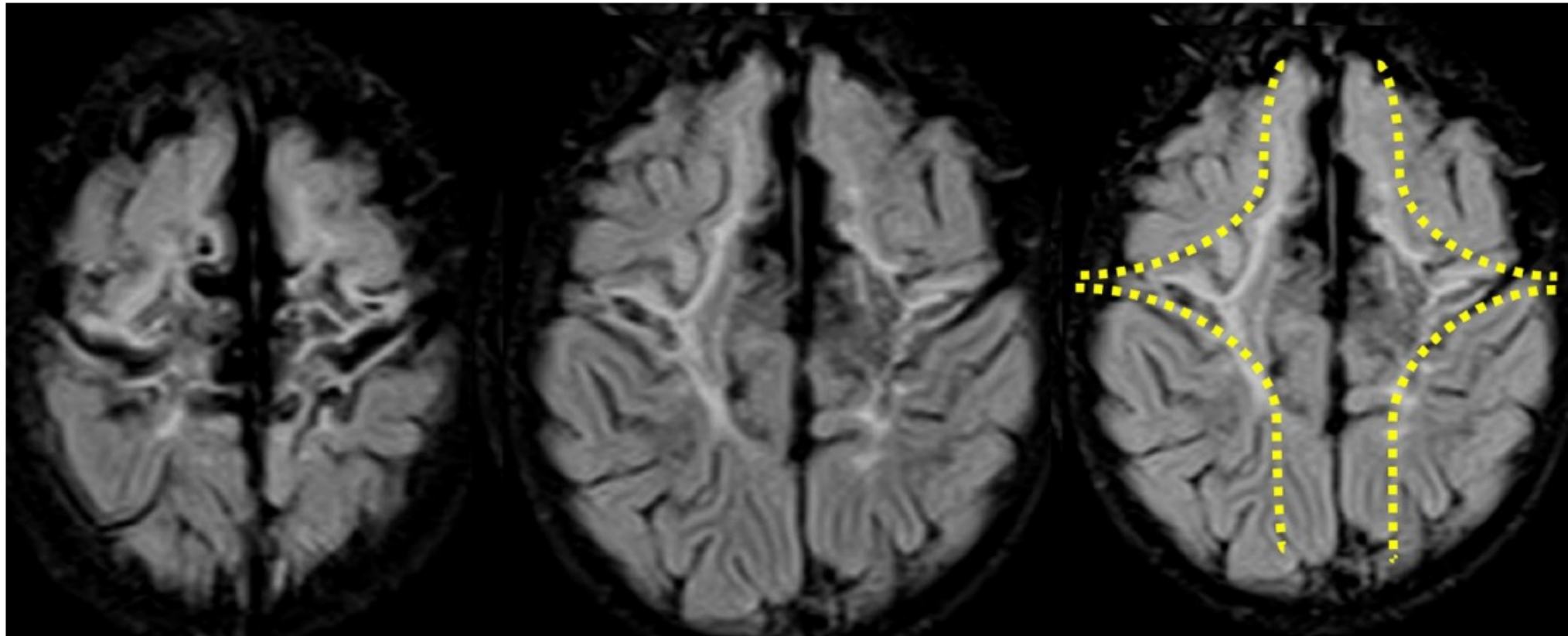
Severe perirolandic (Grade 3) subtype

Fig. 5 The MPI subtype of parasagittal cortex injury including complete destruction of the SMA, with secondary diamond-shaped (yellow dotted line) expansion of the interhemispheric fissure

(MPI) pattern, = an exaggerated form of central hypoxic–ischaemic brain injury.

At this end of the spectrum, shown in Fig. 5, we found a diamond-shaped expansion of the interhemispheric fissure, possibly a consequence of nearly complete destruction of the paracentral lobule, SMA and sensorimotor cortex. The parasagittal scores in this subtype were the highest with the average score measured at 13/15.

(Grade 4) Massive paramedian injury

Table 5 The common findings in all 19 patients with MPI pattern

A common thread…
Term neonates
Appropriate or large for gestational age neonates
Normal antenatal history, all Rhesus positive and syphilis serology negative
No significant chronic maternal conditions
Prolonged labour—more often second stage
Foetal distress, especially with cephalopelvic disproportion
Epidural anaesthesia with maternal hypotension
Grade 3 hypoxic–ischaemic encephalopathy
Low Apgar scores
Metabolic acidosis
Neonatal seizures
Normal immediate postnatal imaging
Metabolic or chromosomal abnormalities excluded
Static/non-progressive phenomena on follow-up imaging
Fairly similar pattern of cerebral injury on imaging
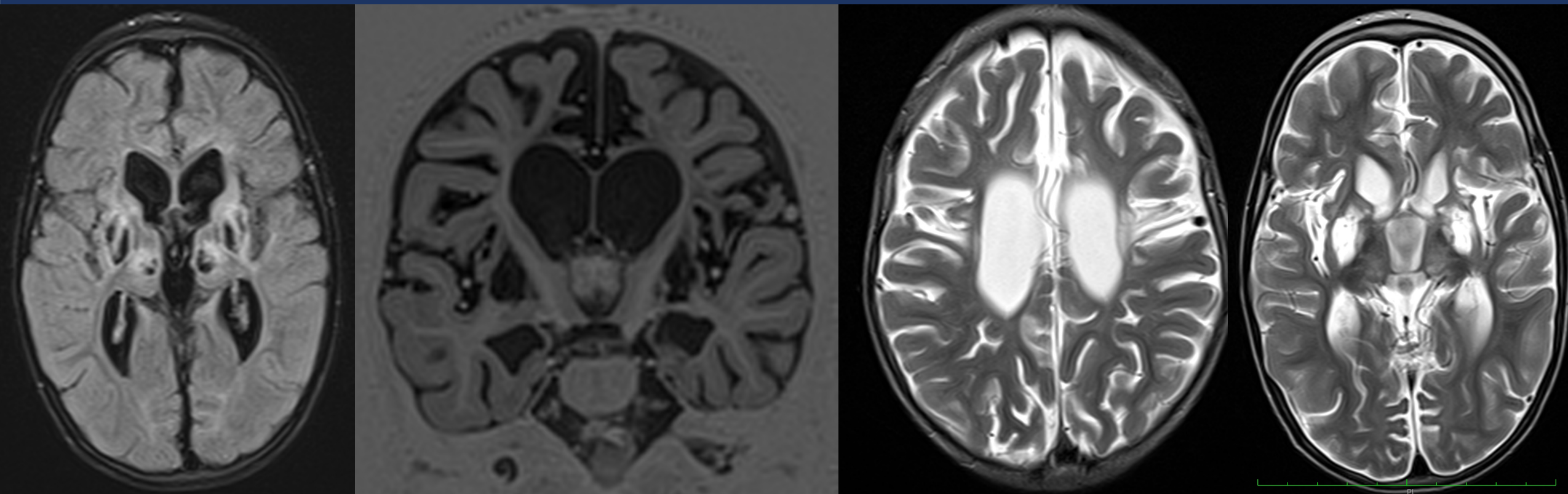
Involvement of the basal ganglia, thalami and hippocampi was noted in all 19 MPI patients, with spongiotic cavitation seen involving much of the thalamus and putamen bilaterally.

The hippocampi were always severely injured.

Overall white matter volume was reduced, involving the central motor core of the brain and much of the pyramidal cortico-spinal tract as well as greater thinning of the corpus callosum.

Secondary ventricular prominence, thinning of the fornix and smaller mammillary bodies.

The loss of volume at the brainstem was also found to be more marked in this most severe category of injury, likely a result of Wallerian degeneration.

(Grade 4) Massive paramedian injury
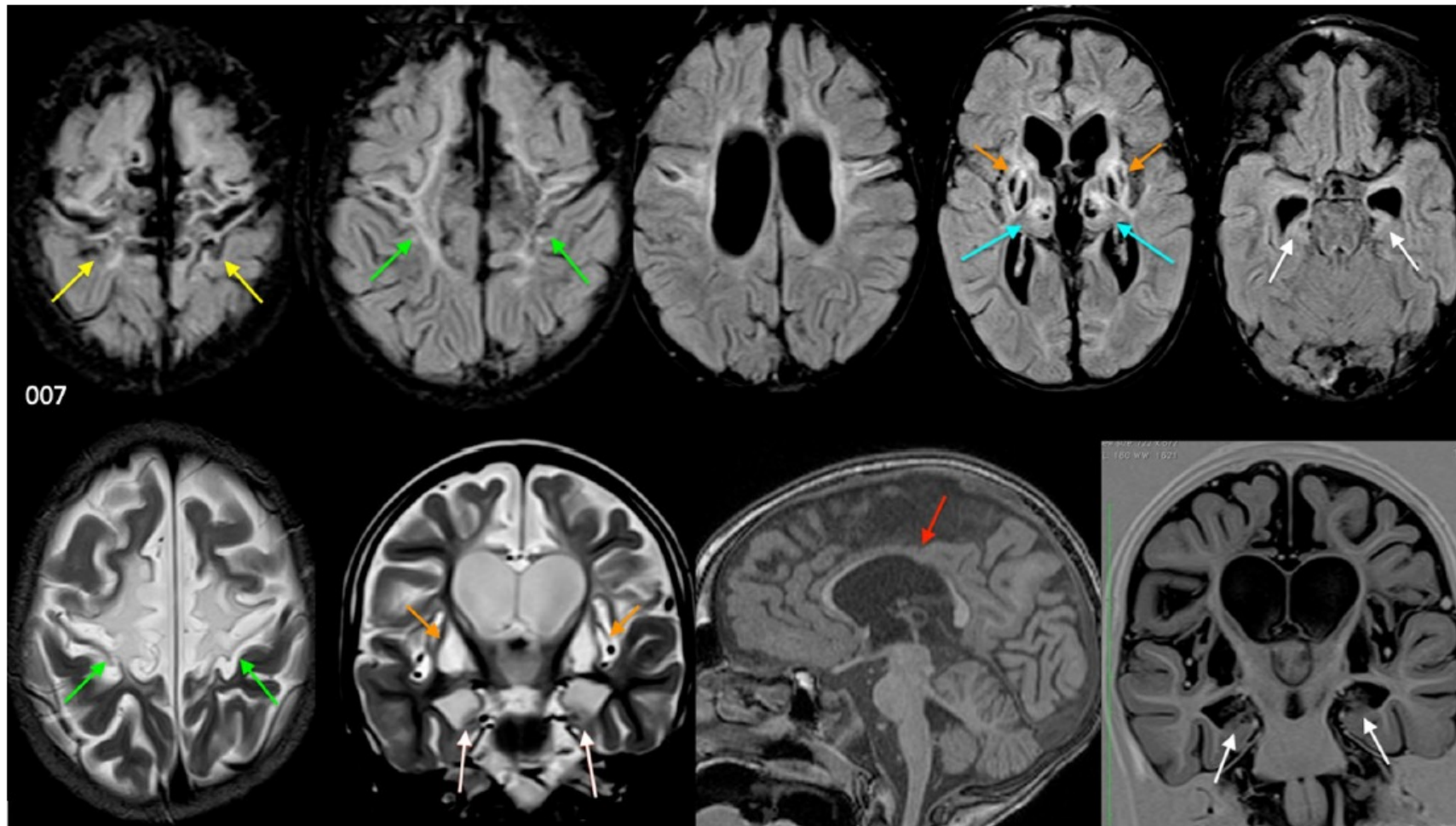
Fig. 7 Collage of MR images demonstrating the key features of the massive paramedian injury pattern. Top row = axial FLAIR and bottom row (from left to right) axial T2-weighted, coronal T2-weighted, Sagittal T1-weighted and coronal inversion recovery sequence images. These demonstrate the perirolandic injury (yellow arrows), diamond-shaped expansion of the parasagittal cortex including the paracentral lobule (green arrows), hippocampal destruction (white arrows), putaminal necrosis (orange arrows) and thalamic (blue arrows) cavitation. The red arrow highlights the severe deafferentation thinning of the body and isthmus of corpus callosum

Table 7 Key features of each subtype of parasagittal central hypoxic–ischaemic injury

Substrate injury		Mild/Mod/Sev (N=64)	MPI (N=19)	Overall (N=83)	P value
IHF Widening, n (%)	Other	6 (31.6)	55 (85.9)	61 (73.5)	<0.001
	Severe	13 (68.4)	9 (14.1)	22 (26.5)	
Pre-central Gyrus Score, n (%)	Other	1 (5.3)	49 (76.6)	50 (60.2)	<0.001
	Severe	18 (94.7)	15 (23.4)	33 (39.8)	
Post-Central Gyrus Score, n (%)	Other	4 (21.1)	52 (81.3)	56 (67.5)	<0.001
	Severe	15 (78.9)	12 (18.8)	27 (32.5)	
SFG Score, n (%)	Other	18 (94.7)	62 (96.9)	80 (96.4)	0.547
	Severe	1 (5.3)	2 (3.1)	3 (3.6)	
Paracentral Lobule Score, n (%)	Other	1 (5.3)	45 (70.3)	46 (55.4)	<0.001
	Severe	18 (94.7)	19 (29.7)	37 (44.6)	
Thalamus Score, n (%)	Other	3 (15.8)	37 (57.8)	40 (48.2)	0.002
	Severe	16 (84.2)	27 (42.2)	43 (51.8)	
Putamen Score, n (%)	Other	1 (5.3)	38 (59.4)	39 (47.0)	<0.001
	Severe	18 (94.7)	26 (40.6)	44 (53.0)	
Heschl Gyrus, n (%)	Other	15 (78.9)	60 (93.8)	75 (90.4)	0.076
	Severe	4 (21.1)	4 (6.3)	8 (9.6)	
Insular Cortex, n (%)	Other	13 (68.4)	60 (93.8)	73 (88.0)	0.008
	Severe	6 (31.6)	4 (6.3)	10 (12.0)	
Hippocampus Score, n (%)	Other	2 (10.5)	30 (46.9)	32 (38.6)	0.006
	Severe	17 (89.5)	34 (53.1)	51 (61.4)	
Cerebellum, n (%)	Normal	12 (63.2)	47 (73.4)	59 (71.1)	0.400
	Involved	7 (36.8)	17 (26.6)	24 (28.9)	

IHF interhemispheric fissure, *SFG* superior frontal gyrus, *other* lower grades of substrate injuries, *Mod* moderate subtype, *Sev* severe subtype, *MPI* massive paramedian injury

Table 8 Factors associated with MPI compared to other subtypes with reference being the severe grade of substrate injuries

Feature	OR	95% CI	P value
IHF Widening	0.08	0.02–0.25	< 0.001
Pre-central gyrus	0.02	0.00–0.14	< 0.001
Post-central gyrus	0.06	0.02–0.22	< 0.001
SFG Score	0.58	0.05–6.77	0.664
Paracentral lobule	0.02	0.00–0.19	< 0.001
Thalamus	0.14	0.04–0.52	0.003
Putamen	0.04	0.00–0.30	0.002
Heschl Gyrus	0.25	0.06–1.12	0.070
Insular cortex	0.14	0.04–0.59	0.007
Hippocampus	0.13	0.03–0.63	0.011

OR odds ratio, *95%CI* 95% confidence interval, *IHF* interhemispheric fissure, *SFG* superior frontal gyrus

Conclusions: We propose a new MR grading system of injury at the parasagittal perirolandic region related to severe, sustained central perinatal term hypoxia–ischaemia. We also introduce a previously undescribed pattern of injury, the most severe form of this spectrum, seen especially after prolongation of the second stage of labour. This constellation of high metabolic substrate, targeted tissue destruction is consistently demonstrated by MRI, termed the *massive paramedian injury* pattern.

Here, we have presented a new perspective with a gradation of the parasagittal cortex injury in children who have suffered severe and sustained hypoxic–ischaemic insults. We propose that this four-tiered gradation correlates with the severity of the perinatal insult and the attendant secondary and subsequent cascades of cellular injury. In this new classification, we have also introduced the most severe subtype of this injury which we have termed the massive paramedian injury in which the entire central motor core of the brain is destroyed. Common clinico-pathological features have been identified with the MPI subtype in all the cases presented here, and in particular, these were all associated with prolongation of the second stage of labour.

HYPOXIC – ISCHEMIC BRAIN INJURY

Research Plan

* Categorise the patterns

* Classify the central patterns

       Identified a new undescribed pattern

* Classify the watershed patterns

       Identified a biomarker for HIBI in watershed patterns

* Other aspects

Thalamus L-Sign: A Potential Biomarker of Neonatal Partial, Prolonged Hypoxic-Ischemic Brain Injury or Hypoglycemic Encephalopathy?
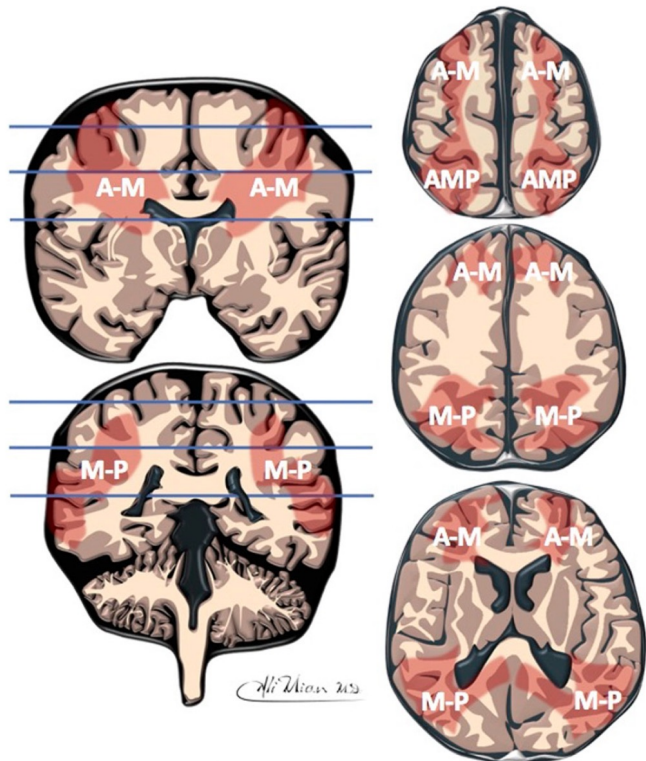
S.K. Misser, J.W. Lotz, R. van Toorn, N. Mchunu, M. Archary, and A.J. Barkovich
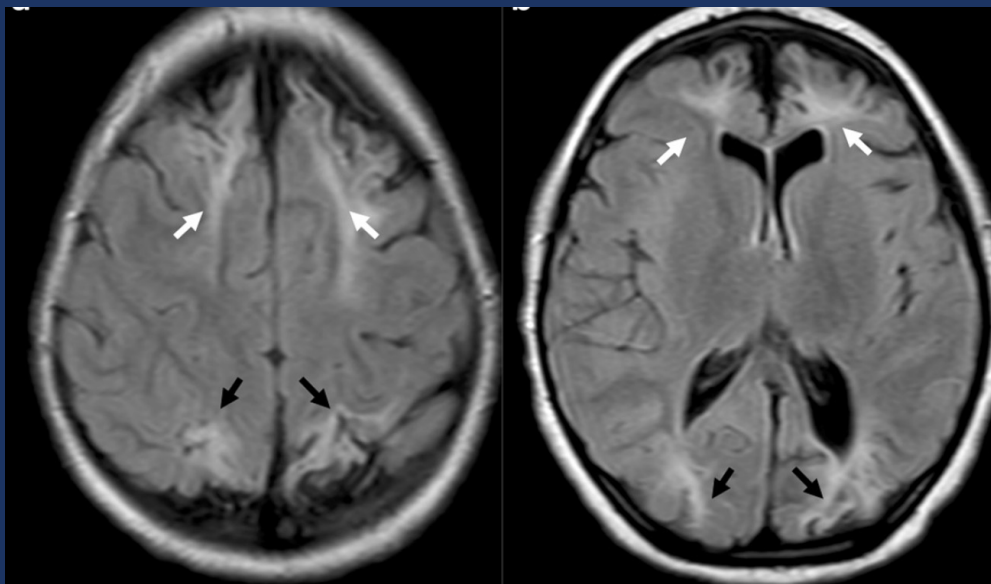
Insights into Imaging

Cortical ischaemic patterns in term partial-prolonged hypoxic-ischaemic injury—the inter-arterial watershed demonstrated through atrophy, ulegyria and signal change on delayed MRI scans in children with cerebral palsy

A-M: ACA-MCA Watershed Region
AMP: ACA-MCA-PCA Watershed Region
M-P: MCA-PCA Watershed Region
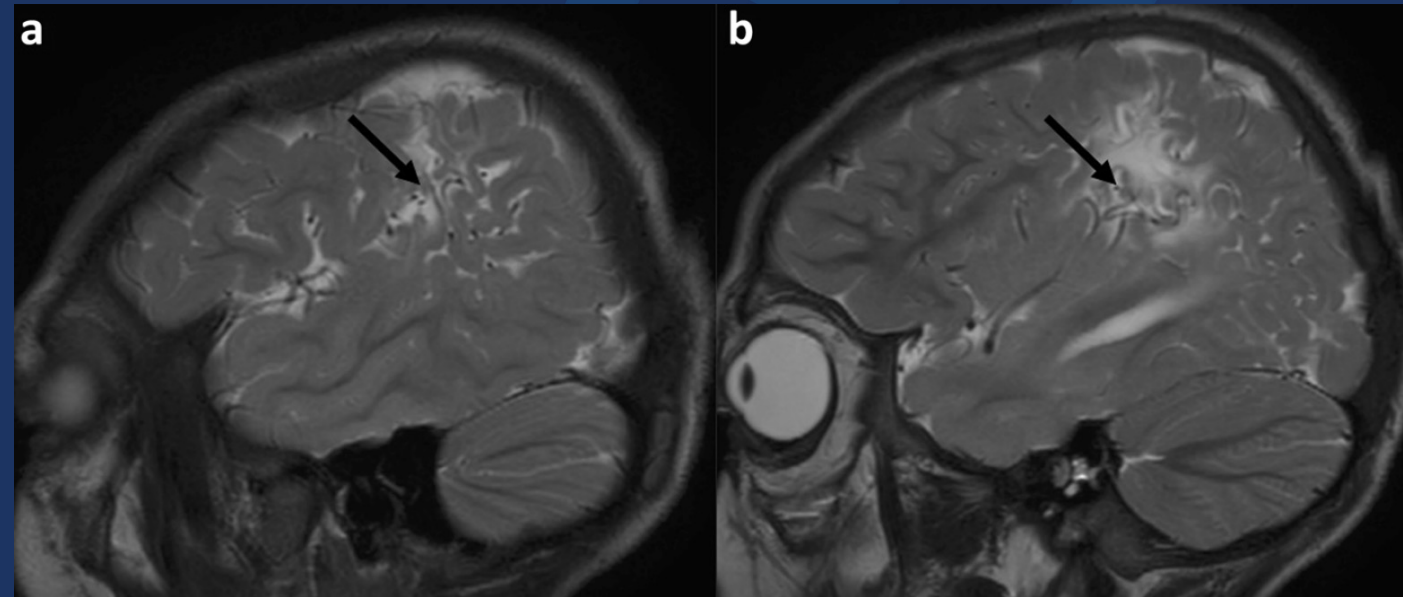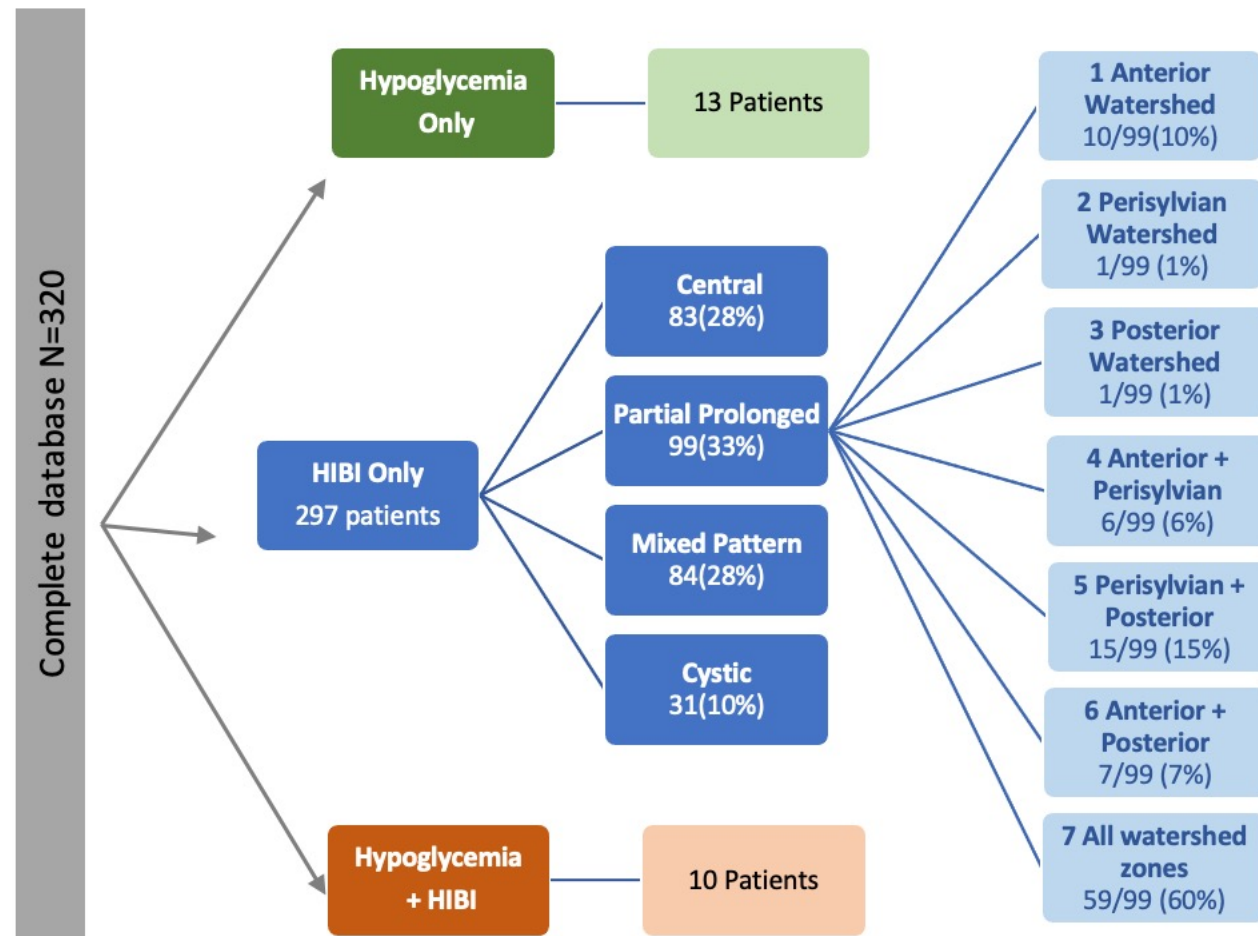
Figure 1. Derivation of the three major study groups, the subgroups of HIBI and the subtypes of watershed patterns of injury in patients who sustained partial prolonged HIBI.

Table 1: Key features of the 7 subtypes of partial prolonged/watershed HIBI

| Lobe/Structure	Features	Subtype 1 Anterior (n = 10)	Subtype 2 Peri-Sylvian (n = 1)	Subtype 3 Posterior (n = 1)	Subtype 4 Anterior + Peri-Sylvian (n = 6)	Subtype 5 Peri-Sylvian + Posterior (n = 15)	Subtype 6 Anterior + Posterior (n = 7)	Subtype 7 All 3 Zones (n = 59)	Overall (n = 99)
Thalamic injury location (No.) (%)	Nil	3 (30.0)			1 (16.7)				4 (4.0)
	Atypical	7 (70.0)			2 (33.3)		1 (14.3)		10 (10.1)
	Thalamus L-sign		1 (100.0)	1 (100.0)	3 (50.0)	15 (100.0)	6 (85.7)	59 (100.0)	85 (85.9)
Thalamus score (No.) (%)	Not/less involved	10 (100.0)	1 (100.0)	1 (100.0)	6 (100.0)	14 (93.3)	6 (85.7)	53 (89.8)	91 (91.9)
	Markedly destroyed					1 (6.7)	1 (14.3)	6 (10.2)	8 (8.1)
Parietal (No.) (%)	Not involved	6 (60.0)			3 (50.0)		1 (14.3)		10 (10.1)
	Involved	4 (40.0)	1 (100.0)	1 (100.0)	3 (50.0)	15 (100.0)	6 (85.7)	59 (100.0)	89 (89.9)
Occipital (No.) (%)	Not involved	7 (70.0)	1 (100.0)						8 (8.1)
	Involved	3 (30.0)		1 (100.0)	6 (100.0)	15 (100.0)	7 (100.0)	59 (100.0)	91 (91.9)
Frontal (No.) (%)	Not involved	1 (10.0)		1 (100.0)		8 (53.3)		1 (1.7)	11 (11.1)
	Involved	9 (90.0)	1 (100.0)		6 (100.0)	7 (46.7)	7 (100.0)	58 (98.3)	88 (88.9)
Temporal (No.) (%)	Not involved	6 (60.0)				3 (20.0)	3 (42.9)	3 (5.1)	15 (15.2)
	Involved	4 (40.0)	1 (100.0)	1 (100.0)	6 (100.0)	12 (80.0)	4 (57.1)	56 (94.9)	84 (84.8)
Cerebellum (No.) (%)	Not involved	7 (70.0)	1 (100.0)		4 (66.7)	10 (66.7)	5 (71.4)	40 (67.8)	67 (67.7)
	Involved	3 (30.0)		1 (100.0)	2 (33.3)	5 (33.3)	2 (28.6)	19 (32.2)	32 (32.3)
Brainstem (No.) (%)	Not involved	10 (100.0)	1 (100.0)	1 (100.0)	6 (100.0)	14 (93.3)	7 (100.0)	49 (83.1)	88 (88.9)
	Involved					1 (6.7)		10 (16.9)	11 (11.1)
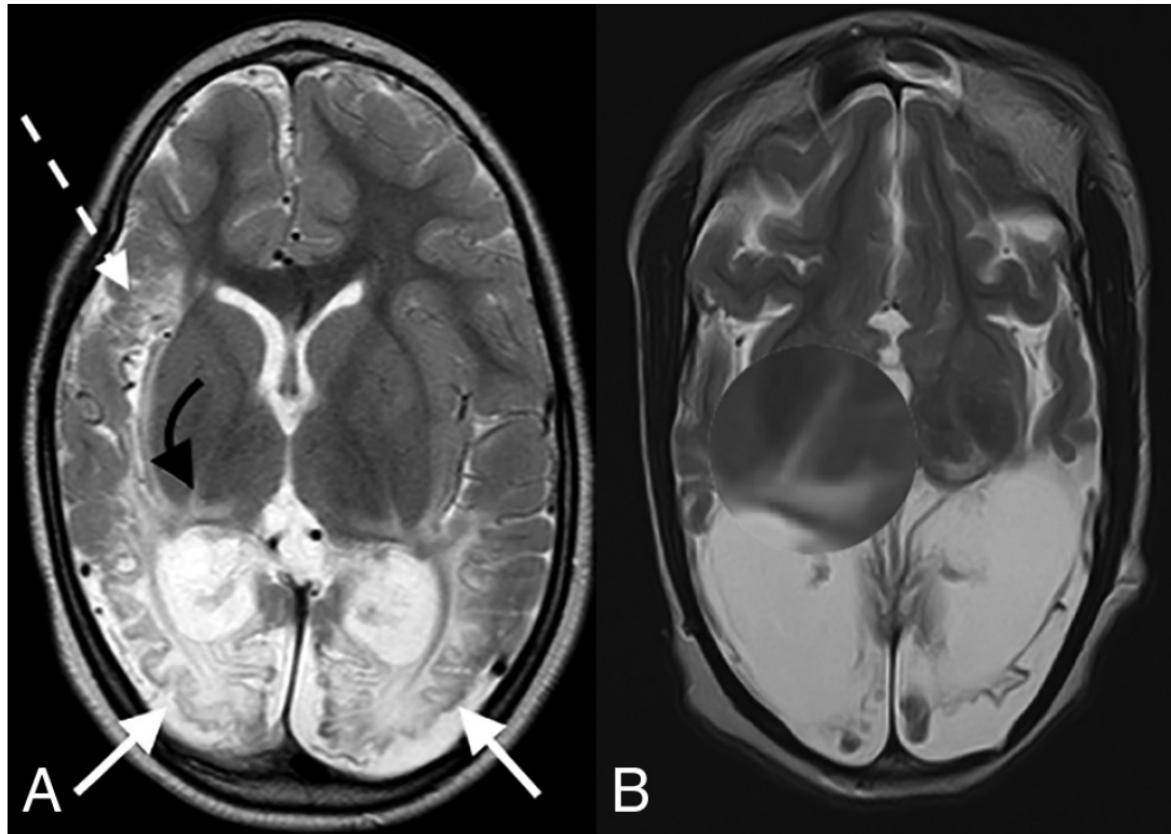
FIG 2. Axial T2-weighted images in a child with partial, prolonged HIBI demonstrating interarterial injuries at the peri-Sylvian (*dashed white arrow*) and posterior parieto-occipital (*solid white arrows*) watershed regions. Note the thalamus L-sign (*curved arrows* in *A* and highlighted by the loupe in a second patient in *B*).

Table 2: Key features involved in thalamus L-sign injury compared with other thalamic injuries (nil and atypical)

Lobe/Structure	Features	Thalamus L-Sign (*n* = 85)	Other (*n* = 14)	Overall (*n* = 99)	*P* Value
Thalamus score (No.) (%)	Not/less involved	77 (90.6)	14 (100.0)	91 (91.9)	<.001
	Markedly destroyed	8 (9.4)			
Parietal (No.) (%)	Not involved	3 (3.5)	7 (50.0)	10 (10.1)	<.001
	Involved	82 (96.5)	7 (50.0)	89 (89.9)	
Occipital (No.) (%)	Not involved	1 (1.2)	7 (50.0)	8 (8.1)	<.001
	Involved	84 (98.8)	7 (50.0)	91 (91.9)	
Frontal (No.) (%)	Not involved	10 (11.8)	1 (7.1)	11 (11.1)	1.000
	Involved	75 (88.2)	13 (92.9)	88 (88.9)	
Temporal (No.) (%)	Not involved	9 (10.6)	6 (42.9)	15 (15.2)	.007
	Involved	76 (89.4)	8 (57.1)	84 (84.8)	
Cerebellum (No.) (%)	Not involved	57 (67.1)	10 (71.4)	67 (67.7)	1.000
	Involved	28 (32.9)	4 (28.6)	32 (32.3)	
Brainstem (No.) (%)	Not involved	74 (87.1)	14 (100.0)	88 (88.9)	.355
	Involved	11 (12.9)		11 (11.1)	

Table 3: Factors associated with the thalamic L-sign injury

Lobe/Structure	RR	95% CI	P Value
Parietal	3.07	1.19−7.93	.020
Occipital	7.38	1.18−46.23	.033
Frontal	0.94	0.76−1.15	.539
Temporal	1.51	0.99−2.29	.055
Cerebellum	1.03	0.87−1.21	.738
Brainstem	1.19	1.09−1.30	<.001
Parietal + occipital	2.79	1.25−6.23	.012

Note:—RR indicates relative risk.

- Critically, the risk of experiencing a thalamus L-sign type injury was 7.38 times higher when an occipital lobe injury was identified compared with when it was not involved, statistically significant.

- Similarly, the risk of experiencing a thalamus L-sign injury was 3.07 times higher when a parietal injury was present compared with when it was not involved, statistically significant.

- The risk of experiencing a thalamus L-sign injury was 1.19 times higher when a brainstem injury was present compared with when it was not involved statistically significant (P<.001).

- The risk of experiencing a thalamus L-sign injury was also higher when the frontal lobe, temporal lobe, and cerebellar injuries were all present compared with when they were not involved
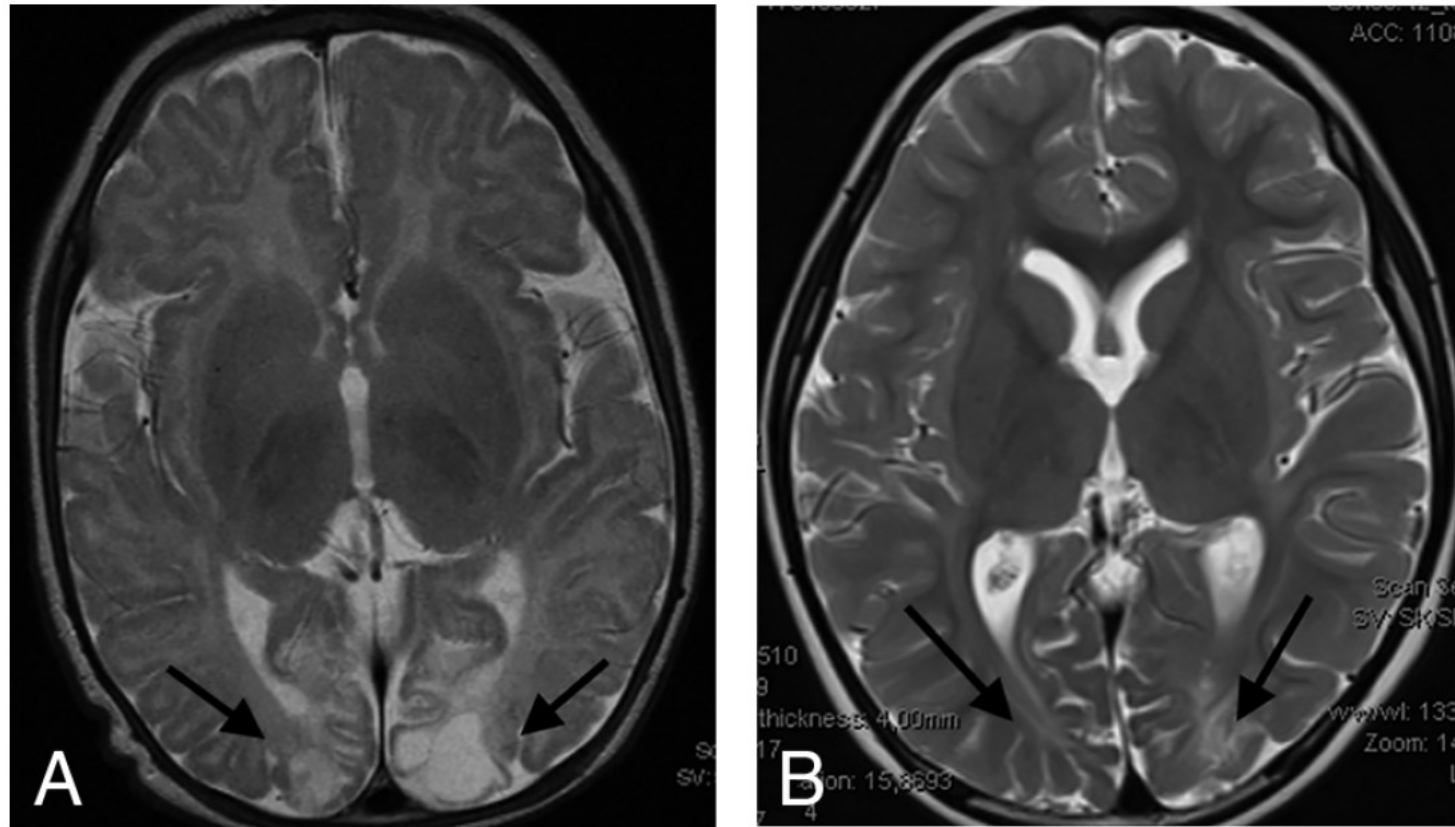
FIG 3. Axial T2-weighted images in 2 children with proved neonatal hypoglycemia. There is bilateral occipital lobe encephalomalacia (*arrows*) related to hypoglycemic brain injury. Note the absence of any thalamic injury.
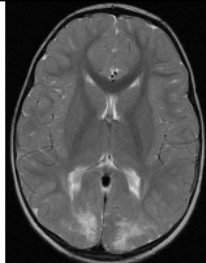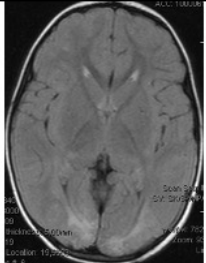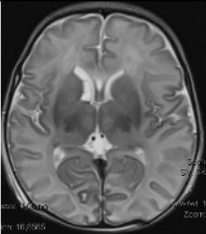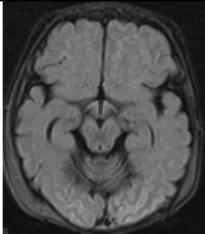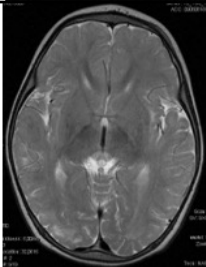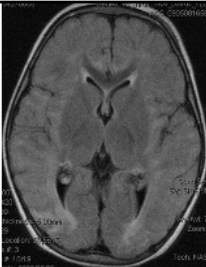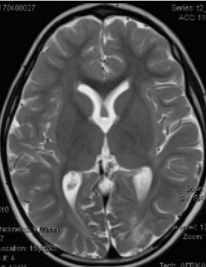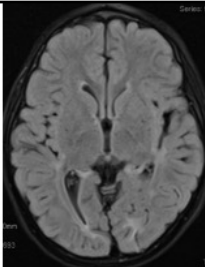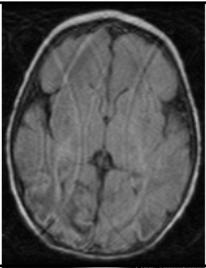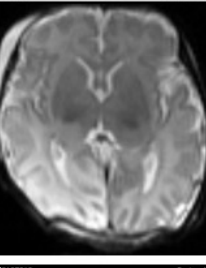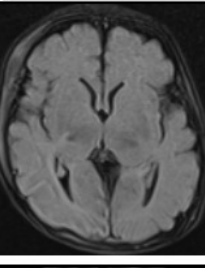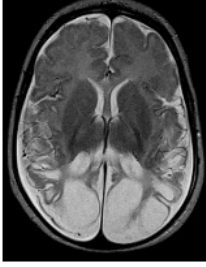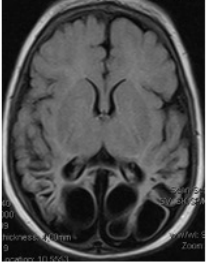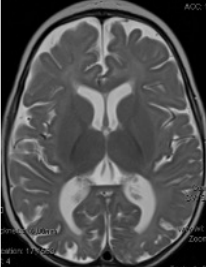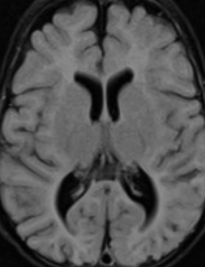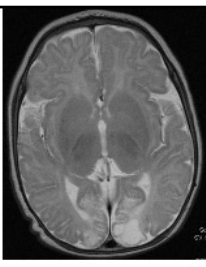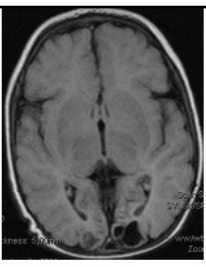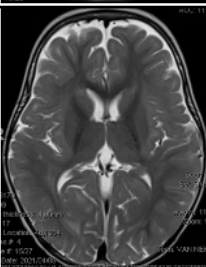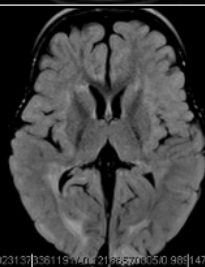
Table A. Axial T2-weighted and FLAIR sequence images of ten patients with documented pure neonatal hypoglycemic brain injury. Note the predominant parieto-occipital cortical injuries as well as distinct sparing of the thalami with absent thalamus L-sign.
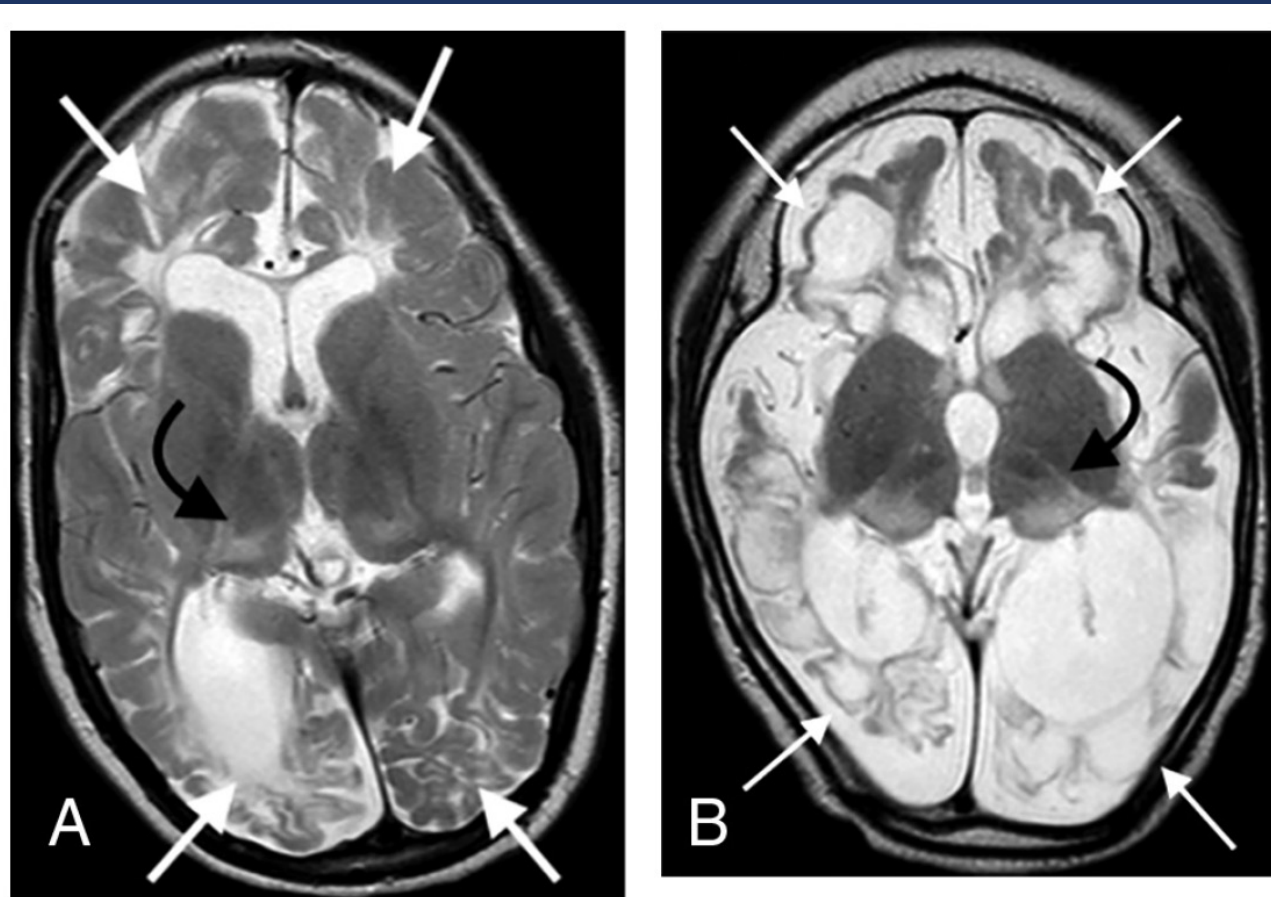
FIG 4. Combined hypoxic-ischemic and hypoglycemic brain injury in 2 children with documented neonatal encephalopathy. Note the exaggerated signal abnormality and thalamic volume loss (*black arrows*). There are multiple watershed areas (*white arrows*) demonstrating encephalomalacia change.
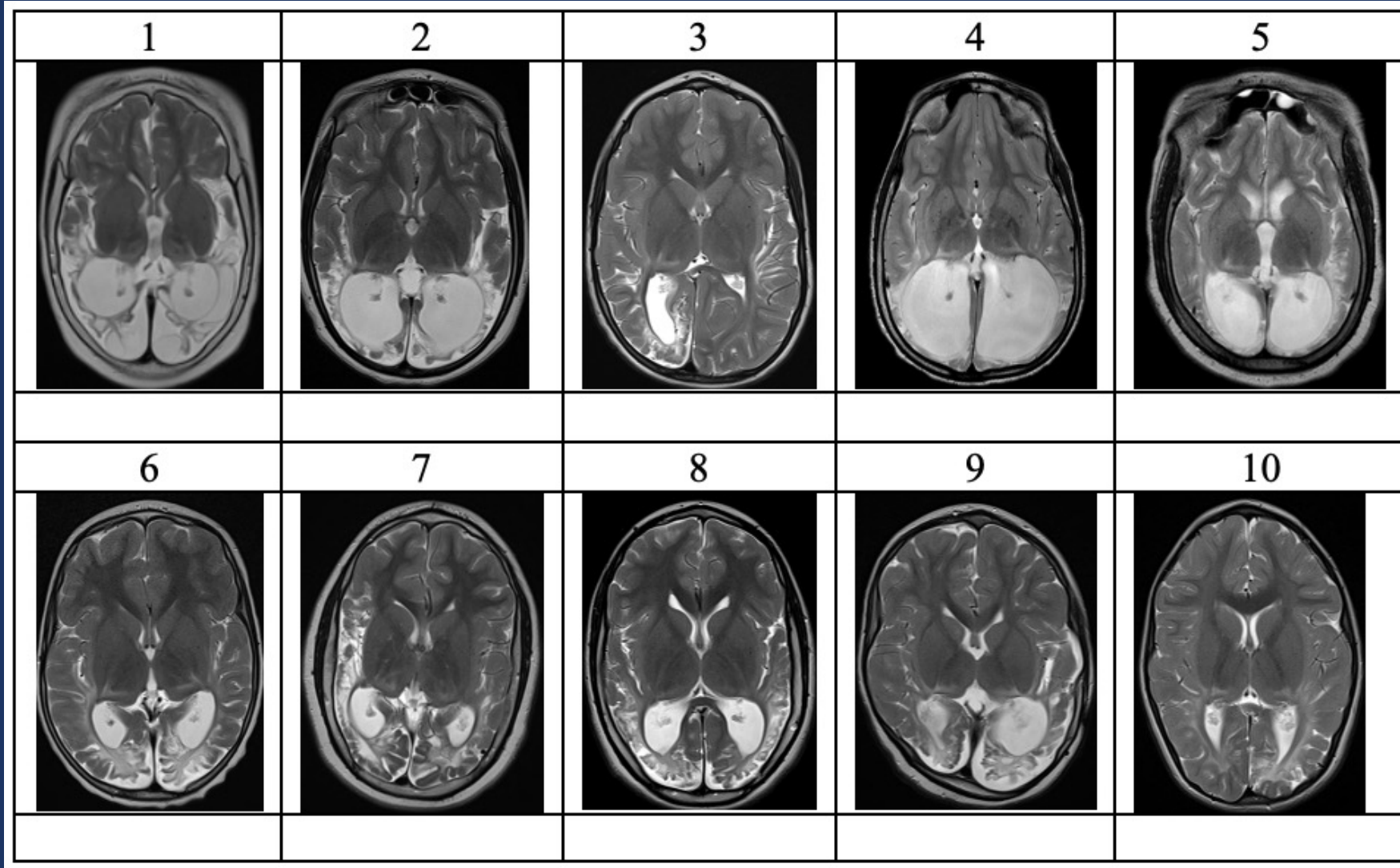
Table B. The third group comprising patients with combined hypoxic-ischemic and hypoglycemic brain injury. Note the presence of the thalamus L-sign and the cortical watershed injuries.
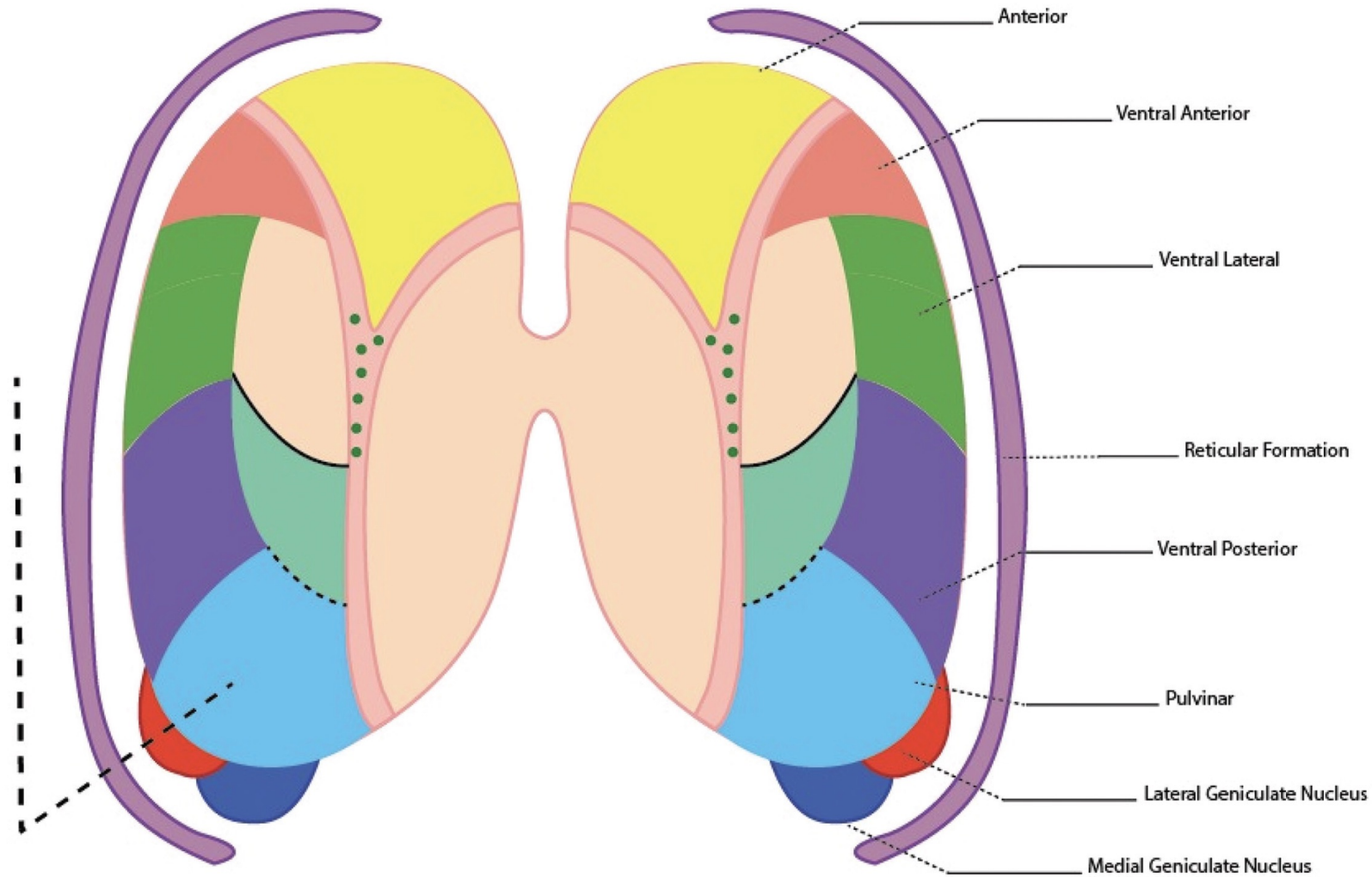
FIG 5. The key thalamic nuclei identified as components of the thalamus L-sign (*dotted line*) include the pulvinar, the lateral geniculate nucleus, and the reticular formation nuclei. Illustration by Neil Northey.

The vicious interplay between hypoxia and hypoglycemia and their attendant secondary inflammatory cascades leads to a combined final common pathway injury, especially in patients whose mother had prolonged labor.

The thalamus L-sign, we propose, is an indication of a partial, prolonged type of HIBI and occurs in patients who have endured additional HGI.

In the patients we presented, who had documented, isolated, pure HGI without HIBI, the thalamus L-sign was not observed.

We, therefore, introduce this sign as a possible biomarker for HIBI of the partial prolonged subtype, particularly when the posterior watershed territories have been involved.

This phenomenon is exaggerated in patients with combined HGI and HIBI due to the compounded lack of usable substrates for brain metabolism.

S.K. Misser, J.W. Lotz, R. van Toorn, N. Mchunu, M. Archary, and A.J. Barkovich

HYPOXIC – ISCHEMIC BRAIN INJURY

Research Plan

* Categorise the patterns

* Classify the central patterns

    Identified a new undescribed pattern

* Classify the watershed patterns

    Identified a biomarker for HIBI in watershed patterns

* Other aspects

References

1. Volpe JJ. Neurology of the newborn. 6th ed. Philadelphia, PA: Saunders; 2018.

2. Blair E, Stanley FJ. Intrapartum asphyxia: A rare cause of cerebral palsy [published correction appears in J Pediatr. 1988 Aug;113(2):420]. J Pediatr. 1988;112(4): 515–519. https://doi.org/10.1016/s0022-3476(88)80161-6

3. Kurinczuk JJ, White-Koning M, Badawi N. Epidemiology of neonatal encephalopathy and hypoxic-ischaemic encephalopathy. Early Hum Dev. 2010;86(6):329–338. https://doi.org/10.1016/j.earlhumdev.2010.05.010

4. Bruckmann EK, Velaphi S. Intrapartum asphyxia and hypoxic ischaemic encephalopathy in a public hospital: Incidence and predictors of poor outcome. S Afr Med J. 2015;105(4):298–303. https://doi.org/10.7196/SAMJ.9140

5. Simiyu IN, Mchaile DN, Katsongeri K, Philemon RN, Msuya SE. Prevalence, severity and early outcomes of hypoxic ischemic encephalopathy among newborns at a tertiary hospital, in northern Tanzania. BMC Pediatr. 2017;17(1):131. https://doi.org/10.1186/s12887-017-0876-y

6. Allen KA, Brandon DH. Hypoxic ischemic encephalopathy: Pathophysiology and experimental treatments. Newborn Infant Nurs Rev. 2011;11:125–133. https://doi.org/10.1053/j.nainr.2011.07.004

7. Rutherford M, Pennock J, Schwieso J, Cowan F, Dubowitz L. Hypoxic-ischaemic encephalopathy: Early and late magnetic resonance imaging findings in relation to outcome. Arch Dis Child Fetal Neonatal Ed. 1996;75(3):F145–F151. https://doi.org/10.1136/fn.75.3.F145

8. Barkovich AJ, Hajnal BL, Vigneron D, et al. Prediction of neuromotor outcome in perinatal asphyxia: Evaluation of MR scoring systems. Am J Neuroradiol. 1998;19(1):143–149.

9. Barkovich AJ, Truwit CL. Brain damage from perinatal asphyxia: Correlation of MR findings with gestational age. Am J Neuroradiol. 1990;11(6):1087–1096.

10. Douglas-Escobar M, Weiss MD. Biomarkers of hypoxic-ischemic encephalopathy in newborns. Front Neurol. 2012;3:144. https://doi.org/10.3389/fneur.2012.00144

11. Volpe JJ. Hypoxic-ischemic encephalopathy: Biochemical and physiological aspects. In: Volpe JJ, editor. Neurology of the newborn. 4th ed. Philadelphia, PA: W.B. Saunders Company, 2001; p. 217–276.

12. Lai MC, Yang SN. Perinatal hypoxic-ischemic encephalopathy. J Biomed Biotechnol. 2011;2011:609813. https://doi.org/10.1155/2011/609813

13. De Vries LS, Groenendaal F. Patterns of neonatal hypoxic–ischaemic brain injury. Neuroradiology. 2010;52(6):555–566. https://doi.org/10.1007/s00234-010-0674-9

14. Inder TE, Volpe JJ. Chapter 20 – Hypoxic-ischemic injury in the term infant: Clinical-neurological features, diagnosis, imaging, prognosis, therapy. In: Volpe JJ, Inder TE, Darras BT, et al., editors. Volpe's neurology of the newborn. 6th ed. Philadelphia, PA: Elsevier, 2018; p. 510–563.

15. Dekker G, Louw HB, Andronikou S, Pienaar M, Hlongwane S, Brandt A, et al. In utero and perinatal hypoxic brain damage. S Afr J Rad. 2006;10(3). https://doi.org/10.4102/sajr.v10i3.164

16. Miller SP, Ramaswamy V, Michelson D, et al. Patterns of brain injury in term neonatal encephalopathy. J Pediatr. 2005;146(4):453–460. https://doi.org/10.1016/j.jpeds.2004.12.026

17. Sie L, Van der Knaap M, Oosting J, De Vries L, Lafeber H, Valk J. MR patterns of hypoxic-ischemic brain damage after prenatal, perinatal or postnatal asphyxia. Neuropediatrics. 2000;31(03):128–136. https://doi.org/10.1055/s-2000-7496

18. Barkovich AJ, Baranski K, Vigneron D, et al. Proton MR spectroscopy for the evaluation of brain injury in asphyxiated, term neonates. Am J Neuroradiol. 1999;20:1399–1405.

19. Barkovich AJ, Miller SP, Bartha A, et al. MR imaging, MR spectroscopy, and diffusion tensor imaging of sequential studies in neonates with encephalopathy. Am J Neuroradiol. 2006;27(3):533–547.

20. Lakatos A, Kolossvary M, Szabo M, et al. Novel structured MRI reporting system in neonatal hypoxic-ischemic encephalopathy – Issues of development and first use experiences. Ideggyogy Sz. 2018;71(7–08):265–276. https://doi.org/10.18071/isz.71.0265

21. Yoshida S, Hayakawa K, Yamamoto A, et al. Symmetrical central tegmental tract (CTT) hyperintense lesions on magnetic resonance imaging in children. Eur Radiol. 2009;19:462–469. https://doi.org/10.1007/s00330-008-1167-7

22. Aguilera-Albesa S, Poretti A, Honnef D, et al. T2 hyperintense signal of the central tegmental tracts in children: Disease or normal maturational process? Neuroradiology. 2012;54:863–871. https://doi.org/10.1007/s00234-012-1006-z

23. Griffiths PD, Radon MR, Crossman AR, Zurakowski D, Connolly DJ. Anatomic localization of dyskinesia in children with 'profound' perinatal hypoxic-ischemic injury. Am J Neuroradiol. 2010;31:436–441. https://doi.org/10.3174/ajnr.A1854

24. Chacko A, Andronikou S, Mian A, Goncalves FG, Vedajallam S, Thai NJ. Cortical ischaemic patterns in term partial-prolonged hypoxic-ischaemic injury – The inter-arterial watershed demonstrated through atrophy, ulegyria and signal change on delayed MRI scans in children with cerebral palsy. Insights Imaging. 2020;11(1):53. https://doi.org/10.1186/s13244-020-00857-8

25. Nikas I, Dermentzoglou V, Theofanopoulou M, Theodoropoulos V. Parasagittal lesions and ulegyria in hypoxic-ischemic encephalopathy: Neuroimaging findings and review of the pathogenesis. J Child Neurol. 2008;23(1):51–58. https://doi.org/10.1177/0883073807308694

26. Myers RE. Two patterns of perinatal brain damage and their conditions of occurrence. Am J Obstet Gynecol. 1997;112:246–276. https://doi.org/10.1016/0002-9378(72)90124-X

27. Volpe JJ, Pasternak JF. Parasagittal cerebral injury in neonatal hypoxic-ischemic encephalopathy: Clinical and neuroradiologic features. J Pediatr. 1977;91: 472–476. https://doi.org/10.1016/S0022-3476(77)81328-0

28. Weidenheim KM, Bodhireddy SR, Nuovo GJ, et al. Multicystic encephalopathy: Review of eight cases with etiologic considerations. J Neuropathol Exp Neurol. 1995;54:268–275.
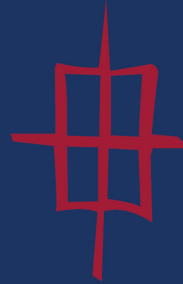
References

1. Barkovich A (1992) MR and CT evaluation of profound neonatal and infantile asphyxia. AJNR Am J Neuroradiol 13:959–972

2. de Vries LS, Groenendaal F (2010) Patterns of neonatal hypoxic–ischaemic brain injury. Neuroradiology 52(6):555–566

3. Huang BY, Castillo M (2008) Hypoxic-ischemic brain injury: imaging findings from birth to adulthood. Radiographics 28(2):417–439. https:// doi. org/ 10. 1148/ rg. 28207 5066

4. Ghei SK, Zan E, Nathan JE et al (2014) MR imaging of hypoxic-ischaemic injury in term neonates: pearls and pitfalls. Radiographics 34:1047–1061. https:// doi. org/ 10. 1148/ rg. 34413 0080

5. Miller SP, Ramaswamy V, Michelson D et al (2005) Patterns of brain injury in term neonatal encephalopathy. J Pediatr 146(4):453–460

6. Sie L, Van der Knaap M, Oosting J, De Vries L, Lafeber H, Valk J (2000) MR patterns of hypoxic-ischemic brain damage after prenatal, perinatal or postnatal asphyxia. Neuropediatrics 31(03):128–136

7. Volpe JJ, Pasternak JF (1977) Parasagittal cerebral injury in neonatal hypoxic-ischemic encephalopathy: clinical and neuroradiologic features. J Pediatr 91:472–476

8. Misser SK, Barkovich AJ, Lotz JW, Archary M (2020) A pictorial review of the pathophysiology and classification of the magnetic resonance imaging patterns of perinatal term hypoxic ischemic brain injury—what the radiologist needs to know…. S Afr J Radiol 24(1):206

9. Mar.n-Padilla M (2011) The human brain: prenatal development and structure. Springer, New York. https:// doi. org/ 10. 1007/ 978-3-642-14724-1

10. Inder TE, Volpe JJ (2018) Chapter 20—Hypoxic-ischemic injury in the term infant: clinical-neurological features, diagnosis, imaging, prognosis, therapy. In: Volpe JJ, Inder TE, Darras BT, de Vries LS, du Plessis AJ, Neil JJ et al (eds) Volpe's neurology of the newborn, 6th edn. Elsevier, Amsterdam, pp 510–563

11. Pasquier F, Leys D, Weerts JG, Mounier-Vehier F, Barkhof F, Scheltens P (1996) Inter- and intraobserver reproducibility of cerebral atrophy assessment on MRI scans with hemispheric infarcts. Eur Neurol 36(5):268–272. https:// doi. org/ 10. 1159/ 00011 7270

12. Kinney HC, Volpe JJ (2018) Hypoxic-ischemic injury in the term infant: neuropathology. In: Volpe JJ, Inder TE, Darras BT, de Vries LS, du Plessis AJ, Neil JJ et al (eds) Volpe's neurology of the newborn, 6th edn. Elsevier, Amsterdam, pp 484–499

13. Chacko A, Andronikou S, Mian A et al (2020) Cortical ischaemic patterns in term partial-prolonged hypoxic-ischaemic injury—the inter-arterial watershed demonstrated through atrophy, ulegyria and signal change on delayed MRI scans in children with cerebral palsy. Insights Imaging 11(1):53

14. Pasternak JF, Gorey MT (1998) The syndrome of acute near-total intrauterine asphyxia in the term infant. Pediatr Neurol 18(5):391–398. https:// doi. org/ 10. 1016/ s0887-8994(98) 00002-2

15. Gunn AJ, Bennet L (2009) Fetal hypoxia insults and patterns of brain injury: insights from animal models. Clin Perinatol 36:579–593

16. Rennie J, Rosenbloom L (2011) How Long have we got to get the baby out? A review of the effects of acute and profound intrapartum hypoxia and ischaemia. Obstet Gynaecol 13:169–174

17. Myers RE (1972) Two patterns of perinatal brain damage and their conditions of occurrence. Am J Obstet Gynecol 112:246–276Ranck JB, Windle WF (1959) Brain damage in the monkey, macaca mulatta, by asphyxia neonatorum. Exp Neurol 1:131–150

19. Windle WF (1968) Brain damage at birth. JAMA 206:1967. https:// doi. org/ 10. 1001/ jama. 206.9. 1967

20. Mallard EC, Williams CE, Gunn AJ, Gunning MI, Gluckman PD (1993) Frequent episodes of brief ischemia sensitize the fetal sheep brain to neuronal loss and induce striatal injury. Pediatr Res 33:61–65

21. Azzarelli B, Caldemeyer KS, Phillips JP, DeMeyer WE (1996) Hypoxicischemic encephalopathy in areas of primary myelination: a neuroimaging and PET study. Pediatr Neurol 14:108–116

22. McDonald J, Johnston M (1990) Physiological and pathophysiological roles of excitatory amino acids during central nervous system development. Brain Res Rev 15:41–70

23. Fatemi A, Wilson MA, Johnston MV (2009) Hypoxic-Ischemic Encephalopathy in the Term Infant. Clin Perinatol 36(4):835–858

24. Johnston MV, Fatemi A, Wilson MA, Northington F (2011) Treatment advances in neonatal neuroprotection and neurointensive care. The Lancet Neurology 10(4):372–382

25. Squier W (2002) Acquired damage to the developing brain: timing and causation. Arnold Taylor & Francis, London

26. Akkal D, Dum RP, Strick PL (2007) Supplementary motor area and presupplementary motor area: targets of basal ganglia and cerebellar output. J Neurosci 27(40):10659–10673

27. Cacciola A, Calamuneri A, Milardi D et al (2017) A connectomic analysis of the human basal ganglia network. Front Neuroanat 26(11):85. https:// doi. org/ 10. 3389/ fnana. 2017. 00085

28. Leh.ricy S, Ducros M, Krainik A et al (2004) 3-D diffusion tensor axonal tracking shows distinct SMA and pre-SMA projections to the human striatum. Cereb Cortex 14(12):1302–1309. https:// doi. org/ 10. 1093/ cercor/ bhh091

29. Leh.ricy S, Ducros M, Van de Moortele PF et al (2004) Diffusion tensor fiber tracking shows distinct corticostriatal circuits in humans. Ann Neurol 55(4):522–529. https:// doi. org/ 10. 1002/ ana. 20030

30. Inase M, Tokuno H, Nambu A, Akazawa T, Takada M (1999) Corticostriatal and corticosubthalamic input zones from the presupplementary motor area in the macaque monkey: comparison with the input zones from the supplementary motor area. Brain Res 833:191–201

31. Milardi D, Quartarone A, Bramanti A et al (2019) The cortico-basal ganglia-cerebellar network: past, present and future perspectives. Front Syst Neurosci 13(13):61. https:// doi. org/ 10. 3389/ fnsys. 2019. 00061